Experimental characterization of API-5L X65 steel and an improved, reliable method for assessing hot cracking susceptibility of materials

Dimitrios E. Statharas

A thesis presented for the degree of
Doctor of Philosophy
At the University of Leicester

Department of Engineering
University of Leicester
United Kingdom
2019

Contents

List of Figures

List of Tables

Abstract

Fusion welding is a complex process that requires a lot of control in order to achieve the desired results. Due to its complexity a number of defects may occur during the process. Weld solidification cracking is one of them and it is a critical defect. The presence of this defect will always lead to failure. This failure can occur during the production process where, if detected, the defect will cause significant setbacks and increased cost of production. If undetected it will lead to failure during service where the impact will be more severe. Overall, failures due to solidification cracking can lead to significant environmental, economic and social damage.

This thesis examines the capabilities of experimental procedures with the ultimate goal to assess the hot cracking susceptibility of materials. In the first chapters the material used for this work is presented along with its production process for manufacturing pipelines for gas and oil transport. Adding to that, literature on the subject of hot cracking is presented. Tests that have been created for assessing the hot cracking susceptibility of materials (weldability tests) are presented and discussed and the two tests that are the focus of this study are analysed in depth.

This thesis is focused on the characterization of the material, weldability tests and post processing of the weldability test samples. During the experimental design of the weldability tests, improvements that allow for increased repeatability and reliability of the tests are presented. These improvements allow for the better control of the application of strain during the tests which is an important parameter for solidification cracking. The results of these tests show that there are significant improvements compared to previous work. This is deemed important since these tests are not standardized and increased control of the tests could lead to standardization of the tests. Furthermore, the post processing by X-ray computed tomography and fractography of the samples provided indications that it is possible to predict the position where a solidification crack will be generated during welding.

Acknowledgements

Before I started the PhD it seemed to me that a PhD is a one man show. Boy was I wrong. Admittedly, I enjoyed the work that had me as the only driver and the only person that had a say to what would happen next, but there were many parts of the work that would not have been possible without the important people that I had supporting me throughout the course of this project.
Firstly I would like to thank Professor Helen V. Atkinson for supervising, supporting me and dealing with my eccentricities throughout the PhD. Thank you Professor you have my utmost appreciation and respect. I would also like to thank Dr. Rob Thornton who took over as my supervisor for my final year. It was a memorable experience for multiple reasons. Thank you very much for the support and patience.
I would also like to extend my appreciation and gratitude to Professor Hongbiao Dong who was not only my second supervisor but also the person who made this possible from the start and brought me here so I can contribute to the field. I would also like to thank Professor Simon Gill who also made this possible by bringing me here at IMPACT CDT for doing a PhD.
Special thanks go to the people in TATA steel. Particularly, Shuwen Wen and John Marsden for supervising me for the industrial part of the project and providing to me not only their expertise, knowledge and equipment but also their patience, hospitality and an open mind that allowed me to achieve my goals. I would also like to thank Adam Bannister, Chris Phillips, Steve Hattersley, Titou Minster and Zulfiqar Husain for aiding me either in experiments, equipment transfer, providing input and opportunities to present my work to the company.
I would also like to thank everyone working in the University of Leicester who helped me in one way or another during the PhD. Technical staff members like Graham Clark, Vinay Patel, Alex Frost, Dipak Raval, Ian Bromley, Andy Underhill and so many others who provided with support and helped with my requests no matter how crazy they were. Administration staff like Charlotte Ratcliffe, Chris Howe and Michelle Pryce who did their best to make my life easier here. Academics who not only provided significant input for the academic part of my PhD and allowed me to teach in their modules but also made me a better person like Dr. Dave Weston, Dr. Hugo Williams, Dr. Mateusz Bocian, Dr Andrew McMullan and many others this list could go on forever. I am glad I met all of them and they were part of this in one way or another.
Last but not least, special thanks to all friends and family who also supported me and created memories since day one that I will remember forever.
This study that was provided by the Centre for Doctoral Training in Innovative Metal Processing (IMPaCT), at the University of Leicester, funded by the UK Engineering and Physical Sciences Research Council (EPSRC), grant reference EP/L016206/1. Thanks for providing me the opportunity to work on this project.

Dedication

This thesis is dedicated to the man that made all of this possible but sadly and suddenly passed away this year. John Sideris you, along with Carmen Medrea and Fotis Fotopoulos brought materials in my life. Without you I would not be where I am now. I think about you every time I see or think about steel. Which is every single day. You were, are and will be the best Professor daskale, I wish you were here to see this. This is for you. Rest in peace.

Dimitris

Nomenclature

AF	Acicular Ferrite
API	American Petroleum Industry
BF	Bainitic Ferrite
BTR	Brittle Temperature Range
CE	Carbon Equivalent
CG-HAZ	Coarse-Grained Heat Affected Zone
CPTT	Cast Pin Tear Test
CT	Computed Tomography
CTOD	Crack Tip Opening Displacement
DCC	Direct Chill Casting
DDC	Ductility Dip Cracking
DP	Degenerate Pearlite
DSAW	Double Submerged Arc Weld
EDM	Electrical Discharge Machining
FW	Friction Welding
GB	Granular Bainitic Ferrite
GMAW	Gas Metal Arc Welding
GTAW	Gas Tungsten Arc Welding
HAZ	Heat Affected Zone
HIC	Hydrogen Induced Cracking
HSLA	High Strength Low Alloy
ID	Inner Diameter
LBW	Laser Beam Welding
M/A	Martensite/Austenite
MCD	Maximum Crack Distance
MCL	Maximum Crack Length
NDT	Non-Destructive Testing
OD	Outside Diameter
PF	Polygonal Ferrite
PMZ	Partially Melted Zone
PWHT	Post Weld Heat Treatment
QF	Quasi Polygonal Ferrite
RW	Resistance Welding
SAW	Submerged Arc Welding
SCTR	Solidification Cracking Temperature Range
SEM	Scanning Electron Microscope
SMAW	Shielded Metal Arc Welding
SSC	Sulphide Stress Cracking
TCL	Total Crack Length

TIG	Tungsten Inert Gas
TMCR	Thermo-Mechanically Controlled Rolled
UKAS	United Kingdom Accreditation Service
UOE	U-Forming, O-Forming And Expansion Process
XRCT	X-Ray Computed Tomography

Chapter 1

Introduction

The presented thesis is the result of a study that focused on developing and improving the experimental process of assessing hot cracking susceptibility of materials. These improvements also led to an improved theoretical understanding of the hot cracking phenomenon. The following sections discuss and present the motivation for this work initiating from a brief history of steel and its applications that acted as a main driver for this work. Following these brief sections the main aspects, which the work was focused on, are described in order to set the scope of the study and describe the structure of this thesis in detail.

1.1 Brief history of steel

Since ancient times the use of materials was driving civilisations and the main materials that were used characterized the era. One of the most important eras in history was the Iron Age (1200 BC to 550 BC). Iron began being used toward the end of the Bronze Age (3300 BC to 1200 BC) and its superiority to bronze was quickly acknowledged. Despite the fact that the rise of steel began during the industrial revolution of the 19^{th} century its story started much earlier. Steel was, like a lot of great discoveries, discovered by accident. Iron workers realised that when iron is left in charcoal fires for long periods the material changed [1]. It became harder and stronger and the tools and weapons that were made with the

use of this material were superior to others. A significant number of techniques for manipulation of steel were developed and the products produced from this material gained in reputation. There are still items from these early times that are to this day legendary because of the amount of material manipulation that was needed in order to create these high quality products even for today's standards. These include Japanese Katana swords, traditional Persian swords and Damascene swords.

Industrial revolution would not have been so successful or even possible if steel was not an option. One of the greatest technological leaps of mankind would not have been possible. Common steel is an iron-carbon alloy which contains a maximum 2% carbon. Other alloying elements are also used for the production of steel. Steel was and still is the most commonly used material. This is because steel is a strong material that can be easily manipulated with a low production cost compared to other materials and it is also indefinitely recyclable. Adding to that, research and work on creating advanced steel alloys is ongoing. A couple of examples include improvements in corrosion resistance by improving the chemical composition of steel [2] or improving steel strength to weight ratio by submitting the material to specific heat treatments [3]. As a consequence, steel is the primary material for multiple industries like automotive [4], oil and gas [5], construction [6] and food [7]. World production of steel reached a total of 1,630 million tonnes in 2016 [8].

1.2 High Strength Low Alloy Steels

Steel is used in numerous applications and it is one of the most widely used metals. This is mainly because of the wide range of the alloy's composition, microstructures and properties [9]. Steels can be divided into four main categories:

- carbon steels
- alloy steels
- stainless steels and

- tool steels

Each category can be divided into subcategories depending on the application, the composition or the alloying elements of the steels. One interesting category of steels is the high strength low alloy steels (HSLA).

HSLA steels are alloys with a low percentage of carbon (usually <0.3%wt.) and with alloying elements like manganese (up to 2.0% wt.), silicon, molybdenum, nickel and chromium usually less than 1% wt. individually [9]. Their high strength is primarily a result of the production process. This results in steels with yield strength above 275 MPa, adequate formability and weldability [10]. HSLA steels are produced usually with thermo-mechanically controlled rolling and the alloying elements are actually micro alloyed in the steel, mainly to control its structure. Figure 1.1 shows a comparison in the yield strength of HSLA steels relative to other steels and also how the size of the grains affects the yield strength [11].

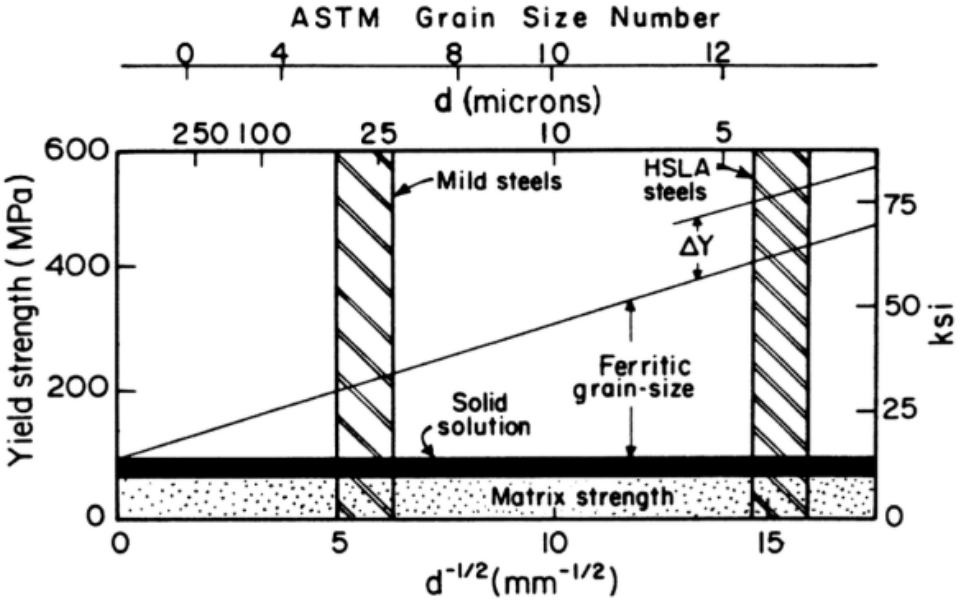

Figure 1.1: Yield strength versus $d^{-1/2}$ where d is the grain diameter for HSLA steels in comparison with mild steels [11].

The micro alloying process of these steels also results in improved mechanical properties, corrosion resistance and increased weldability. HSLA steels can reach up to 485 MPa yield strength without further heat treatment [12].

1.2.1 Alloying elements and HSLA steels

Research on the effect of the alloying elements that are used for HSLA pipelines steel is significant. Generally alloying elements have different effects on the microstructures and properties of steel. Understanding the basic effect that the most significant elements used for alloying HSLA steel have, but also steel in general, is considered important. Alloying elements like manganese, aluminium, titanium and chromium are commonly used in HSLA steels.

Manganese is present in almost all commercial steels. This is because it enhances the de-oxidation properties in the melts of steel and its tendency to combine with sulphur and form manganese sulphides that increase machinability. It also contributes to the steel hardenability but with not as strong an effect as other elements [13]. The problem with increased manganese concentration is that it decreases ductility and weldability of the steel, a property that in the current application is not desirable [13].

Silicon is also a deoxidizing element that is used in steels and it also increases the strength of ferrite without having a severe effect on the overall ductility of the steel. The usual range of composition in silicon is between 0.15% to 0.30% wt. If other types of deoxidizing elements are present the composition of silicon can be reduced [10, 13].

Chromium is a strong carbide forming element and it is also used as a solid solution hardening element. The chromium carbides dissolve in austenite at a slow rate which means that before quenching steel containing chromium a sufficient amount of heating time is required [14].

Vanadium is an element that is usually added to reduce the grain growth in steels. This leads to improved strength of steels and the composition that is required usually does not exceed the 0.05% wt. point. Further increase in vanadium composition usually results in reduction of the strength of the steels since it forms carbides that are hard to dissolve in austenite. Niobium additions to steel significantly increase the yield strength of the material. These additions are

usually around 0.02% wt. Niobium is a significant element in steels that are processed using thermo-mechanically controlled techniques. Titanium is used as a grain size control element that improves strength. It also forms carbides and nitrides and can be used as a deoxidizer [10, 13, 15].

Molybdenum can increase the hardenability of steel. It also reduces the effect of temper embrittlement in steels, and increases the creep and tensile strength of steel at high temperatures. Adding to that it reduces the speed of transformation of austenite to pearlite significantly more than it reduces the speed of transformation of austenite to bainite thus making it possible to obtain bainite structure from continuous cooling. Aluminum additions also improve the control of austenite grain growth and it is used as a deoxidizer [10, 13, 16]. All the elements used in HSLA steels are significant contributors in de-oxidation of steel and in the control of the grain size, which are two key factors for the production process of HSLA steels.

The effect of titanium has been investigated in steels like API 5L-X70 pipeline steel [17] which showed that X70 steel with increased content of titanium in the weld metal exhibits improved impact toughness because titanium drives the formation of more acicular ferrite in the microstructure of the steel. On the other hand research on the X65 steel showed that the formation of titanium carbonitride precipitates reduces the fracture toughness of the material and they act as crack initiation sites [18].

This is one of the classic problems engineers face in their search for appropriate materials and compositions for demanding applications. The trade off in properties is something that must be taken under consideration constantly and finding the optimal process for each application is essential. Since the HSLA pipeline steels are welded a focus on the alloying elements in the welds is also a topic that is extensively researched as the demands for higher quality materials are increasing.

API 5L-X70 steel samples with different compositions in manganese and titanium were examined for their susceptibility in hydrogen-induced cracking (HIC) and sulphide stress cracking (SSC) which essentially revealed the same conflicting problem as the previous example where the amount of manganese improved the materials hardness as it was increased but it also increased its susceptibility to

SSC. Adding to that titanium based inclusions acted as beneficial hydrogen traps that reduce the HIC susceptibility but they reduce the fracture toughness of the material [19]. Another study on API 5L-X80 steel showed that the increase of molybdenum can increase the yield and tensile strength of the material but also reduce its toughness [20].

In these studies the observed presence of acicular ferrite was deemed as a desirable microstructure in welds because it can increase HIC and SSC resistance especially in combination with Ti (C,N). However, increased amounts of any of these structures will have an adverse effect on the material. Adding to that it must not be forgotten that each element behaves in a specific way in the changes of temperature that can affect significantly the performance of the material. For example molybdenum is an alloying element that is used in HSLA steels but if the production process parameters are not carefully controlled it might lead to secondary hardening [10].

1.2.2 Microstructure of HSLA steel for offshore pipelines.

The microstructure of HSLA steels is not only guided by the alloying elements used but also from the production process of the steel. HSLA steels for offshore pipelines are produced mainly through a process called Thermo-Mechanically Controlled Rolling (TMCR). This process is a significant driver that leads to the exceptional properties of HSLA steels for these applications. An outline of the process is presented in Figure 1.2. During TMCR the steel is subjected to a simultaneous application of deformation and heat. This leads to a refined microstructure. By adding this process to the production cycle of the micro/-alloyed HSLA steel the conflicting requirements of strength, toughness and weldability are addressed through grain refinement [21].

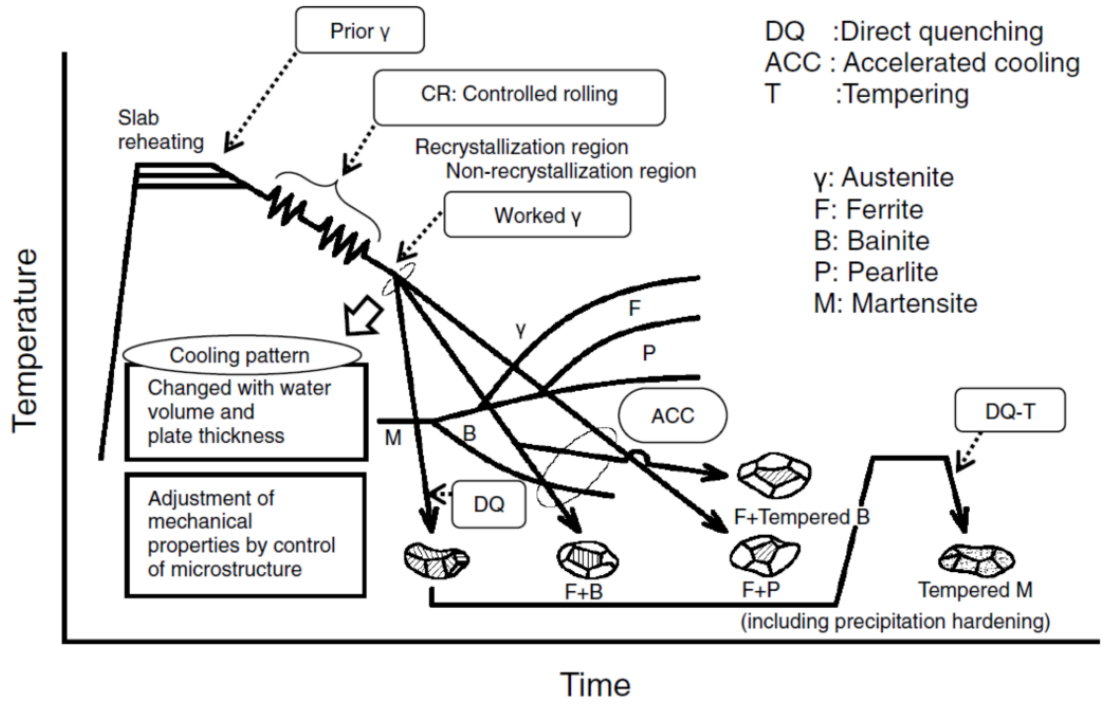

Figure 1.2: Schematic description of various typical TMCR processes [22].

This grain refinement is driven primarily by the recrystallization of the austenitic structure during deformation of the material. This occurs during the process where the steel is reheated in the range of 1200°C-1300°C in order to be formed/rolled to the desirable thickness. This deformation leads to the breaking down of the coarse microstructure and recrystallization of the austenite [13]. The micro alloying elements that are added in the material inhibit the growth of the grains by pinning the grain boundaries [22].

Recrystallization is an integral part to thermo-mechanical rolling. The definition of recrystallization can be describes as follows. When a new grain structure is formed in a deformed material, driven by the stored energy of deformation, then the process is called recrystallization [23]. This process occurs in two steps. Nucleation and growth which a structural transformation originally recognized by Gibbs [24]. This transformation has an extensive effect in the structure of the material. In the first step a new grain is formed (nucleated) and on the second step it grows generating a new structure [25].

The microstructure that results from this process is most commonly a

ferrite-pearlite structure with the ferrite being the dominant phase. These two phases have specific characteristics that distinguish them from the typical phases that result from normalizing and slow cooling.

Because after the TMCR the material is undergoing an accelerated cooling process the resulting pearlite is more homogenous than the normalized pearlite. This occurs because the cooling process inhibits the C diffusion which results in a lack of a lamellar structure. The resulting pearlite is usually referred to as Degenerate Pearlite (DP) or pseudo-pearlite [26, 27]. Because of the increased cooling rate of these steels the formation of pearlite is significantly hindered. This results in a ferrite dominant microstructure. The manufacturing process of the HSLA steel will produce different morphologies of ferrite that will affect the properties of the material. The morphologies that ferrite can manifest are the following [28] which are also described in Figure 1.3.

- Ferrite that is formed at the highest temperatures and slow cooling rates and presents equiaxed grains which is called polygonal ferrite (PF).
- Ferrite that is formed by short range diffusion across the interface of ferrite and austenite. It assumes irregular boundaries with a high density of dislocations. It also includes martensitic and austenitic constituents that are brittle thus reducing toughness. This is called quasi-polygonal ferrite (QF).
- Ferrite that forms at the same temperature as bainite but at slower cooling rates. This structure has retained austenite or martensite/austenite constituents dispersed in a ferritic matrix. This is called granular bainitic ferrite (GB).
- Another form is called bainitic ferrite (BF), which has many ferritic lath bundles that contain a high density of dislocations and are separated with high angle boundaries.

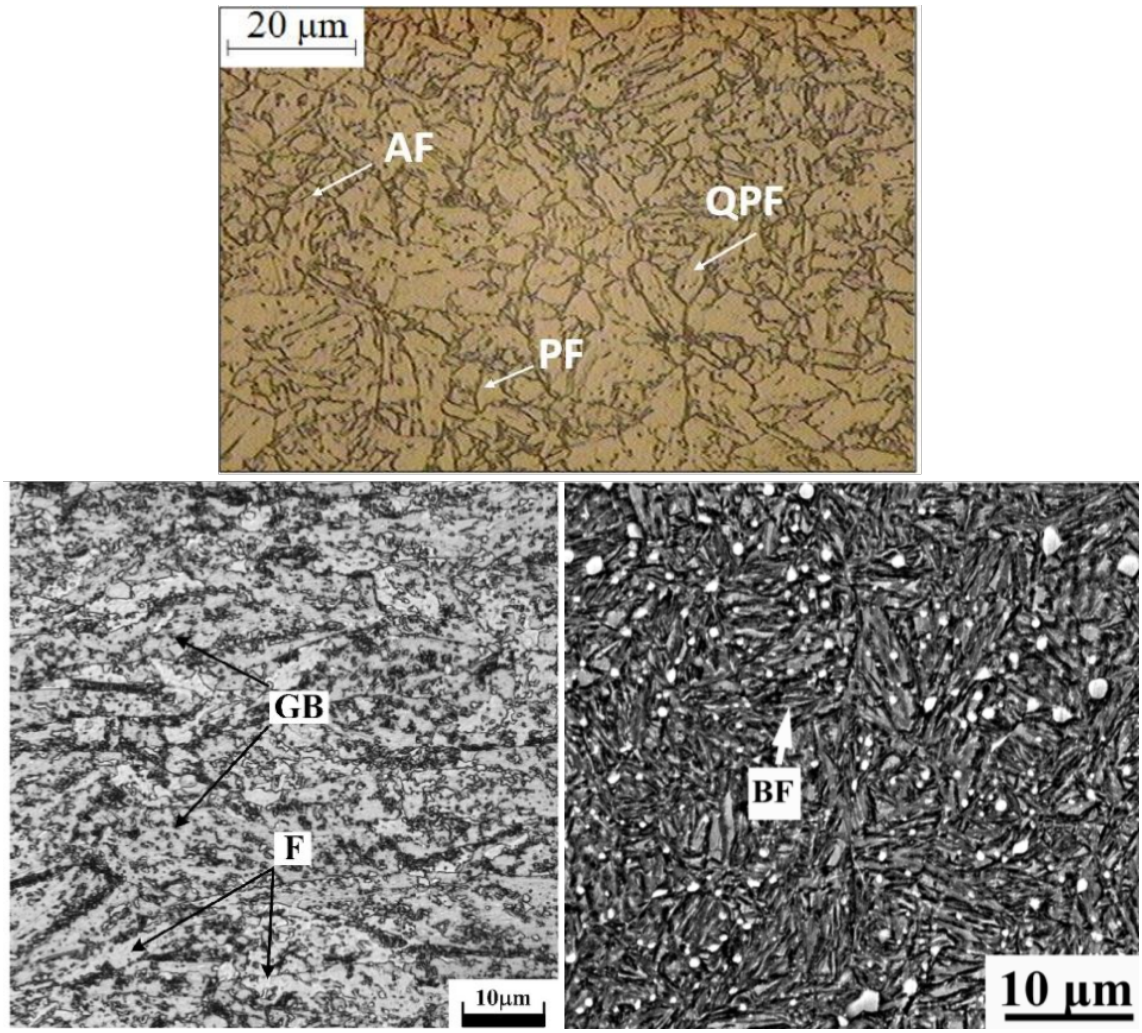

Figure 1.3: Microstructures of different types of ferrite [29–31].

All of these forms of ferrite can be observed in a form of ferrite that is called acicular ferrite (AF). This form is present in HSLA steel usually with irregular grain boundaries and small sub-grain boundaries. Acicular ferrite can also obtain a needle like shape which is randomly oriented when the material is welded. A type of ferrite that is effectively competitive in nature with the acicular ferrite and forms at high temperatures is the Widmanstätten ferrite which grows from the austenitic grain boundaries [32].

The microstructure of HSLA steels and their welds has been extensively researched. Study that was carried out on the weld metal in X70 steel revealed that the ferrite structures discussed were also detected in the weld of the material with the addition of lamellar pearlite ferrite-carbide aggregate and of coarse upper and lower bainite morphologies [33]. Another research of a Ti-Nb-Mo

micro-alloyed HSLA steel showed that the structure is predominantly ferritic but the cooling rate affects the size of the interphase carbide precipitates [34]. The influence of microstructural aspects of Submerged Arc Welding (SAW) HSLA steel joints has also been examined. The micro-structure of the weld joint is, as expected, affected by the heat input during welding which affect the size of the ferritic laths and alters the CGHAZ from bainite/martensite to coarse granular bainite. As the heat input was increased the toughness of the material decreased [35, 36]. It is noteworthy that in many cases HSLA steels and their microstructure is examined under welding conditions because HSLA is a steel that is broadly used in the oil and gas industry for the production of pipes. Its increased use has led to the formation of specific standards for this industry [37].

1.3 API-5L standard and X65 HSLA steel

The American Petroleum Institute (API) is a national trade association that among other activities has led the development of petroleum, natural gas and petrochemical equipment and operating standards. API 5L standards define all the parameters and limits in mechanical properties, size (pipe diameters, pipe wall thickness), welding techniques, composition and mandatory tests that the steel must comply with, in order to be characterized as an X65 steel. The main objective of the specification is to provide standards for pipe suitable to transfer water, gas and oil [37].

API-5L X65 steel is the grade of steel that has specific properties. These properties are defined in these standards. An API-5L X65 steel was mainly used in this study. X65 has a minimum yield strength of 448 MPa and a maximum of 600 MPa. Its ultimate tensile strength ranges from 531 to 758 MPa. Properties that are not defined by the standards have been examined in the literature. The impact toughness (Charpy energy) of the steel has been measured between 280 J and 360 J. Its fracture toughness has been measured between 115 MPa $m^{1/2}$ and 280 MPa $m^{1/2}$. As far as corrosion resistance is concerned. Depending on the environment X65 has a corrosion resistance ranging from 0.02 mm/y to 0.8 mm/y [38–43].The standards define two Product Specification Levels (PSL 1 and PSL 2). These

specifications have some differences in the limits that are set and the manufacturer should always state which the specification level for the steel manufactured is. The composition of the steel is given in the following table (Table 1.1).

Table 1.1: Chemical Composition limits of X65 Steel [37].

Grade & Class	**C Max (% wt.)**	**Mn Max (% wt.)**	**P Max (% wt.)**	**S Max (% wt.)**	**Nb Max (% wt.)**	**V Max (% wt.)**	**Ti Max (% wt.)**
PSL 1	0.26	1.40	0.030	0.030	The sum must not Exceed 0.15%		
PSL 2	0.22	1.45	0.025	0.015			

The API specification defines parameters considered critical for the applications of X65 and other grades of HSLA steel. The analysis of the standards is not in the scope of this study. X65 steel is the material that will be used and discussed in this study. Its microstructure will be examined and it will be used in order to develop/improve a method of assessing hot cracking susceptibility of materials.

1.3.1 Pipelines

Pipelines are a critical component of infrastructure in the energy and energy transport sectors. Due to its size and importance, the oil industry continues to be a significant driver in the development of pipeline technology. Figure 1.4 illustrates some of the most significant changes that occurred during the 20th Century [44].

Categories	Before	After
Materials Innovations	Brittle Low Toughness iron	Ductile High Toughness steel
Design changes	Lap Welds	Submerged arc welds or seamless pipe
	Threated Joints	Welded joints
	Small Diameter Pipe	Large Diameter pipe
	Solely onshore construction	Offshore and deep-water construction
Demand Changes	Low pressure operation	High pressure operation
	Oil Pipelines	Oil gas and product pipelines
Regulatory Changes	No standards	Benchmark standards
	No regulations	Safety regulations

Figure 1.4: Materials innovations, design, demand and regulatory changes for pipelines that occurred during the 20th Century.

In general, pipelines that are used today can be divided into two categories: onshore and offshore (Figure 1.5).

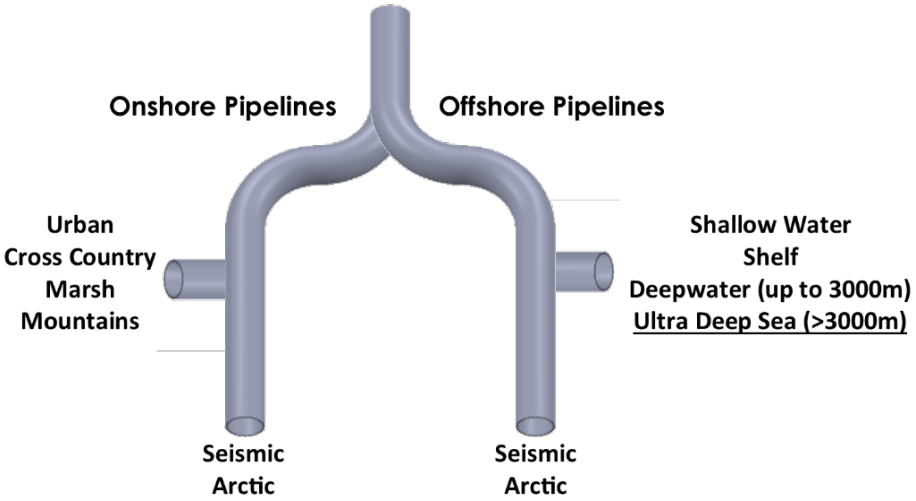

Figure 1.5: Pipeline types summary.

Generally, production of the pipes can be outlined as follows. A plate or strip of steel is formed at the desired shape (hollow pipe) followed by a welding process. After that the pipe is heat treated, the weld is inspected and the pipe undergoes a process of sizing in order to obtain a specific size and then it undergoes a process of finishing [45]. Figure 1.6 shows an outline of this process.

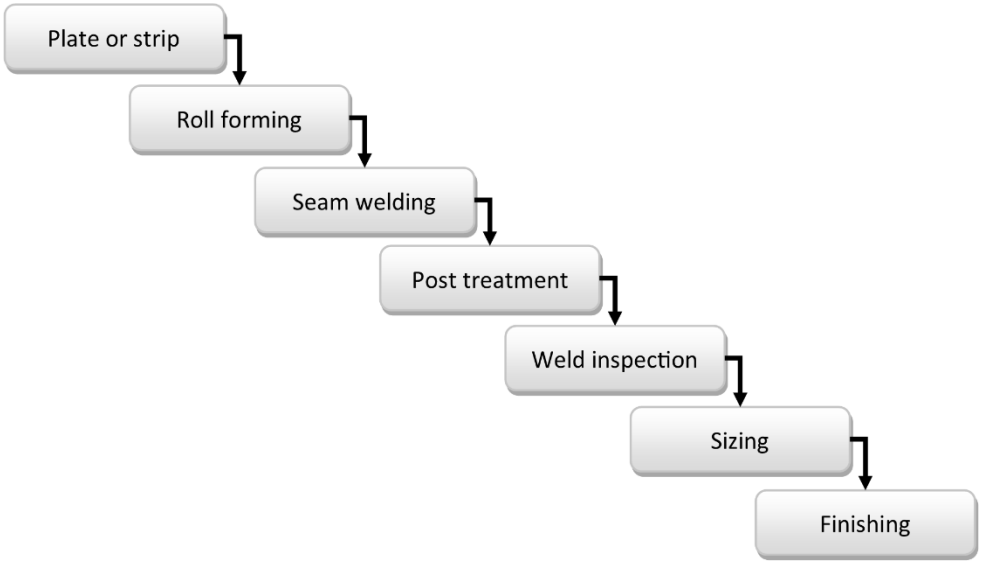

Figure 1.6: General outline for the production of pipes.

The demands for oil and gas are constantly increasing [46, 47] and the demands on pipeline materials are constantly increasing since oil and gas reserves are increasingly found in demanding environments (low temperatures, high pressure) which could not previously be accessed. This will not only require improvements in materials but also a focus on the maintenance of older pipelines that need to continue providing service [44]. The operation of pipelines at deep sea (up to 3000 m depth) and ultra-deep sea (more than 3000 m depth) is an example of a demanding environment. This is one of the main drivers for this research. The materials used for these applications must be tested thoroughly and reliably because of the challenges that these types of applications exhibit.

1.3.2 Demanding environments

One challenging topic in materials' applications is the use of materials in demanding environments. These are environments in which materials may be required to sustain

extremes of:

- High/low temperatures
- High/low pressure
- Corrosion/erosion
- Excess load bearing
- High impact
- High/extended lifetimes

Pipelines that are intended for use in deep sea applications and even in ultra-deep sea applications are made of steel that faces severe stresses both during its installation and its service. Pipes that are used for deep sea applications have to not only pressures that are higher than 30 MPa at depths of 3000 m or more and temperatures of 3°C. During the installation of the pipes stresses higher than 400 MPa can be applied depending on the way they are installed their length, their thickness and the depth of the installation [38]. Furthermore, the pipes must survive in this environment which is also corrosive for periods of more than 20 years. Additionally, except the harsh environment of the installations, the hydrocarbons transferred through the pipe contain H_2S and CO_2 which are characterised as sour hydrocarbons that affect the properties of the steel [39]. For these reasons the materials used for these applications are tested in all aspects of performance, like; strength, toughness, weldability, fatigue etc. Given the importance of the application that these pipes are used for, a lot of research has been done in order to assess aspects of the application like the welding process of the pipes, the stresses that they can withstand, the hot and cold cracking of the welds, corrosion and many more.

1.4 Welding

Welding is a process that is utilised in order to join two, usually metallic, parts. The goal is to make these two separate parts one solid part [48]. The process of joining

can differ significantly depending on the situation and the materials required to be joined together. Some of the main parameters that are taken under consideration are the following:

- How critical is the application
- Are the materials similar or dissimilar
- How the resulting microstructure will affect the performance of the material
- The thickness of the material to be welded
- The position of the weld

There are numerous welding processes. The three major groups are gas welding, arc welding and high energy beam welding. Each group includes multiple types of fusion welding processes with its own advantages and disadvantages. For example, as described in Figure 1.7 high energy beam welding inflicts less damage to the workpiece than gas welding but has a high cost [49]. This section provides a brief description of welding techniques followed by the most common defects that occur in welds.

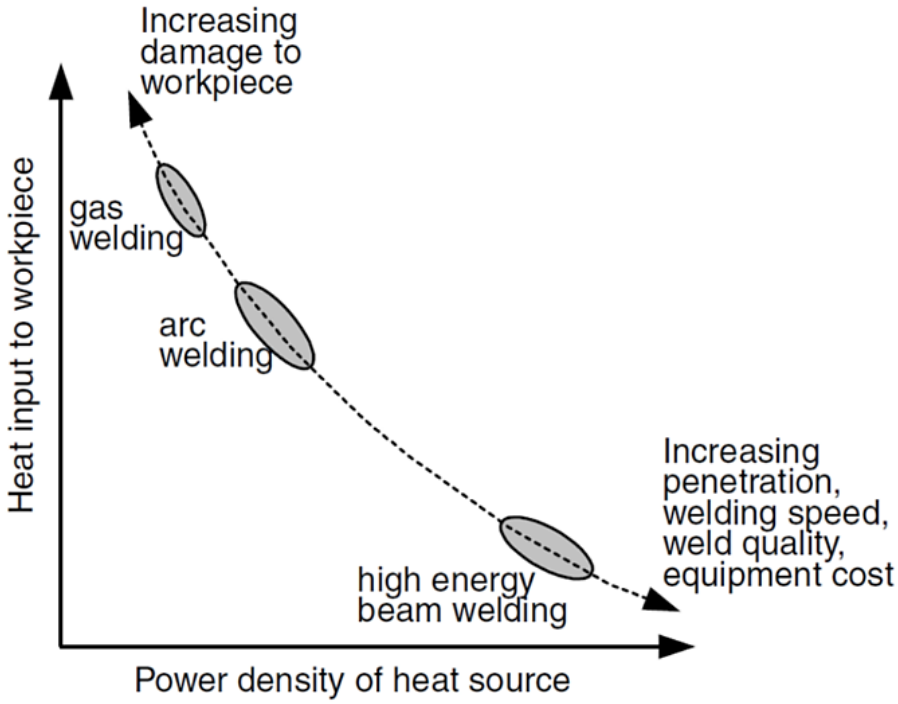

Figure 1.7: Variation of heat input to the workpiece with power density of the heat source [49].

In most cases, welding processes heat the base materials in order to join them. The high heat input has significant effects on the microstructure of the materials, which can be detrimental to the mechanical properties of the joint [50]. The differential cooling, experienced by the material in regions away from the welding point, divide the joint section into different zones (Figure 1.8):

- the fusion zone (FZ)
- the heat affected zone (HAZ) and
- the thermally unaffected zone usually referred to as base metal (BM)

The HAZ can be further sub-categorised as: the coarse grained heat affected zone (CG-HAZ) which is the part closest to the FZ; the recrystallized zone; the partially transformed zone; and the tempered zone. In the boundary of the FZ and CG-HAZ there are areas that during the welding process are partially melted and re-solidified during the welding process. These areas are sometimes referred to as mushy zones [51, 52].

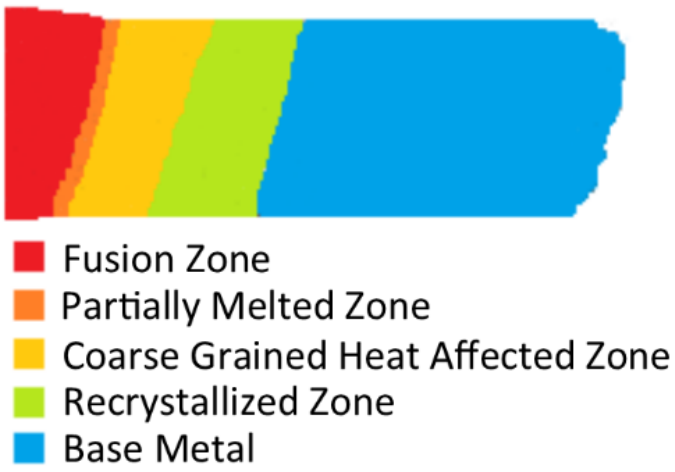

Figure 1.8: Cross section of a weld and the zones that are created during a welding process. Left side is the centreline of the weld were the material is liquid and where fusion is occurring. Due to the different temperatures that the material is subjected different zones are created as the distance from the fusion zone increases.

1.4.1 Welding techniques and defects

Welding is used for multiple applications. Each application requires different properties and used different materials. The choice of welding technique is usually driven by the application requirements. Some of the most common welding techniques will be presented in this section. Shielded metal arc welding (SMAW), which is usually referred to as manual metal arc welding, is a process that uses a metallic consumable electrode covered in flux in order to deposit the weld. Electric current, direct or alternating, is used in order to generate an arc and form a weld pool by melting the electrode [53].

Gas metal arc welding (GMAW) is similar to SMAW but instead uses a shielding gas to protect the weld during the welding process [48]. This technique has been used in the manufacturing of pipelines due to its high production rate and automation capabilities [54]. Defects that have been observed and studied, that are connected with this welding technique are pinholes and tunnel porosity [55].

Submerged arc welding (SAW) is a process where the consumable electrode is covered with a powder like flux that protects the weld and the arc generated is not visible because it is 'submerged' under the flux [56]. This technique is also widely used for the manufacturing of pipelines. Due to the larger sized weld pools compared to other techniques and the high welding speeds that are achieved by SAW hot cracking is usually a defect that must be taken under consideration [56, 57].

Gas tungsten arc welding (GTAW) is a process that is similar to GMAW. It uses a non-consumable tungsten electrode and inert gas to protect the weld [58].

Some other, less common, welding processes include laser beam welding (LBW), resistance welding (RW), friction welding (FW).

Fusion welding defects are significant because of their detrimental effects on the final product. These defects manifest as cracks. The way these cracks are generated or appear allows for them to be separated into four categories:

- Hot cracks or solidification cracks,

  - are cracks that manifest in the fusion zone during the solidification of the weld.

- HAZ micro fissures
  - initiate in the partially melted HAZ section of the HAZ.
- Cold cracks, or hydrogen induced cracking
  - are the result of the contamination of the weld microstructure by hydrogen. Cold cracks can occur months after the welding process has taken place.
- Lamellar tearing
  - is cracking that occurs beneath welds. Rolled steel is quite susceptible to this, especially when the welding bead is parallel to its rolling direction. These cracks can reach the surface of the material but they usually remain under the weld and can be detected by performing ultrasonic testing [52].

Since this study is focused on improving the testing procedures and understanding of hot cracking and hot cracking susceptibility of materials, further analysis of hot cracking phenomena is presented in the literature review section.

1.4.2 Welding HSLA steel for oil and gas pipeline applications

Welding is an integral process in the production of pipes for oil and gas applications. In this section the manufacturing process of pipes made of HSLA steel will be briefly described, focusing on the welding process.

The manufacturing process of the pipes consists of many steps and every step affects the material properties. A simplified illustration of the manufacturing process that is used for some pipes is shown in Figure 1.9.

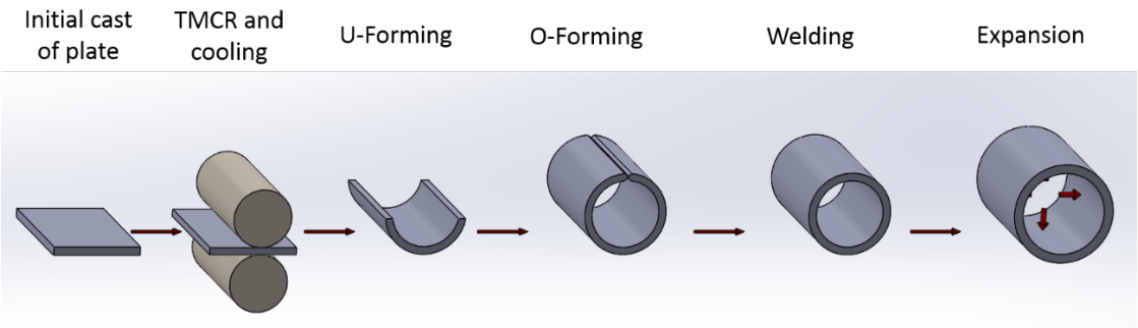

Figure 1.9: Outline of manufacturing process for HSLA pipes.

The production of the steel pipes using X65 steel follows the following process. The metal plates go through a thermo-mechanically controlled rolling process (TMCR) with accelerated cooling. After the process the plates go through a forming process that consists of three steps. The process of forming is usually referred to as UOE forming because of the steps that are used in the process. The steps of this process are the following:

- U-forming, where the plate is bent initially so that it forms a U shape.
- O-forming, where the U shaped plate takes the form of a pipe and the welding process is taking place.
- Expansion, where the welded pipe is expanded to meet the final sizing requirements.

Because the forming process is an integral part in the production of pipes research on the UOE process of the pipes has also been carried out. One of the aspects examined was the collapse pressure of the pipes and the way the UOE process affects these properties. Research showed that if the strain of the pipe during the expansion stage is decreased and the strain during the O forming is increased the collapse pressure of the pipe will be improved [59].

As it can be seen the manufacturing process of pipes from HSLA steel is a complex process that includes many steps.

Between the O-Forming step and expansion the pipe is welded on both its inner and outer diameter. using Submerged Arc Welding (SAW) [60]. Figure 1.10 provides

a basic outline of the SAW process. The process takes place as follows. The pipe is joined along the seam with an arc that is generated between a consumable wire electrode and the HSLA steel. The flux that is supplied from the flux hopper is also partly melted and in combination with the unmolten flux the arc is protected during the process. This way there is no reason to use shielding gas because the flux separates the weld from the environment. The flux also inhibits spatter and heat losses which allows for higher welding currents and deposition rates. Additionally, this process allows for multiple electrodes to be used thus increasing the deposition rates and for thicker welds to be achieved [49].

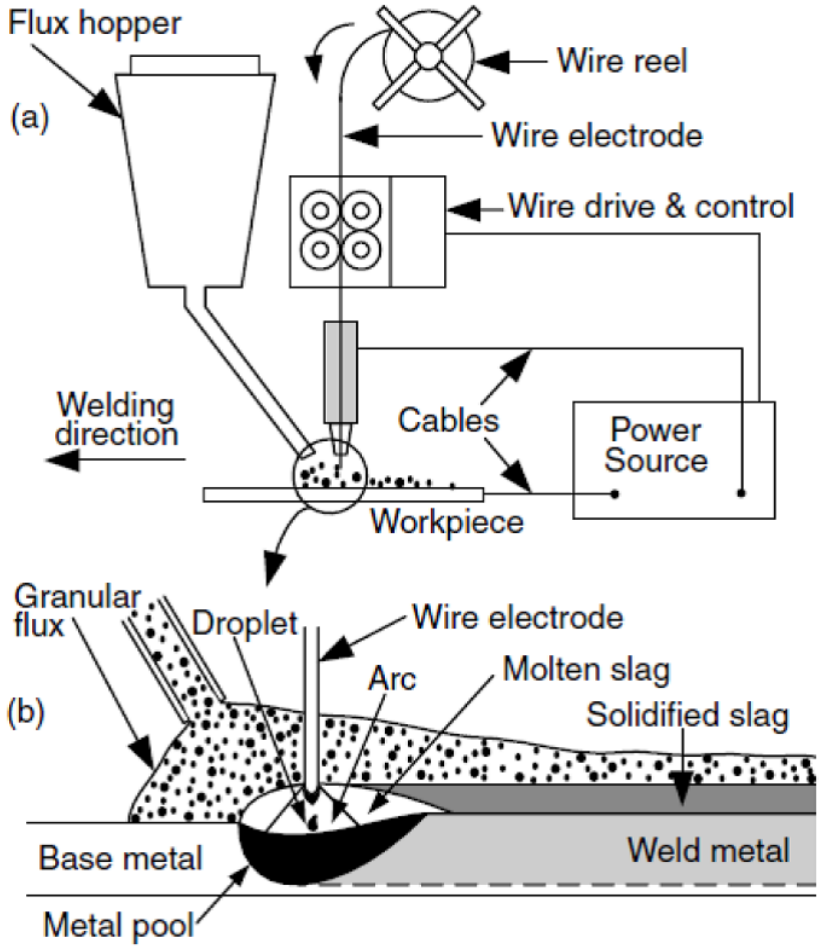

Figure 1.10: Schematic illustration of the submerged arc welding process showing, a) overview of system components, b) detailed view of the welding process and interaction with the base metal [39].

Welding is a very important part of the manufacturing process of pipes since it is not only used during the production of the pipes but also during the installation

of offshore pipelines. The scientific approach to welding is a complex and diverse endeavour. This is because there are many parameters that affect the end result of a welding process. For example, one set of parameters is the welding process itself (MIG, TIG, SAW, LASER, etc.) which results in different quality of welds and mechanical properties due to the effect they have on the material microstructure. Also each welding process is susceptible to different defects that are possible to occur.

The effect of heat input that is used during SAW welding duplex steel UNS S31803 was studied and it demonstrated how critical the heat input is for the quality of the weld joints [57]. Different types of welding have also been compared as far as their fracture mechanisms are concerned. SAW and Flux Core Arc Welding (FCAW) were applied to various materials and then crack tip opening displacement (CTOD) fracture toughness tests were carried out in order to compare the results of the welding methods. The results of the research showed differences in microstructure of the materials according to the welding process but they have also shown how critical the control of the welding parameters is, since they indicated different fracture mechanisms even if the microstructures were similar [61].

HSLA steels have been tested using SAW in order to examine their microstructures and compare them when they are subjected to different thermal cycles during welding. One of the conclusions from the tests on X80 steel was that there is a probability that micro crack nucleation may occur from M/A particles at the intersection of prior-austenite grain boundaries [62]. This finding was also supported by later research on X65 steel where the role of Ti (C, N) was examined [18].

The underwater welding of HSLA steels was also examined in order to examine the possible defects, the microstructure and mechanical properties of the steel when it is welded under these conditions. The results showed that with increasing water depth, the oxygen content increases as the alloying element decreases. The significant drop of manganese and silicon contents happens from 11 to 25 m. Additionally the mechanical properties of the welds drop when the depth is increased due to

increased porosity and the oxidation of alloying elements [63]. Research on HSLA steel has been very intensive and many aspects spanning from the microstructure and alloying elements of these steels to the mechanical properties and applications have been examined.

Another aspect of welding that needs to be discussed is the carbon content of the steel that needs welding. The carbon content of steel must be low in order for the steel to be weldable. Usually below 0.35% carbon is required. The issue that arises is that HSLA steel and generally steels that are being welded for advanced applications are alloyed. Alloying elements affect the weldability of steels directly. For that reason a mathematical expression that converts the effect of alloying elements to a carbon percentage is usually used in order to estimate weldability. This is called Carbon Equivalent (CE), and the equation for HSLA steels that have a carbon percentage below 0.12% is the following.

$$CE = C + \frac{Si}{30} + \frac{Mn}{20} + \frac{Cu}{20} + \frac{Ni}{60} + \frac{Cr}{20} + \frac{Mo}{15} + \frac{V}{10} + 5B \text{ [64]} \quad (1)$$

When the carbon is above 0.12% the CE formula changes to the following.

$$CE = C + \frac{Mn}{6} + \frac{(Cr + Mo + V)}{5} + \frac{(Ni + Cu)}{15} \text{ [37]} \quad (2)$$

Research on welding processes and its effects in materials has been taking place for many years. Many aspects of welding have been examined on various materials and processes. In 1941 Rosenthal presented a mathematical approach to calculating the heat distribution during welding [65]. In order to develop this model that applies on flat plates some assumptions were made in order to simplify the problem at hand. The assumptions, were that the heat flow was in a steady-state, the heat source is a point in space, the thermal properties are constant, the heat of fusion is negligible, there are no heat losses from the workpiece surface and there is no convection in the weld pool. Using these assumptions the calculation of the temperature gradients and isothermal curves was made possible. Another tool that has been provided is that these calculations could be expanded from a two dimensional space to a three dimensional space and include the movement of the heat source (Figure 1.11).

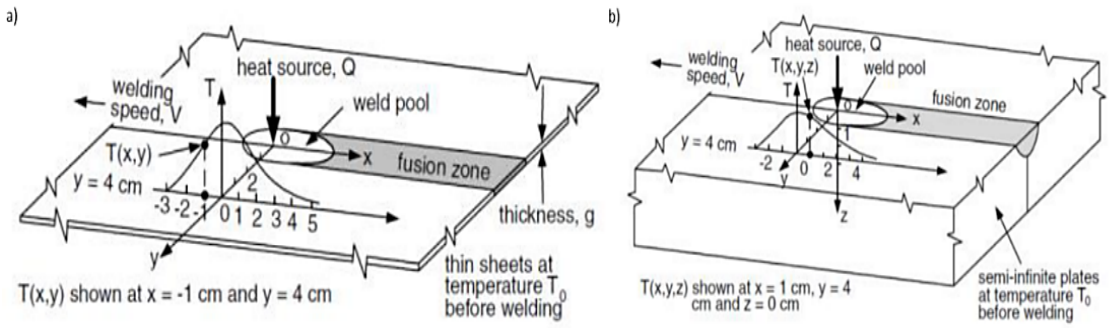

Figure 1.11: Heat flow during welding a) two dimensional (thin plates) b) three dimensional (thick plates) [51]

Research on the cooling rate in the welding of plates has used the Rosenthal's equation to predict the size of HAZ. The results showed that the accuracy of the analytical solution of Rosenthal's equation on thin and thick plates is high and reflects experimental results [66]. Conducting the calculations of the analytical solution of this equation is a simple process and so the Rosenthal equation is deemed a useful tool for calculating the cooling rate of a weld when applied on a plate. It has been mentioned though that since this equation applies only to flat plates,its use for more complex geometries is limited.

1.4.3 Brief history of hot cracking tests

Hot cracking is a defect that is detrimental to the welding processes. For this reason multiple ways have been developed and proposed towards assessing the hot cracking susceptibility. In the early 60's Prokhorov et al. [67, 68] and Matsuda et al. [69–73] defined the term Brittle Temperature Range (BTR) and introduced the working principle of Varestraint and Transverse Varestraint (Trans-Varestraint) tests in order to quantify and assess hot cracking susceptibility. Other methods for assessing hot cracking susceptibility include the cast-pin tear test [74, 75], ductility-dip cracking [76] and Gleeble tests [77–79]. All these methods for assessing the hot cracking susceptibility of materials, have managed to improve the assessment and quantification of hot cracking susceptibility. However, there is a need for further improvements and standardization, in order to achieve the repeatability and reliability required to state that there is a definite measure of hot

cracking assessment [80].

1.5 Research objectives

The objectives of this study can be separated into two main categories:

- Experimental characterization of API-5L X65 steel
- Assessing the hot cracking susceptibility of API-5L X65 steel.

Initially, research that has been carried out for characterizing the steel will be reviewed. Following that, a series of experimental procedures will be decided in order to add more information to the literature concerning the steel. Since experimental procedures are constantly improving and in recent years there is new research focused on hot cracking [18, 81], a review of the current methods of assessing the hot cracking susceptibility of materials will be carried out. Subsequently, an evaluation will be carried out and suggested improvements will be presented. By pursuing these objectives the study aims to contribute new information on the steel at hand on both its characterization and its hot cracking susceptibility. Additionally, since hot cracking is a defect that occurs in many materials, the examination of hot cracking susceptibility experimental procedures could be potentially used to provide solutions that will contribute to the assessment of hot cracking susceptibility of materials in general.

1.6 Scope of the thesis

In order to address the objectives that have been defined, this study adopts an experimental approach. This is because the ultimate aim of the study is to develop or improve experimental procedures that could be potentially be used as a basis for standardizing industrial tests. A specific experimental procedure was chosen and improvements in the design and the method are proposed. The theoretical

background is provided, and in cases that demand it, it is probed further. This study was driven and guided from the industrial use of steel for offshore pipelines. For that reason the main material for this study is an advanced steel for subsea pipeline applications. Details for this material will be provided in the chapters following the introduction.

1.7 Structure of the thesis

The succeeding chapters will address the objectives that have been presented. Briefly the structure can be described as follows. A theoretical background will be provided and the current state of the research on the subject at hand will be identified. Following that, the experimental processes that will be carried out will be described and analysed before proceeding to the demonstration of the results. The results will be analysed and discussed in order to reach to the conclusions of the study and evaluate its contributions to the field. The following list provides an outline of the contents of the main chapters.

- Chapter 1
  - Brief introduction to the subject and an outline of what will be studied
- Chapter 2
  - Literature review of the subject guided by the objectives of the research
- Chapter 3
  - Detailed description of the experimental methods and materials that will be used
- Chapter 4
  - Presentation of upgrades that were carried out in experimental equipment
- Chapter 5
  - Presentation of results of the experimental procedures

- Chapter 6
  - Analysis and discussion of the results presented in Chapter 5
- Chapter 7
  - Evaluation of the study and the importance of its findings.

1.8 Summary

The construction of pipelines for the transfer of oil and gas has become an integral part of the energy and energy transfer sectors. Steel is an important material for the manufacturing of pipelines. The process of manufacturing steel pipes has been improving and evolving constantly. The production process is a multistage process with a lot of critical stages. Welding is an important part of this process.

The issue is that occasionally, during welding, defects that are categorized as hot-cracks manifest. These defects are detrimental to the material and if they occur they will lead to significant problems such as production halt, increased cost etc. This means that materials that are to be used for these applications need to be meticulously tested in order to ensure that the production process will be set in a way that parameters and stresses that cause defects like these would not occur. For that reason there is a demand for assessing the material's susceptibility for hot cracking.

Tests have been developed and used in order to address this issue but no standards and regulations have been set for the testing procedures. For this reason a lot of research has been carried out around this subject. This thesis will focus mainly on the hot cracking defects that can occur during welding.

The study will focus on high strength low alloyed (HSLA) steels because they are materials that are used in the oil and gas industry where welding is a significant part of the industry. The structure of this thesis consists of a literature review in order to set the context of the work that will be presented, followed by all the experimental work that was carried out in order to achieve the objectives that have been set in

this chapter. At the end the results will be discussed and the conclusions will be drawn.

Chapter 2

Literature Review

This section provides the theoretical background that is required for this study. The terminology for hot cracking is presented along with literature on the subject. Following this experimental procedures for assessing the hot cracking susceptibility of materials are presented leading to a detailed analysis of the Varestraint and Trans-Varestraint tests that are the focus of this study.

2.1 Production and mechanical properties of HSLA steels

The welding process for the pipes occurs after the O-forming of the plate as described in Section 1.3.1. The plate is initially tack welded and after that the inner diameter of the pipe is welded using multiple feed lines of filler material. Following the inner welding process a similar process is followed for the outer weld. This means that since multiple filler wires are used and they are not necessarily accurately centred during the process the heat input on one side of the joint can be different than the other [82, 83]. Research on the expansion process that takes place during the production of pipelines has shown that the process of the expansion increases the tensile strength along the hoop direction [84]. During this process a tool called 'expander' is used (Figure 2.1). There have been cases that expander segments have

failed due to improper EDM processing during their manufacture [85]. Another parameter that has been studied is the minor deformations that are caused from residual stresses. Research that measured the residual stresses in pipes that have been manufactured using the UOE method has shown that the residual stresses are not evenly distributed through the material [86].

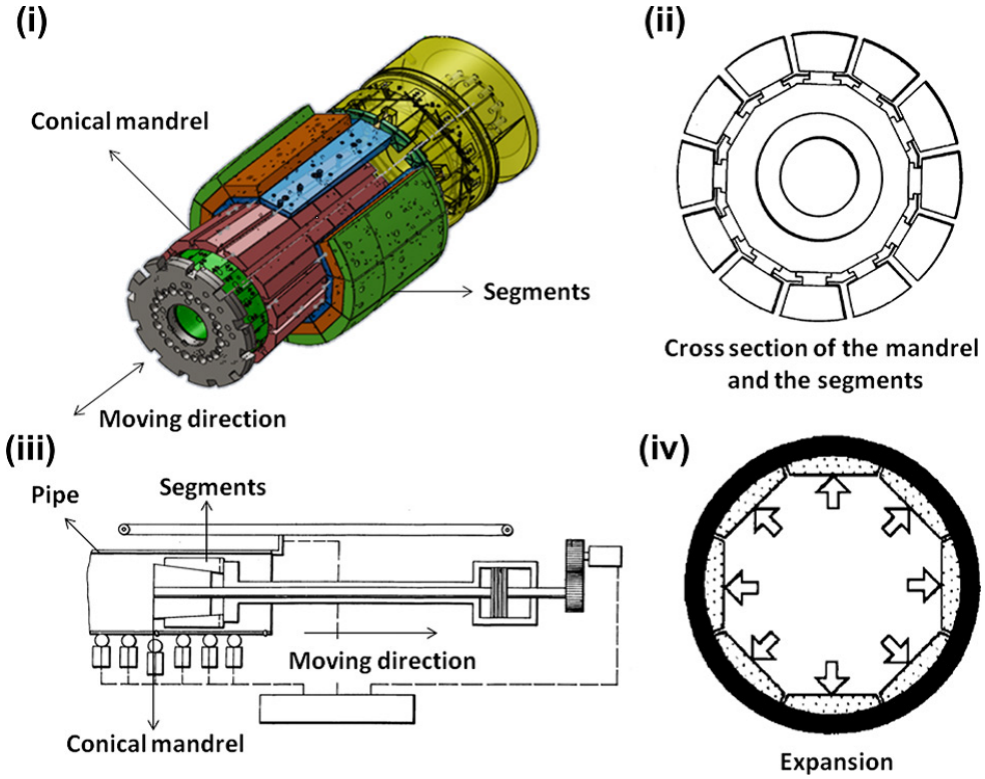

Figure 2.1: A 3D model of the conical mandrel (i), the cross section of the segments and the conical mandrel (ii), the side view of the expander machine (iii), and the cross sectional view of the segments during expansion (iv) [85].

In research on fracture toughness of HSLA steels the fracture toughness of the FZ and HAZ has been compared. Specifically, HSLA X80 steel has exhibited it lowest fracture toughness at its interface between the FZ and HAZ [87] compared to the fracture toughness of the rest of the weld joint. However these tests do not identify clearly the amount of FZ and HAZ that is present in the CTOD samples. Nevertheless obtaining values exactly on the interface between the FZ and HAZ of a weld joint is rare.

2.2 Solidification of steel

Plain carbon steel is usually manufactured by being cast using machines that enable continuous casting. The steel is worked at a high temperature and slow cooled to room temperature [88]. Steel is formed into slabs, blooms, or billets in a continuous casting machine. The solidified product is pulled by rollers before being straightened and cut at the end of the machine. This process can continue for days or weeks without interruption. However during the solidification of the material during its production, due to the intense heat gradients and internal stresses and strains, defects that are called hot tears or hot cracks can manifest. These are problems that create important issues during production. The hot cracking defects and their mechanisms will be discussed in the sections below.

After going through this process the resulting microstructure is the one described by the Fe-C phase diagram (Figure 2.2). During the casting process the material undergoes some specific transformations. Steel is predominately iron with a small addition of carbon. Iron is an allotropic material that changes phases as its temperature drops. Allotropy is a word which is originated from a two part Greek word. Allotropia (Αλλοτροπία), ἄλλος (állos, "other"), and τρόπος (trópos, "way, manner"). It is a property that some materials have which allows them to obtain different crystal structures at different temperatures.

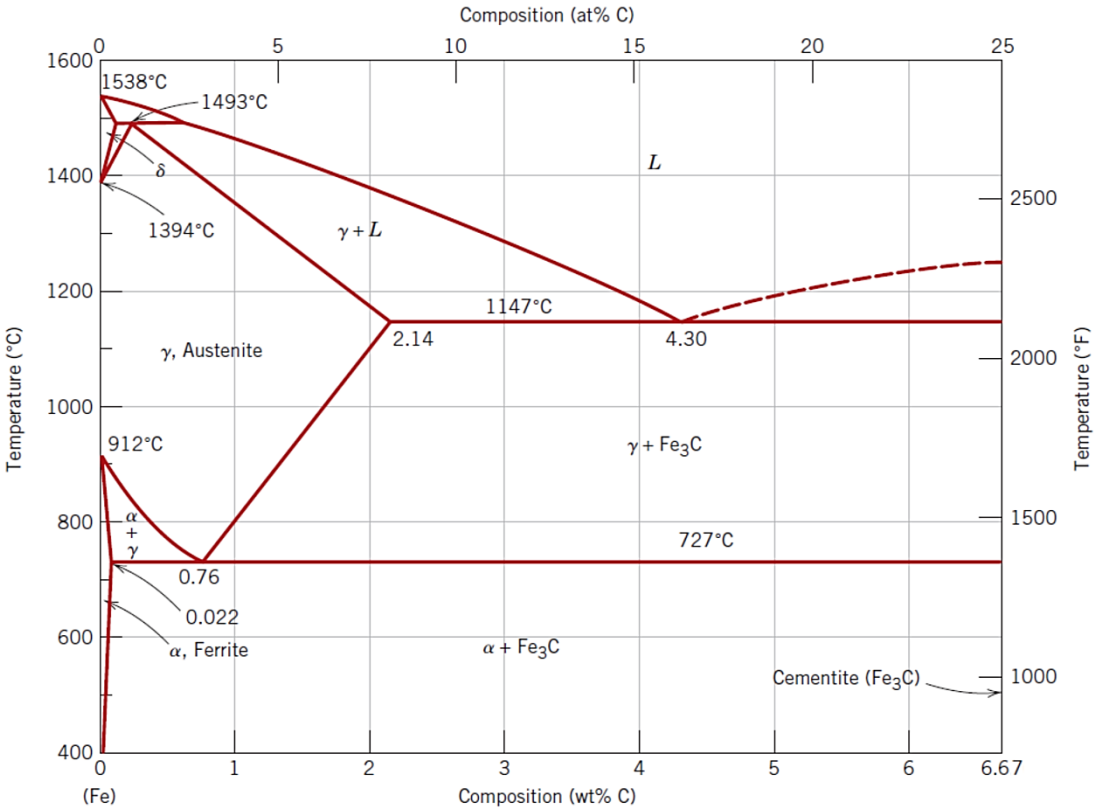

Figure 2.2: Fe-C metastable phase diagram [89]

After iron is solidified its crystal structure changes from body centred cubic (b.c.c.) to face centred cubic (f.c.c.) and back to b.c.c. at room temperature. Iron at room temperature is called ferrite or iron-α and has a b.c.c. structure (Figure 2.3). As the temperature elevates to 912°C the structure changes to f.c.c. and it is called austenite or iron-γ. This crystal structure changes again at 1394°C to b.c.c. which is called iron-δ or δ ferrite [89]. These different phases to be generated which have different properties can be exploited during manufacturing.

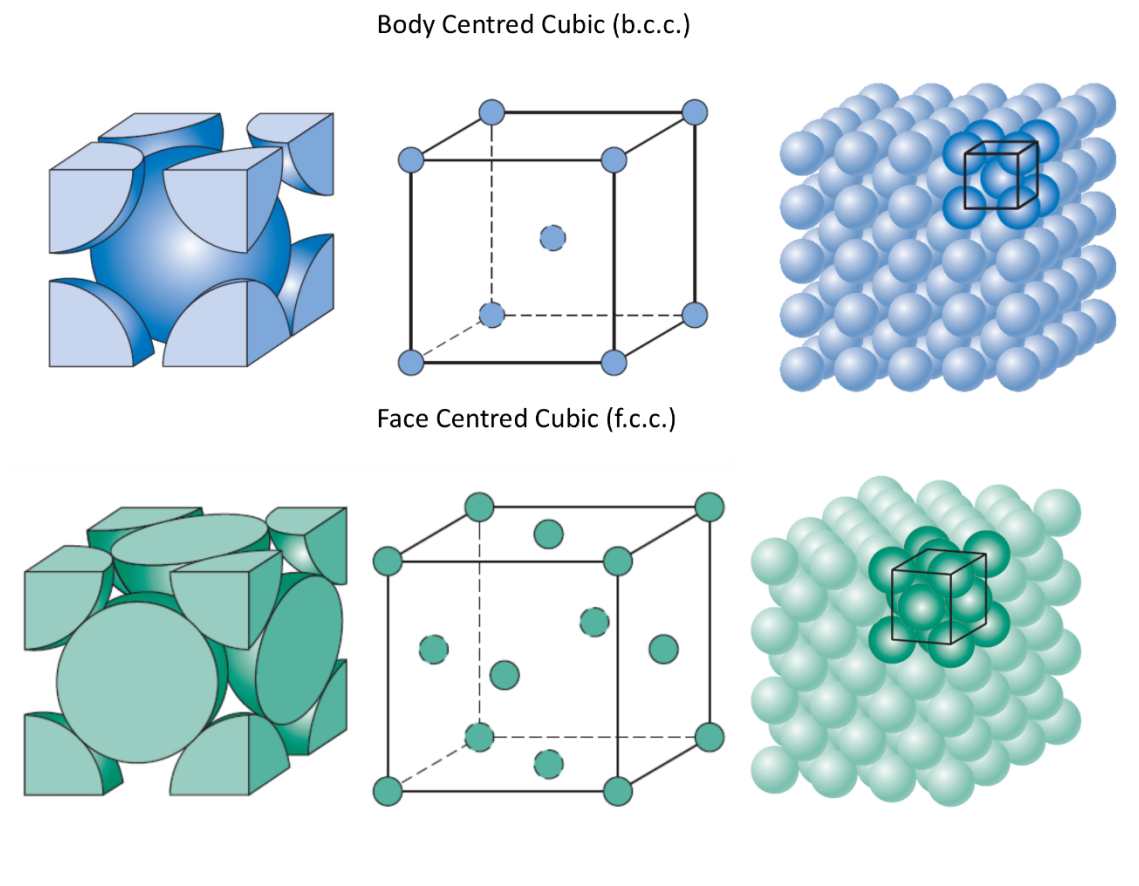

Figure 2.3: Crystal structure of iron-δ, iron-α (b.c.c.) and iron-γ (f.c.c.) [89].

Solidification of steel is an important aspect of its processing. Given that welding is integral part of the manufacturing of pipes, the way that the material behaves during solidification is critical. During welding the material is liquefied and as it cools the solidification process initiates. Generally, the solidification process takes place as follows. As the liquid material releases heat to its environment its temperature drops to a point when initially small nuclei form at various positions. These nuclei start to grow as surrounding atoms assume positions that allow for the growth of the crystal structure. As these formations grow, they form crystal structures at random orientations that inevitably collide with adjacent crystal structures and form grains [89].

Solidification in general is affected by the temperature gradients that are forming during the process and the direction of heat flow [90]. During welding the heat flow is not the same as it would be during the free solidification of materials because of the movement of the heat source and the existence of solid material at the edge

of the weld pool. This acts as nucleation area for the solidification of the material and allows for the material to solidify in specific direction forming columnar grains that are orientated towards the heat source [91]. Adding to that the grains that grow during this process are competing for their growth in a similar way that grains compete during the directional solidification [92, 93].

Because of the heat exchange and the difference in temperature during the solidification, material properties like density and heat capacity are changing. These changes in combination with the changes in the composition of the molten liquid on the solidification front have been shown to create strains and stresses in the solidifying materials [93, 94]. It is during these processes, both during welding and casting, that defects like hot cracking manifest.

2.3 Hot Cracking

Hot cracking is a complex phenomenon that occurs during welding. As a result of this, some terms have been used interchangeably in the literature for many years [39, 95]. Terms like hot crack, hot tear and solidification cracking have been used in many cases to describe either different types of defects of similar defects with different names [96–104]. Therefore, in order to better understand the mechanisms and the theory of the phenomenon a series of definitions, which are used in this study, are specified.

For hot cracking the initial definition of the phenomenon can be made macroscopically. Hot cracking is the phenomenon that includes cracking defects that occur during welding. Because there is more than one cracking defect that can occur during welding a multi-level definition is introduced herein. This still focuses on the macroscopic features of the phenomenon. This is the position where these cracks manifest. The position can be at the fusion zone or in the partially melted zone (PMZ) of the HAZ. This separates the hot cracks between solidification cracks (cracks in FZ) and liquation cracks (cracks in PM-HAZ). Figure 2.4 describes these definitions which will be useful as the exploration of hot

cracking continues.

LEVEL 1 **TYPE OF CRACKING DEFECT**	HOT-CRACKING		WARM CRACKING	COLD CRACKING
LEVEL 2 **STAGE OF WELDING THAT IT MANIFESTS**	DURING WELDING WHILE MOLTEN MATERIAL IS PRESENT		AT ELEVATED TEMPERATURE DURING POST WELD HEAT TREATMENT	AT LOW TEMPERATURES HOURS OR EVEN DAYS AFTER WELDING
LEVEL 3 **POSITION THAT IT MANIFESTS**	SOLIDIFICATION FRONT/ WELDING BEAD	PARTIALLY MELTED ZONE (PMZ) OF HAZ	WELDING BEAD	BASE METAL / HAZ
LEVEL 4 **SUBSET OF DEFECT**	SOLIDIFICATION CRACKING	LIQUATION CRACKING		

Figure 2.4: Levels of hot-cracking definition (macroscopically).

By using the same method of defining cracking defects that occur during welding processes, it is possible to clearly define other defects like warm cracking and cold cracking. Nevertheless analysing these defects is not in the scope of this study. However, as the definitions are currently set, it is established that when the term solidification cracking is mentioned it means the cracks that occur in the FZ of the material during welding (Figure 2.5). This lies as a subset under the greater category of hot cracking. The current thesis focuses on the solidification cracks of materials. Before presenting and analysing the mechanisms of hot cracking, the information presented in Figure 2.4 will be expanded to further levels under the solidification cracks. The reason is that as the hot cracking phenomenon can be divided into sub-categories on the macroscopic level, the solidification cracking can be analysed further and separated into different categories at a microscopic level.

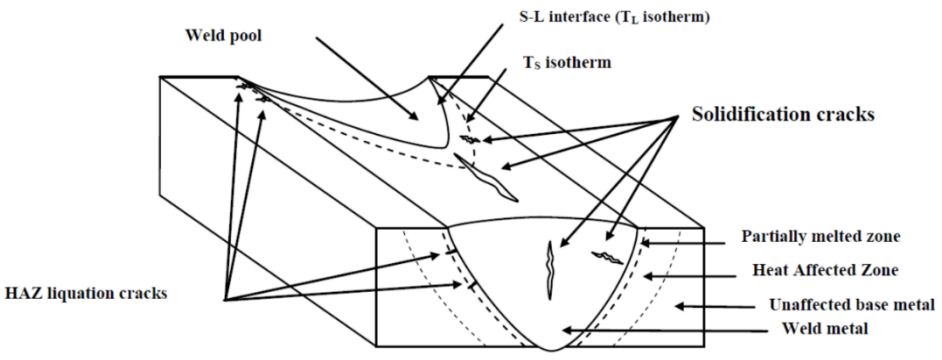

Figure 2.5: Positions in the FZ where solidification cracking can occur [105].

Existing solidification cracking theories can be initially summarized in the following statement. As a welding process takes place the solidification front trails the heat source. As the material solidifies, the difference in heat gradients and percentage volume of liquid on the solidification front introduces both thermal and mechanical strains that result in the generation of cracks in the FZ [106–108].

Since the solidification front is an integral part in the phenomenon a more attentive approach is required. Casting has provided a useful approach in the categorization of solidification cracks by connecting them to the amount of liquid that is present during solidification [103]. This approach could be incorporated in the hot cracking theory and classification and allows for improved definitions on hot cracking.

Figure 2.6 illustrates how the mechanical properties of a material depend on the amount of liquid existing during the solidification. When the presence of liquid is above 10% the cracks that form exhibit an inter-dendritic fracture morphology and they are called hot tears. On the other hand when the liquid present is below 10% then the cracks exhibit an inter-granular fracture morphology and they are called hot cracks.

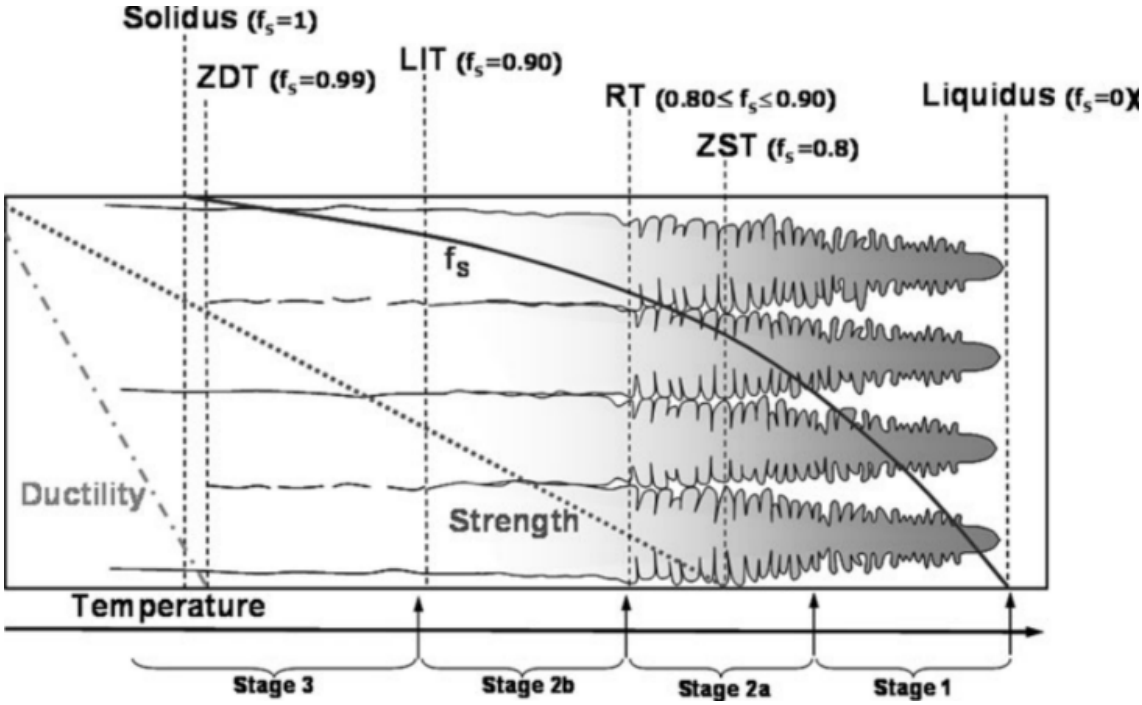

Figure 2.6: Schematic illustration of the structure and mechanical properties at various stages of the solidification [103].

By taking under consideration this information then the levels of hot cracking definition that were presented in Figure 2.4 can be further enhanced and separated between macroscopic and microscopic levels.

Figure 2.7 illustrates this analysis. If the definition of hot cracking is analysed in depth it can potentially be divided into seven different levels. This map allows for a more strict definition of the hot cracking defects.

Figure 2.7: Levels defining hot-cracking.

The focus of this thesis is hot cracking defects that fall under the subcategory of solidification cracking so the analysis of other defects will not be carried out. Nevertheless breaking down cracking defects that occur in welds into these levels could potentially help for better definitions of all defects.

2.3.1 Tests for assessing hot cracking susceptibility of materials

Multiple experimental procedures have been developed and tested in order to assess the hot cracking susceptibility of materials. The Gleeble test has been designed

aiming to measure multiple parameters that are useful in the hot cracking assessment of materials. The test comprises of a tensile testing of a number of cylindrical samples at the temperatures below solidus and determining their hot strength and ductility [78]. Gleeble can also be used to simulate thermal cycles during welding.

Using these capabilities materials like X80 steel have been tested using different thermal cycles to observe how they affect the structure of welds of the steel [109]. This test has been used on 316 stainless steels in order to predict its hot cracking susceptibility in the HAZ [110] based on the fact that a correlation between hot ductility and hot cracking at the HAZ has been observed [111].

Generally the Gleeble is a thermomechanical simulator that unfortunately cannot accurately simulate welding procedures. This is because most of the tests do not or cannot adequately simulate the development of residual stresses in a weldment as it cools after the weld process is over. Moreover, those tests that impose stresses on cooling from the peak temperature to simulate weld residual stress do not accommodate for the changes that can occur in a post weld heat treatment (PWHT) procedure [80]. Nevertheless tests have been carried out using Gleeble setups in order to simulate PWHT procedures in Ni-base super alloys [77].

Another test that has been developed and used for the purpose of assessing hot cracking susceptibility is ductility-dip cracking (DDC) where, samples are manufactured by repeated welding processes with a filler wire made from the material to be examined [112]. A significant amount of research has been carried out on this test in order to improve it. This research has initially pointed out that these tests provide with increased thermal control for the tests and the specimens are easier to make, compared to other methods. Furthermore, tests on Ni-based alloys indicated that the addition of Nb and Ti in small quantities improve the DDC resistance of the alloys but excessive additions cause hot cracking in the weld metal [76, 113, 114]. Other findings indicated, for the alloys and temperatures tests that were used, that grain size does not affect the DDC [115]. Direct chill casting (DCC) AISI 316L weld metals indicated severe localized and thermal plastic deformation which allowed the grain boundaries to slide in the ductility-dip temperature range under strong restraint conditions. This led to the formation of

micro-voids [116].

Another test is the cast pin tear test (CPTT). This test was developed and used between the 60's and 70's [117, 118]. The test was carried out by levitation melting and casting of small charges of material in copper moulds to produce conical cast pins with varying geometry. The mass was constant and small (only 19 g) and the sensitivity of the test was controlled by the pin length and geometry. After the pins were cast they were examined for circumferential cracks and the total crack length was plotted versus the mould length [119]. The test had an important positive aspect. It required a small amount of material in order for the test to be carried out and extract results that could be useful for the development of novel materials. Nevertheless the test initially had issues with the mould filling and control so improved versions of CPTT were introduced [75, 120, 121].

All these testing procedures have contributed in the field of hot cracking and its study. The fact that research in welding, casting and as a result hot cracking has been ongoing for more than seventy years indicates how important it is for engineering applications to do whatever is possible to either, eliminate, or minimize detrimental defects like hot cracking. All the methods discussed so far have potential applications to both casting and welding. The issue is that with these applications the welding process is 'approximated' or simulated in order to extract results and study the phenomenon of hot cracking.

There are however, test methods that are indeed designed to study hot cracking susceptibility of materials during welding. The tests are the Varestraint and the Transverse Varestraint (Trans-Varestraint) tests. These tests will be the focus of this study. Improvements will be introduced that will facilitate the study and assessment of hot cracking susceptibility of materials. The tests will be discussed in the following section.

2.3.2 Varestraint and Trans-Varestraint tests

The Trans-Varestraint and Varestraint tests were established in the early 60s and 70s [69, 74, 122, 123]. These tests involve placing a specimen on a rig with a similar arrangement to a three point bend test, initiating a welding process and towards the end of the welding process bending the specimen to achieve a pre-determined strain, using a former of a prescribed radius. The direction of the weld is either in the plane of bending (Varestraint) or perpendicular to the plane of bending (Trans-Varestraint), as illustrated in Figure 2.8.

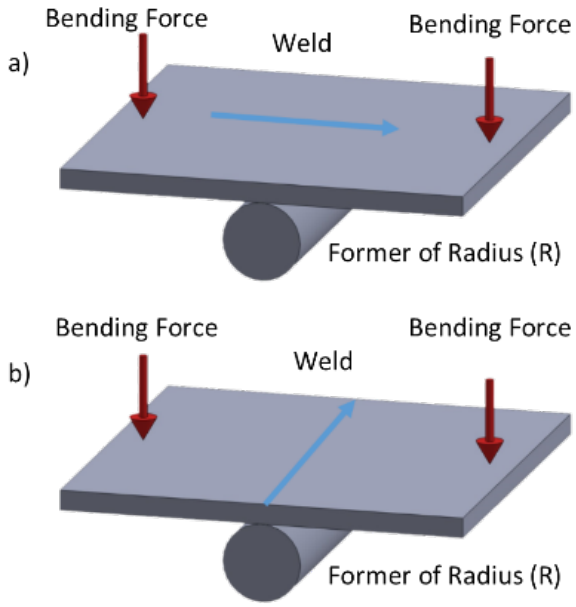

Figure 2.8: a) Varestraint test b) Trans-Varestraint test.

The radius of the former (R) is determined from the specimen thickness (t) and the target strain to be applied (ε), according to Equation 3 . This strain is defined as the 'augmented strain'.

$$\varepsilon = \frac{t}{2R} \times 100 \tag{3}$$

The term augmented strain is defined as follows. During the solidification of the weld strains are generated at the solidification front due to shrinkage (Equation 4). These strains are augmented by the strains imposed by bending [124].

$$\varepsilon_{augmented} = \varepsilon_{shrinkage} + \varepsilon_{bending} \tag{4}$$

As the bend is applied during the welding process significant strain is applied on the welding bead and, consequently, on the solidification front. This results in crack initiation. After the end of the tests the length of cracks that are formed on the surface of the specimen are measured, usually with the use of a stereoscope, and plotted against the augmented strain. Because the orientation, position and number of cracks differs between the two tests, three different crack measurements have been utilized for these tests. Maximum Crack Length (MCL), Total Crack Length (TCL) and Maximum Crack Distance (MCD). TCL is the sum of the lengths of all the cracks present after the experiment. MCL is the length of the biggest crack. MCD is the maximum distance parallel to the welding path that a crack has travelled. In the case of the Varestraint test, because the cracks are not generated along the centreline of the weld, the MCD and MCL may refer to different cracks. For the Trans-Varestraint test the MCL and MCD can refer to the same crack as the biggest cracks are generated along the centreline of the weld (Figure 2.9). Cracks are measured by observing the sample directly above the weld usually using an optical stereoscope.

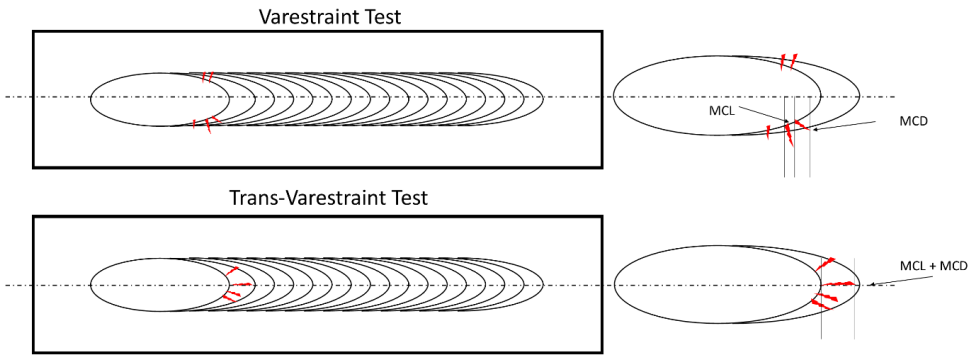

Figure 2.9: Definition of maximum crack length (MCL) and maximum crack distance (MCD) and their differences between the Varestraint and Trans-Varestraint tests.

The exact time that the bend would occur was not fixed and no parameters were set for this [125]. Given that when welding the process is not in a steady-state from the moment of initiation, delaying the time of the bend would allow for the welding process to reach a steady-state. Using these tests allowed for some specific parameters and properties to be quantified and connected to the hot cracking susceptibility of the materials.

Briefly the key milestones in the development of these tests were the following. In the early 60s, a Brittle Temperature Range (BTR) was identified, during which materials presented low ductility [67, 68]. This was determined by measuring the temperature of the weld pool and by correlating crack lengths with the temperature gradient to identify the BTR of the material (Figure 2.10).

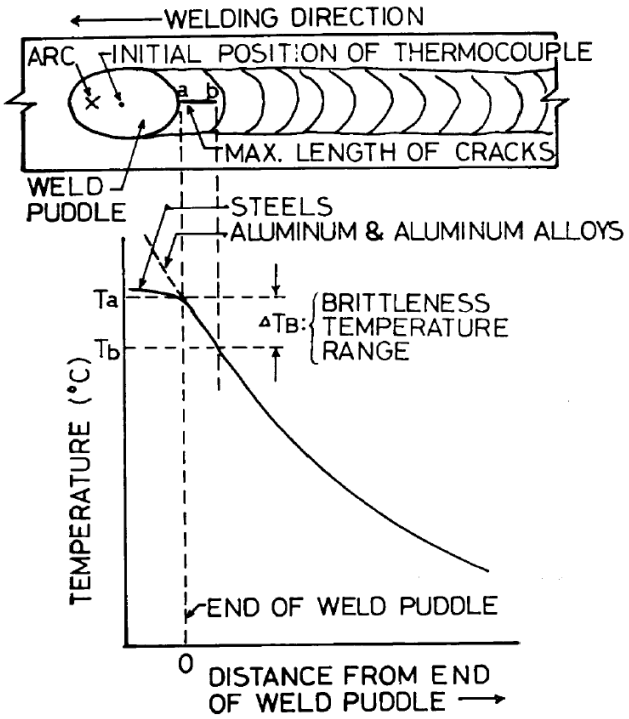

Figure 2.10: Definition of the brittle temperature range (BTR) using the results of Trans-Varestraint test [69].

In order to incorporate the energy input on the weld the Solidification Cracking Temperature Range (SCTR) was introduced. This was determined by conducting the test as previously described, resulting in a plot of augmented strain vs crack length (Figure 2.11). The augmented strain above which the crack length ceased to increase was then identified and defined as the 'saturated strain' condition.

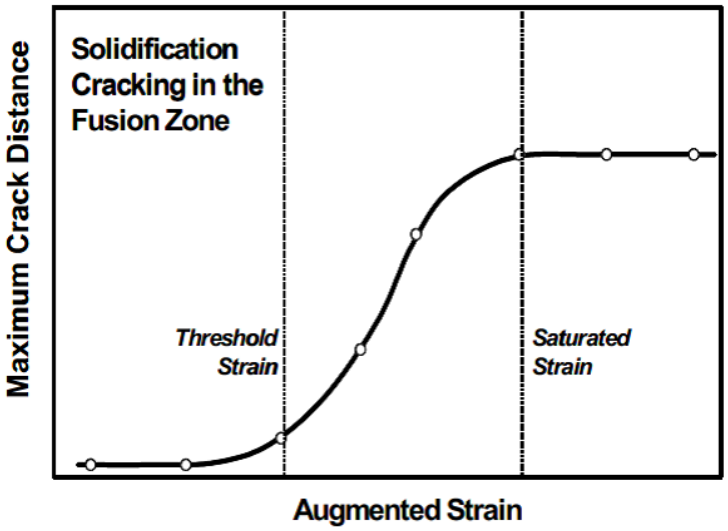

Figure 2.11: Augmented strain vs crack length [80].

This saturated strain crack length was used in combination with the welding speed and cooling rate to calculate the SCTR according to Equation 5 and Figure 2.12.

$$SCTR = Cooling\ rate \times \frac{Maximum\ Crack\ Distance\ (MCD)}{Welding\ Velocity\ (V)} \tag{5}$$

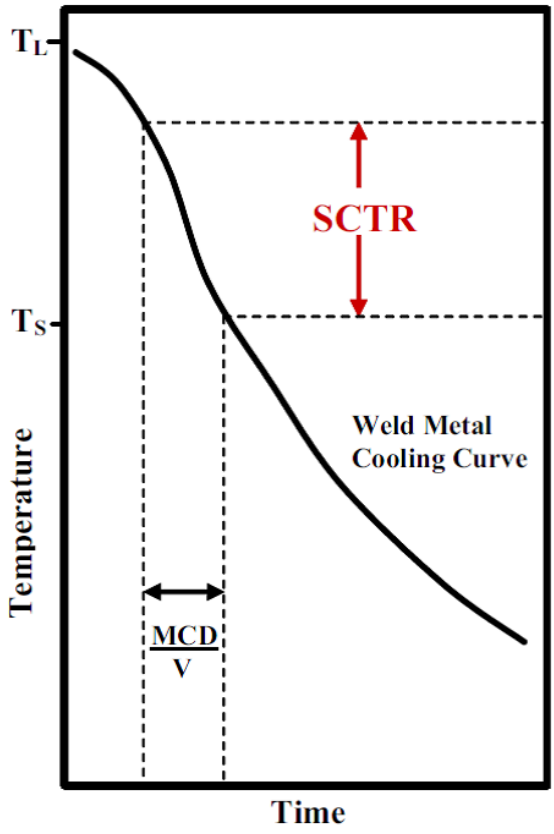

Figure 2.12: SCTR calculation on a time vs temperature graph [80].

The Varestraint test was introduced and applied initially in the mid to late 60's [74, 126] and the test was described as follows. For this test, a specimen is held over a removable die-block with a specific radius as a cantilever beam and a TIG arc melt run is made along the centreline. At a predetermined point the specimen is rapidly bent around the die-block. As a result strain is induced on the top surface. If the strain is sufficient then cracks will be generated. After the tests, the total count of cracks, their total crack length and the maximum crack length are recorded and plotted against the augmented strain. This information will provide a qualitative means of assessing hot cracking susceptibility [125].

Taking under consideration that these were the initial steps in a new experimental procedure which has a solid working principal that can be used to study the hot cracking phenomenon the following must be noted. The way these tests are described and defined presents some key issues that need to be addressed. Initially the mentioned predetermined point is not clearly defined. Adding to that, the

amount of bend or its speed is not defined either. Research that was carried out after the introduction of these tests, proposed another variation of the test. The reasoning behind this change was that since the hot cracks occur mostly along the centreline of the weld, the Varestraint test will not produce these types of cracks necessarily [69]. For this reason a similar setup to the Varestraint test was introduced with the difference of the position of the weld. By applying the strain in the transverse direction the crack generation along the centreline was ensured. This test was named Transverse-Varestraint test, Trans-Varestraint for short.

The researchers that introduced this new test went forward and tested multiple materials using this test in order to assess their hot cracking susceptibility [70, 71, 73, 127–129]. In these reports, hot cracking was studied along with the effect that alloying elements have in the hot cracking susceptibility of materials. Their focus was mainly on multiple grades of fully austenitic stainless steels and aluminium alloy metals. It is during these tests that the difference in the hot crack morphology was first identified.

The names that were given in the different morphology of the hot cracks were type D for the region of the cracks that exhibit dendritic protuberances (inter-dendritic fracture), type F for the areas that exhibit a more smooth area where inter-granular fracture occur and type D-F in for the areas that a transition from one morphology to the other occurs [130]. As research progressed both Varestraint and Trans-Varestraint tests were used in order to assess hot cracking susceptibility of materials.

Varestraint tests on Ti-6Al-2Nb-1Ta-0.8Mo and Ti-6Al-4V were carried out using the Varestraint test. Results indicated that Ti-6Al-2Nb-1Ta-0.8Mo is more susceptible to hot cracking than Ti-6Al-4V and that heat input may have an effect on the total crack length of the specimens [131]. A comparison between Al-2.2Li-2.7Cu, alloy 2024 and alloy 5083 was also carried out using a Trans-Varestraint indicating that alloy 5083 was the most weldable alloy and Al-2.2Li-2.7Cu was the least weldable one by comparing their BTR and their MCD [132]. Research that has been carried out in experimental steels that also compared results between the Varestraint and Trans-Varestraint tests revealed some important features on both testing procedures. By

comparing the tests the difference on the orientation and the size of the hot cracks generated from the test it was revealed that depending on the test utilized the cracks generated will be different.

What is noteworthy though, is that the results of maximum crack length vs augmented strain did not show the expected evolution as presented in Figure 2.11 on all of the specimens that were used [132]. Additionally the tests were not carried out on identically sized specimens. The intensity of research that was focused on the Varestraint and Trans-Varestraint tests after the late eighties has dropped compared to the years before that. Nevertheless research still continued using various materials like stainless steels, duplex stainless steel and even magnesium alloys [133–135]. The tests were even used in additive manufacturing materials research like Inconel 718 alloy [136].

Figure 2.13 shows the inconsistencies discussed by gathering data for steel samples from multiple sources where the Trans-Varestraint tests were used towards the assessment of hot cracking susceptibility of materials.

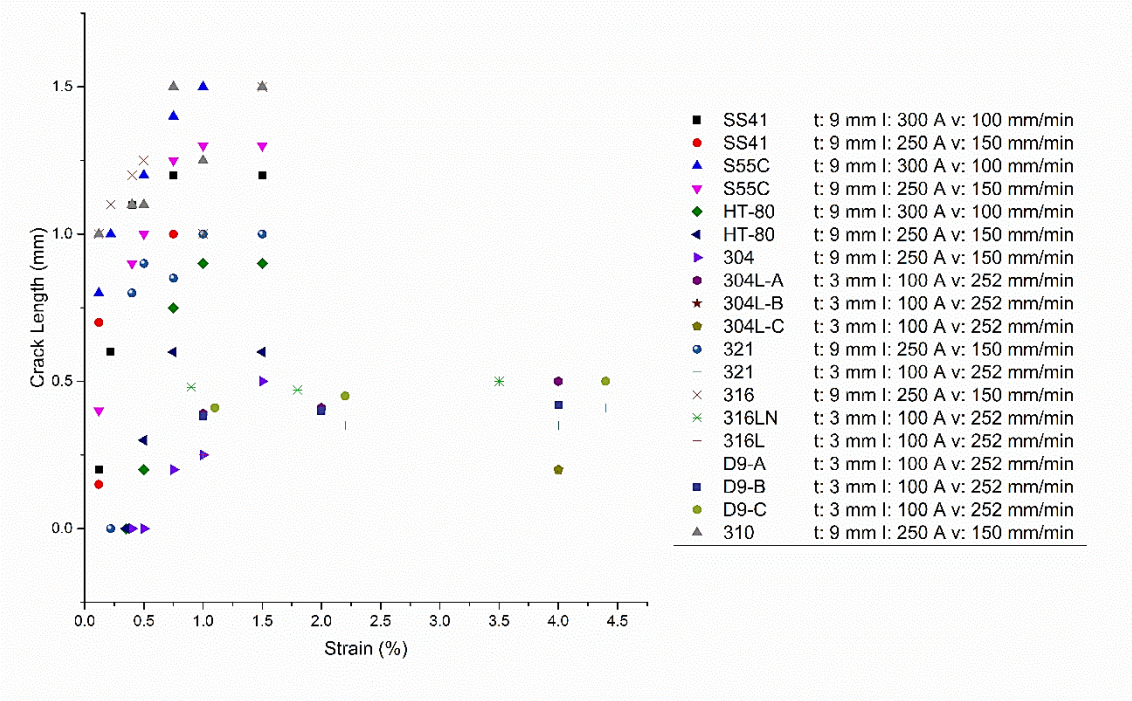

Figure 2.13: Trans-Varestraint data from multiple tests and materials (steel) showing inconsistencies between results and examinations that are focused in the range of 0 to 2.5% augmented strain mainly [69, 127, 132, 137].

Figure 2.14 provides with similar data to the ones presented in Figure 2.13 but it outlines research that has been carried out in aluminium alloys. Data are focused in the area of 0% to 2.5% augmented strain with multiple welding parameters and specimen thicknesses. Furthermore the specimens used for the testing of these materials were sheets of thickness below 10 mm.

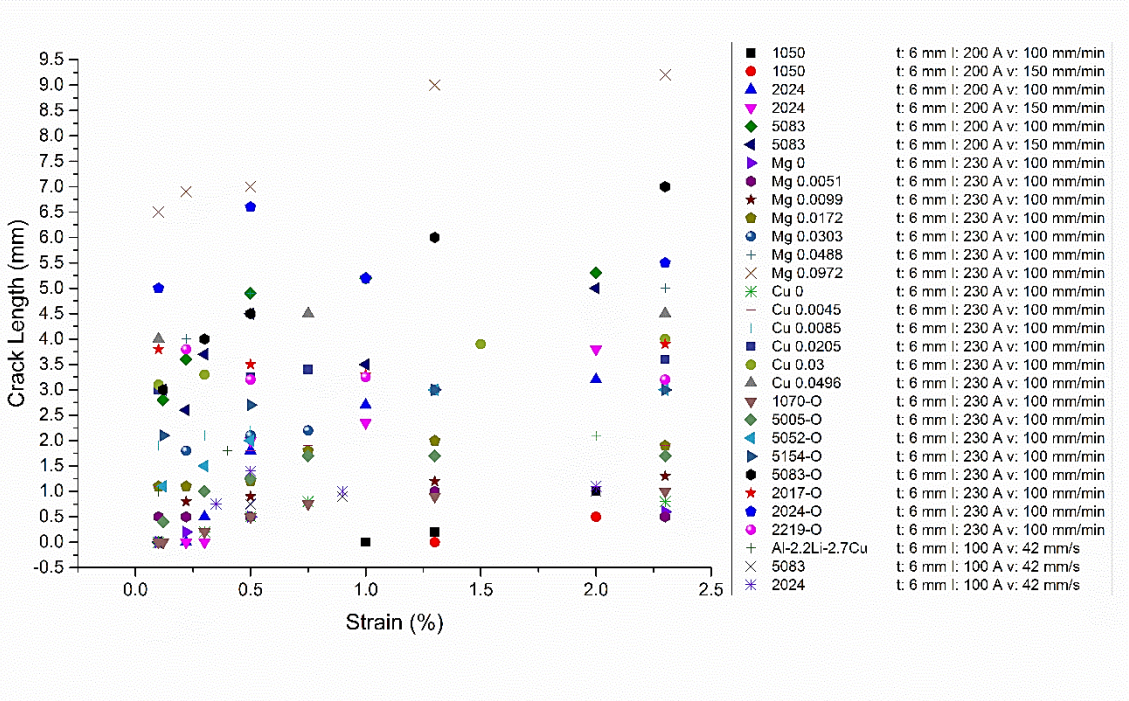

Figure 2.14: Trans-Varestraint data from multiple tests and materials (aluminium) showing inconsistencies between results and examinations that are focused in the range of 0 to 2.5% augmented strain mainly [69, 127, 132, 137].

By focusing on identical or similar materials (2024 alloys) that have been tested a number of observations can be made. The first observation is that the results presented do not seem to approximate the suggested pattern presented in Figure 2.11. Figure 2.15 shows this clearer and by comparing these results to Figure 2.11 it appears that the experiments are limited to the area of the threshold strain.

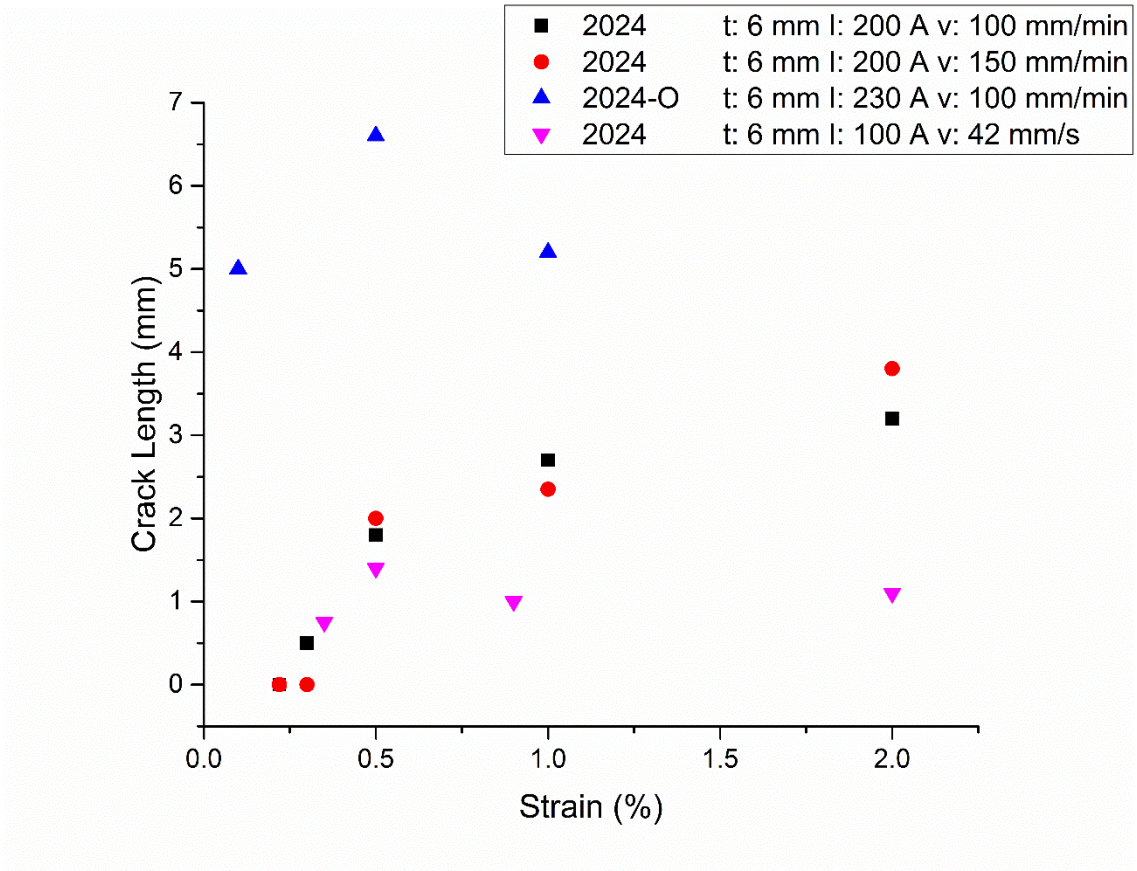

Figure 2.15: Crack length measurements from similar materials that were tested either from the same or different studies referenced in Figures 2.13 and 2.14.

Another observation is that the results from these experiments in some cases are not similar which suggests that the same material does not present the same hot cracking susceptibility constantly. This is demonstrated clearly in the results of 2024 alloy where using different welding parameters produces cracks of 1 mm to 4 mm at 2% augmented strain. By looking at the welding parameters used for these experiments the logical conclusion that welding parameters affect significantly the hot cracking susceptibility of materials can be reached. However, when examined carefully, this conclusion does not hold to scrutiny. The experimental procedure does not state that different formers were used for different strains and the bending conditions are also not stated. The fact that a significant amount of parameters was not clearly set and replicated for these experiments renders the results incomparable. Adding to that, the number of specimens used was not defined nor presented in these studies. As a result it is not possible to arrive to conclusions concerning the hot cracking susceptibility of these materials and it is not possible to extract

repeatability measures since information of the amount of tests and specimens is not presented.

The tests have also been through performance assessment. This assessment concluded that these tests can be potentially used for assessing the hot cracking susceptibility of materials but also pointed out that further research on the topic is required [138]. Reviews that are focused on the hot cracking phenomena in welds have also included these tests as prime candidates for assessing the hot cracking susceptibility of materials, but one common and usual conclusion is that there is a lack of standards and control for these tests [119, 139]. There has also been a discussion around the subject of standardization of these tests [140].

Recent research has also suggested an alternative setup in order to perform Varestraint and Trans-Varestraint tests [105, 124, 141] which is suggested that it will allow increased control of the test while at the same time the classic setup is abandoned. Despite these developments, a global agreement on how hot susceptibility should be tested has not yet been reached. Some of the main reasons preventing a standardized approach are:

- Lack of an optimal apparatus setup to conduct the experiments with.
- Lack of a specific way to apply the augmented strain during the experiment.
- Lack of an optimal strain rate that should be used for the experiment.
- Lack of specimen specifications.
- Lack of specification of welding time.

Taking under consideration that there have been more than 140 hot cracking test procedures have been developed for determining the hot cracking susceptibility [142], shows that assessing hot cracking susceptibility is an important issue and standardized tests have always been integral to the assessment of the properties of materials.

Additionally, investigators have recently stated that controlling the strain and strain rate, during these experiments, is a challenging issue that has not yet been addressed

[119]. These are key parameters that need to be specified since they are critical to the mechanism of the phenomenon that is examined. Since hot cracking is a strain driven phenomenon the control of the strain was considered as the primary parameter that needs to be controlled if the experiments were to be improved.

2.4 Summary

Steel is a diverse material that has a lot of applications. HSLA steels comprise a group of steel that has a low amount of carbon and its alloying elements are added in very small concentrations. HSLA steels are manufactured by using a specific process that is what gives them their properties. These steels are weldable and widely used in the oil and gas industry for on shore and off shore applications. Welding is an important part of this industry and because the applications are demanding and critical a lot of research has been carried out around these types of steel.

The effect of their alloying elements in the microstructure and properties of the steel is one aspect that has been examined along with how these elements affect their welding properties and quality. Because the applications of the industry are demanding, the welding defects that may occur have been researched as well, in order to better control the welding process and if possible eliminate the possibility of defects during manufacturing.

One of the critical defects that may appear during welding is hot cracking. Multiple tests have been developed and introduced in an attempt to quantify hot cracking susceptibility of materials with an ultimate aim to categorize materials according to their hot cracking susceptibility. This endeavour has been proven to be challenging and hard to achieve. Research to this day still tries to tackle this issue with various results. One of the tests that have been used for this aim is the Varestraint test and its alternative the Transverse Varestraint test. These tests were introduced in the 60's and despite the fact that their principal mechanism is valid, they were proven to not always provide reliable and repeatable results. Additionally because of the multiple methods that have been employed for these tests, standardization

has proven difficult.

Chapter 3

Experimental Process

This section will provide with information about the experimental processes that were carried out during this study. For the processes that standards are available, these standards will be referenced and outlined. Processes that do not have or do not follow standards will be described in detail. Furthermore new methods and processes that have been developed in order to achieve the objectives of this study will be analysed in detail in this chapter.

The experimental procedures that were carried out for the purpose of this study are organized in three groups. The first group of experiments focuses on the characterization of the material that is the focus of this study. The material is API 5L-X65 steel provided by TATA steel for the purposes of this research. The second group includes the small scale and industrial scale hot cracking susceptibility experiments. The third group is the non-destructive testing, fractographic and microstructural examination of the specimens generated from the hot cracking susceptibility tests.

3.1 Characterization Methods and Material

Multiple characterization methods have been used for this study. Tests that have been carried out were the following:

- optical microscopy
- scanning electron microscopy (SEM)
- hardness tests
- crack tip opening displacement (CTOD) fracture toughness.

Each one of them will be analysed in the following sections. In order to conduct the tests mentioned a sample of X65 steel was used (Figure 3.1). This part is a sample extracted from a pipe that was manufactured using the process described in Section 1.3

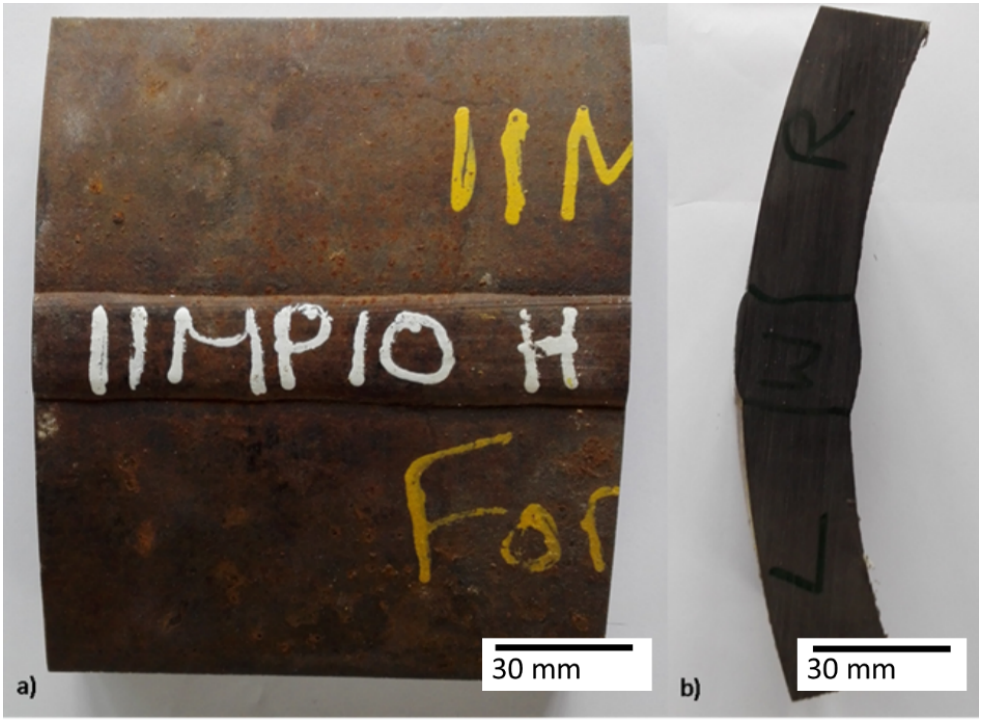

Figure 3.1: Part of steel pipe manufactured from X65 steel a) top view b) side view.

For each experiment specimens were extracted from the main sample according to the requirements of the test.

3.1.1 Microscopic examination

Microscopic examination (metallography, fractography) of specimens was carried out using optical and scanning electron microscopy. The preparation of specimens for

metallographic inspection was carried out according to ASTM E3-11 standards [143]. For the preparation of the metallographic specimens (sectioning, mounting, grinding, polishing) the following equipment was used:

- Buehler Abrasimet 250 Abrasive Cutter
- ATM Brillant 220 cut off machine
- Struers CitoPress-1 hot mounting press
- ATM Saphir 520 metallographic grinder and polisher
- Nital 2% (For etching)

For the consumables that were used for these processes a series of mounting material, grinding papers, polishing pads and diamond suspensions from MetPrep were used.

Grain size measurements were carried out according to ASTM E112 standards for determining average grain size [144]. The measurement was carried out using an inverted microscope (Olympus GX51) and a circular intercept procedure. Grain size measurements were carried out on sixteen sites (eight on either side of the weld). The number and the position of the measurements will provide with enough information to accurately determine the grain size of the material and also identify potential differences on the grain size between the right and left site of the weld.

For the metallographic and fractographic examination of the samples microscopes with a magnification range of X100 to X2000 were used. The stereoscopes had a maximum magnification X36. The SEM parameters used a working distance of 5 or 10 mm, spot sizes from 3 to 5 and beam energy of 20kV. The equipment that was used was the following:

- Olympus GX51 inverted microscope equipped with an Olympus SC30 camera.
- Olympus SZX12 stereo microscope
- Inspex HD 1080 stereo microscope

- Phillips XL 30 ESEM
- FEI Quanta 650 FEG SEM
- FEI Sirion 200 FEG SEM

3.1.2 Hardness testing

According to ASTM standards, hardness testing is a means of determining resistance to penetration (or permanent deformation), which (in the case of ductile metals) is occasionally used to approximate yield strength [145]. Hardness testing is a procedure that is commonly used in industry and research and there are many different methods for measuring hardness of materials [146]. Some of the most common methods of hardness testing are the following:

- Knoop
- Vickers
- Rockwell
- Brinell
- Shore

Each method is carried out by using different ways of indenting a sample and measuring its hardness. For this study the method employed for the hardness measurements that were carried out was the micro hardness Vickers method. The method was carried out using ASTM E384 standards as a guide [147]. Hardness testing was carried out on specimens that were extracted from the sample previously presented (Figure 3.1). The specimens were selected so that they will include all the areas that required characterization (FZ, HAZ, BM) (Figure 3.2). For the hardness measurements a Wilson Tukon 1102 hardness tester was used. The measurements were carried out using a 0.2 kgf for a 10 second dwell time. The position of the indents was in the form of a matrix that had 28 rows and 350

columns for a total number of 9800 measurements. The distance between rows was 0.5 mm and between columns 0.2 mm. The measurements were done in an area of 70 mm x 14 mm (980 mm^2). The equipment was calibrated before the hardness measurements were carried out as ASTM E384 describes, by using standard test blocks which were certified by the United Kingdom Accreditation Service (UKAS). Their nominal hardness values were 213.7 HV02/2096 MPa, 512.1 HV02/5022 MPa and 636.1 HV02/6238 MPa.

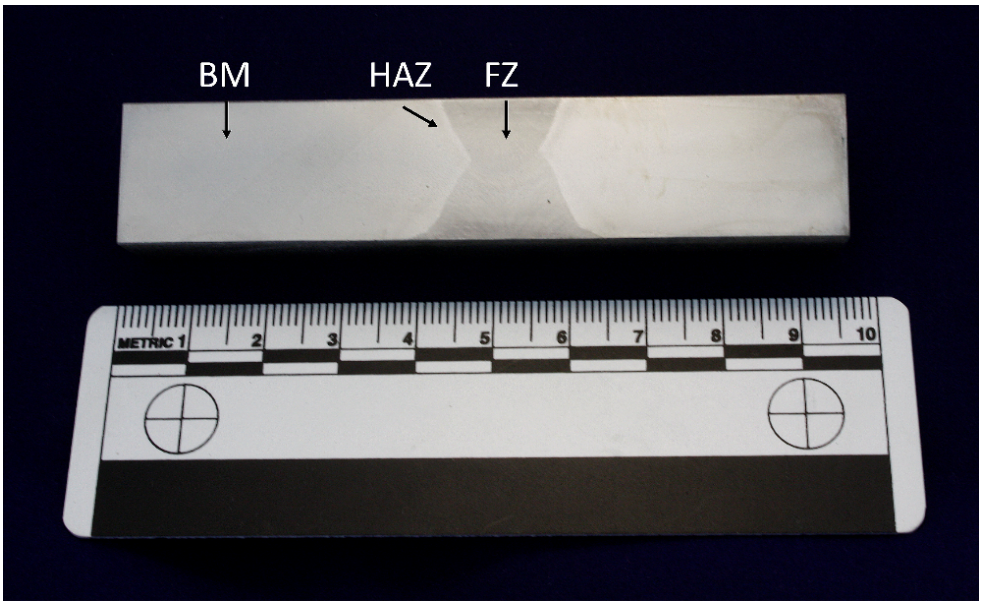

Figure 3.2: Specimen extracted for hardness measurements.

3.1.3 Fracture toughness of CTOD bend specimens

Fracture toughness is a measure that describes the resistance of a material to failure due to crack propagation [148]. The test method for performing the tests is standardized and described in ASTM E1290, ASTM E399 and ASTM E1820 [149–151]. The standards that are used usually depend on the material that is tested and its application. Previous work on fracture toughness of the X65 SAW weld joint has focused in the fusion zone of the joint [39]. The work that was carried out also revealed that Ti (C,N) have an important role in the fracture toughness of weld joints because they act as crack initiation points [60].

The present study is focused on the SAW weld joint, on the fusion interface between

FZ and HAZ of the X65. The change in the position of study will offer more information on how the fracture toughness differs from site to site in a weld joint. Furthermore, since hot cracks also nucleate at the interface of the FZ with the HAZ obtaining more information on the fracture toughness is important. The issue is that because of the shape of the weld joint the extraction of samples is challenging. The process of manufacturing the specimens is as follows. The main part was sectioned using wire cutting electrical discharge machining (EDM) to get slices from the part in order to be machined afterwards. The shape and dimensions of the specimens are in accordance to the ASTM 1820-01. The designs which indicate the cutting of slices and the positioning of the specimens are in the following figures (Figure 3.3, Figure 3.4).

It is essential to point out that because the fracture toughness experiment was planned to be carried out with the notch placed at a position so that it contains 50% FZ and 50% HAZ the design and positioning of the specimens was crucial. Each specimen was identified by its position and orientation relative to its original position at the weld joint (ODF: Outer diameter of the pipe, IDF: Inner diameter of the pipe). Before the specimens were notched and tested a preliminary examination was carried out.

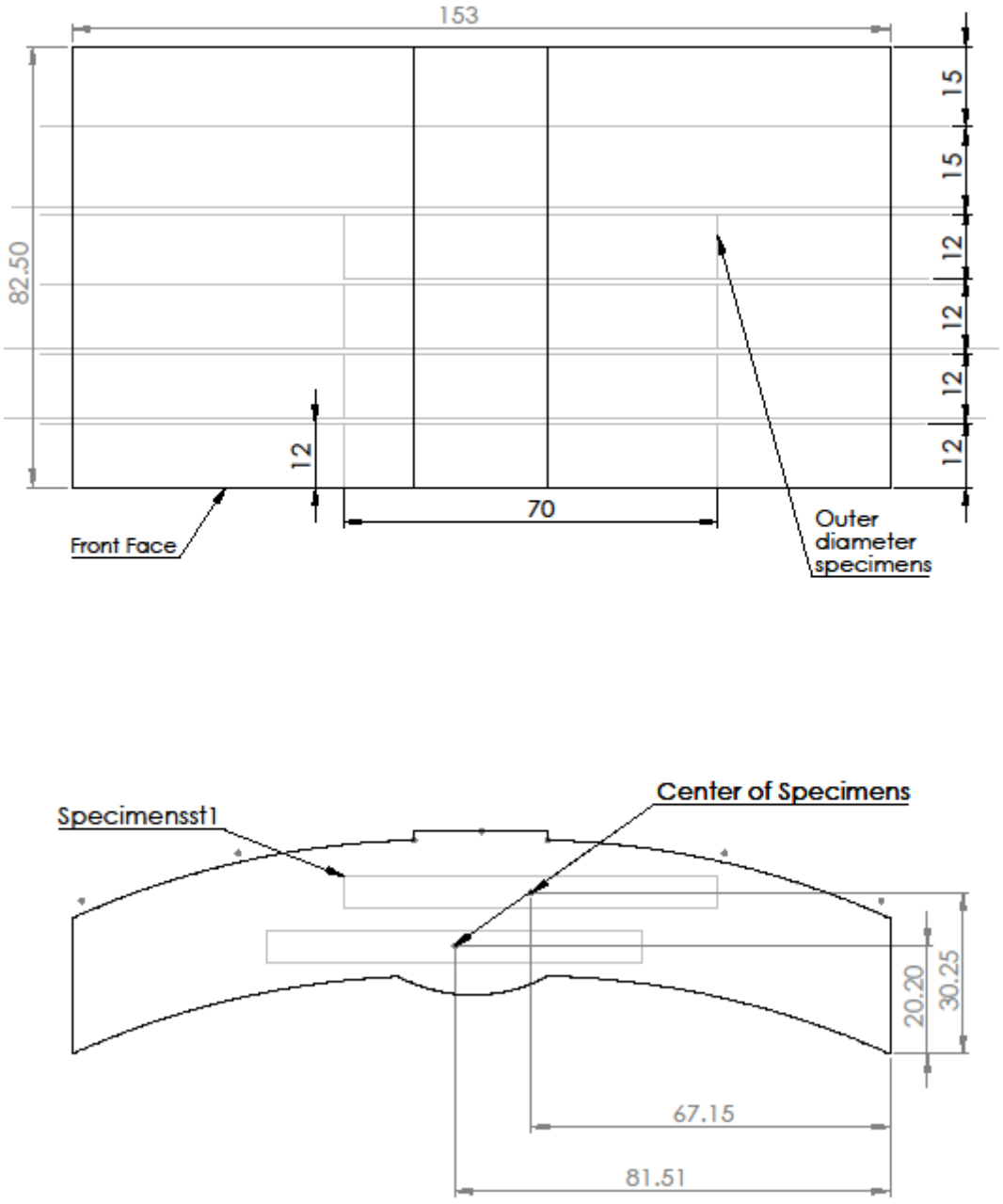

Figure 3.3: Positioning of the specimens with allowance for material loss during cutting. All measurements are in mm.

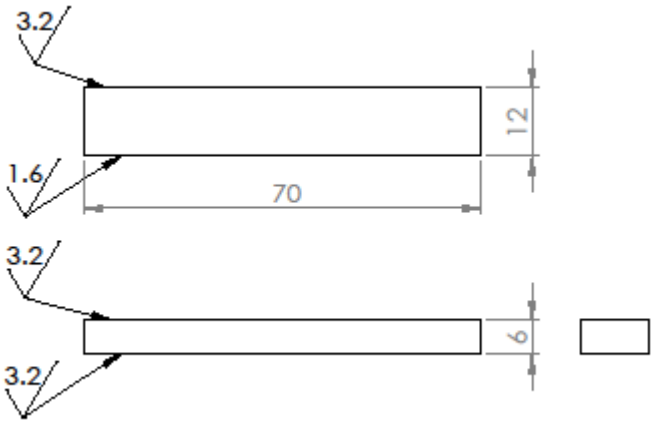

Figure 3.4: Last stage of specimens before sending them to TATA steel. All measurements are in mm.

The specimens were hardness tested and then they were etched in order to reveal the fusion zone of the part. This helped identify the position where the notch needs to be placed for the fracture toughness test. The examination of the specimens revealed that there is a high probability that even if the notch is accurately placed on the specimens it will not contain exactly 50% HAZ and 50% FZ because the weld varies in width along the length of the pipe (Figure 3.5, Figure 3.6). This will cause deviations on the samples.

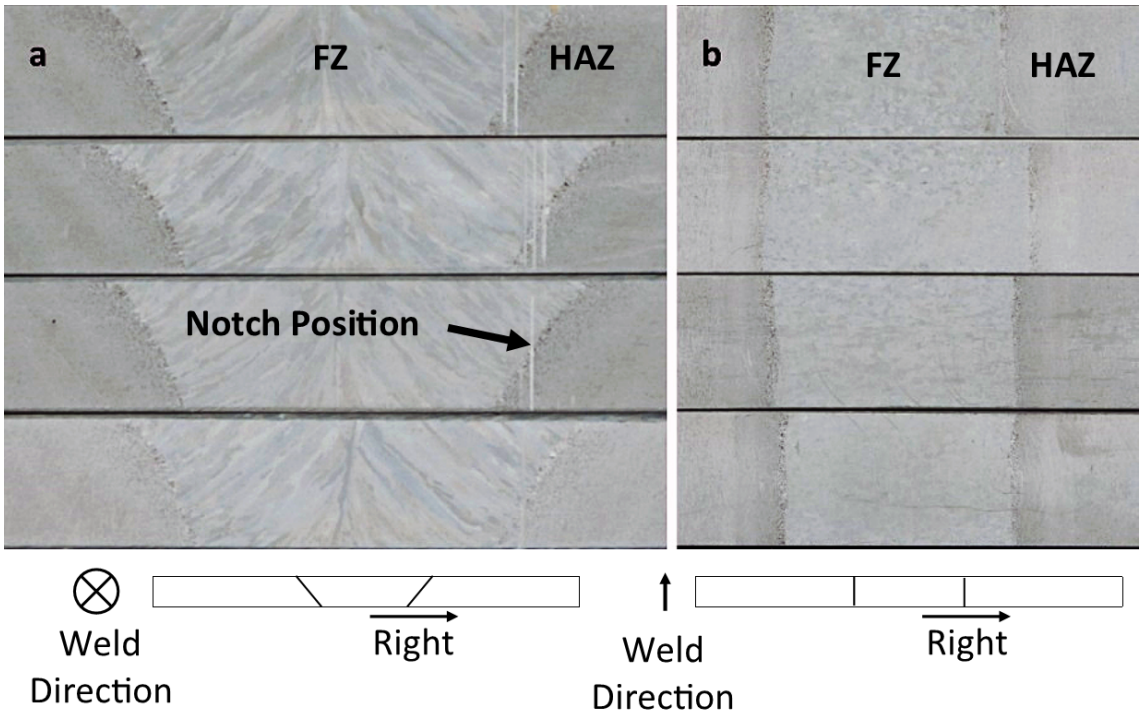

Figure 3.5: Etched CTOD specimens. a) front face where notch will be positioned b) top face of the sample width of the weld changes.

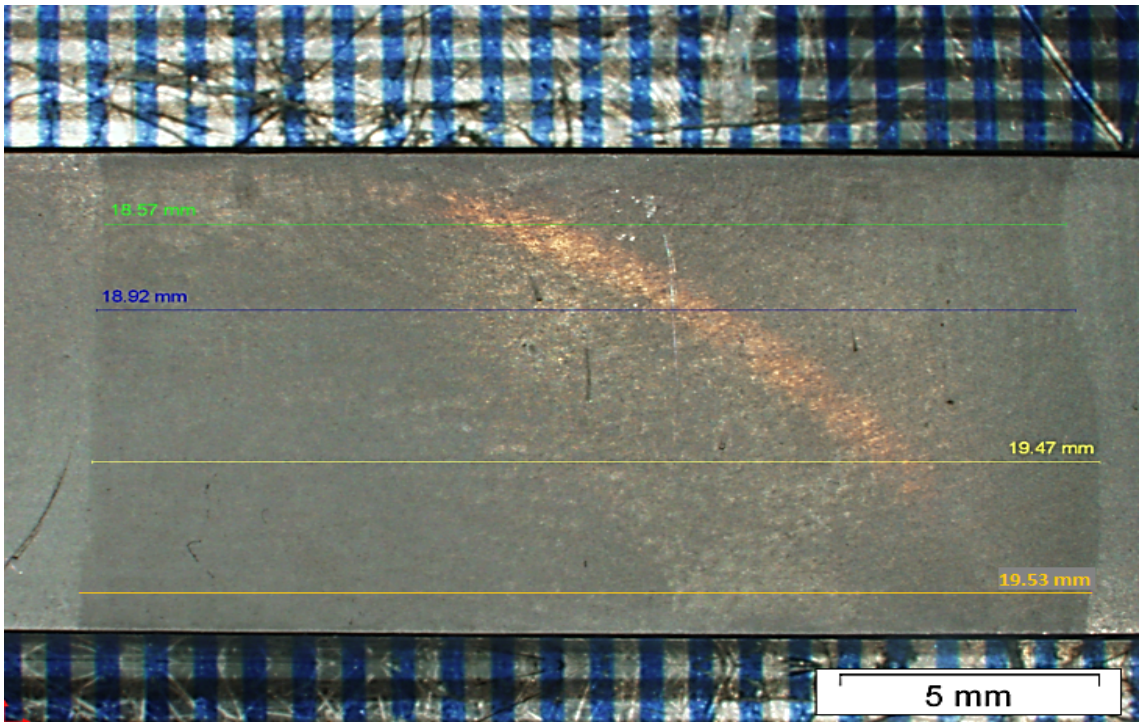

Figure 3.6: Difference in weld width.

Therefore, in order to identify the position of the notch for the fracture toughness experiment, measurements were carried out on every specimen separately. For all the

specimens the distance for the notch was measured from the front right face (Figure 3.5 a) of the specimen in order for the positioning of the notch to be correlated to each specimen from a specific position. The measurements were taken as shown in the next figure (Figure 3.7).

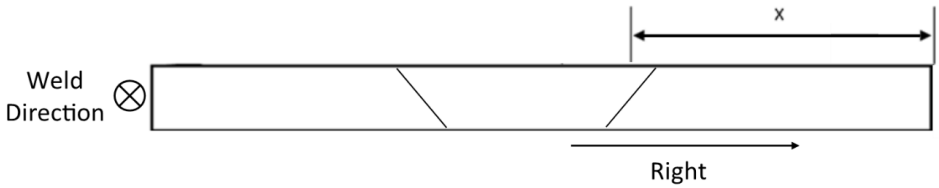

Figure 3.7: Front face of CTOD specimens.

As shown in the figure the distance for the position of the notch is measured on the front face of each specimen and from the right side of the specimen which is marked with an engraver on each specimen. The measurements for each specimen can be found in the following table.

Table 3.1: Position of the notch measured as shown on Figure 3.7

Specimen Code	**X (mm)**	**Specimen Code**	**X (mm)**
IDF001	48.83	**ODF001**	35.76
IDF002	50.29	**ODF002**	36.97
IDF003	49.41	**ODF003**	36.00
IDF004	49.66	**ODF004**	36.86

After the position of the notch was identified the samples were machined according to ASTM E1820-09. Figure 3.8 shows the dimensions of the specimens and the drawing of the notch that was machined on the specimens. After machining the specimens were pre-cracked. Pre-cracking was carried out by a fatigue pre-cracking procedure with an initial maximum load of 3 kN and a minimum load of 0.3 kN. The final maximum load was 1 kN and the minimum was 0.1 kN. On average pre-cracking was carried out in 13000 cycles. Following pre-cracking the three point bend test was carried out. On average the K Rate (The rate stress intensity factor increases as the crack grows) was 1.85 MPa $m^{1/2}$/s, the loading range was 0.125 kN/s and the

displacement rate was 0.008 mm/s. The tests provided with values for the critical stress intensity factor (K_{IC}), the plastic-elastic fracture toughness (J) and the crack tip opening displacement (CTOD).

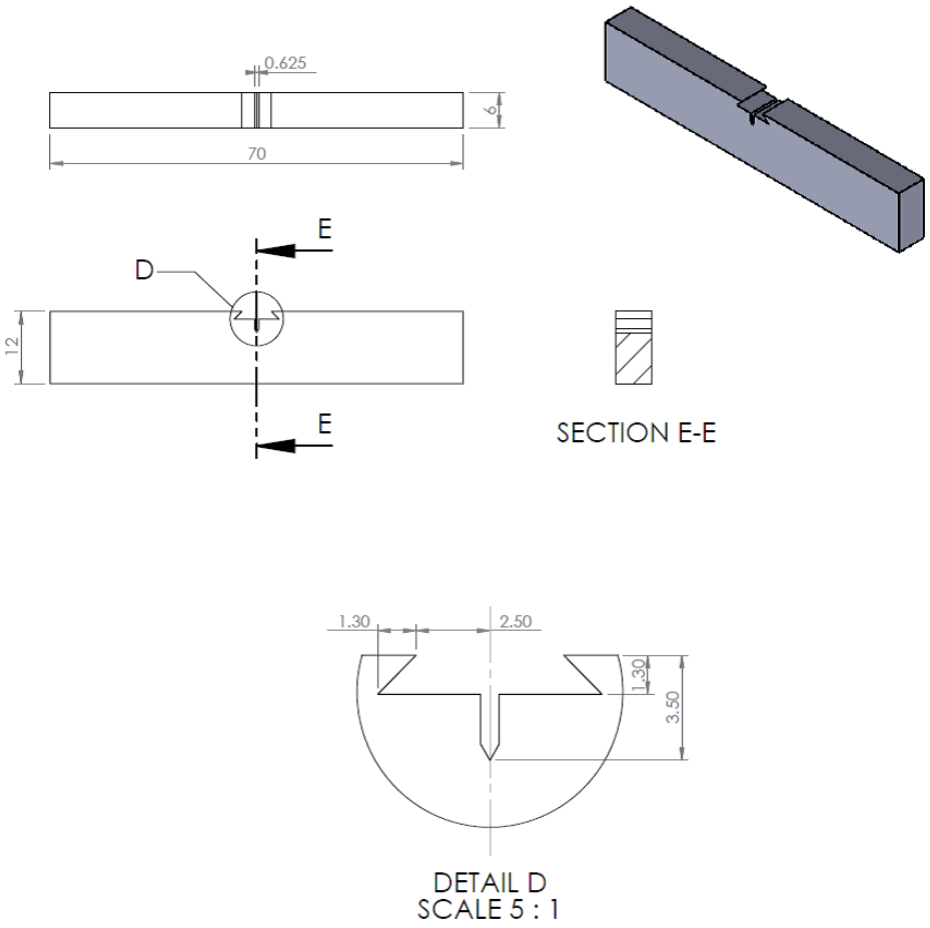

Figure 3.8: CTOD specimens drawing. All measurements in mm.

The following figure (Figure 3.9) illustrates a force-clip gauge graph that was obtained during the experiments. In order to determine the P_Q value a line that has the 95% of the slope that the original loading line has been drawn (red line). The initial slope is drawn on the elastic line where the force-displacement evolution is linear. The second line (blue line) is a line that goes through the maximum load and has the initial loading slope. This line passes from the total notch displacement point at the x-axis.

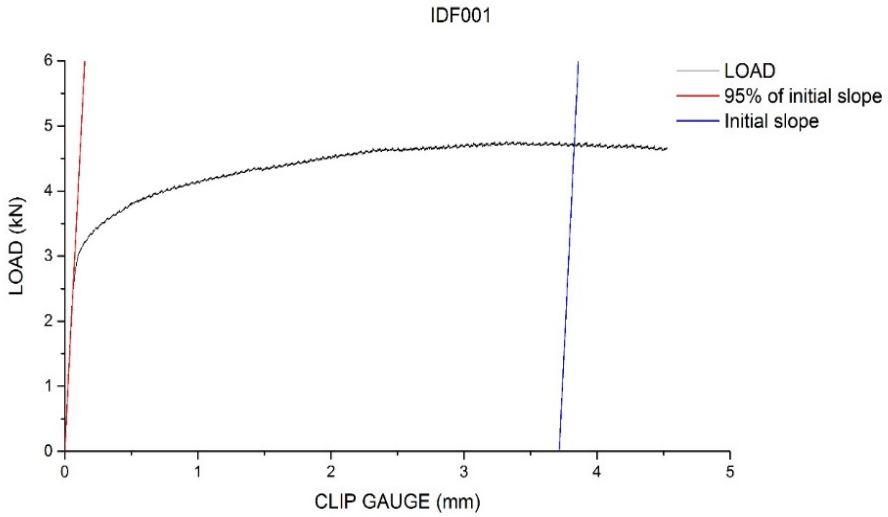

Figure 3.9: Load-clip gauge graph (see Figure 3.10 for detail).

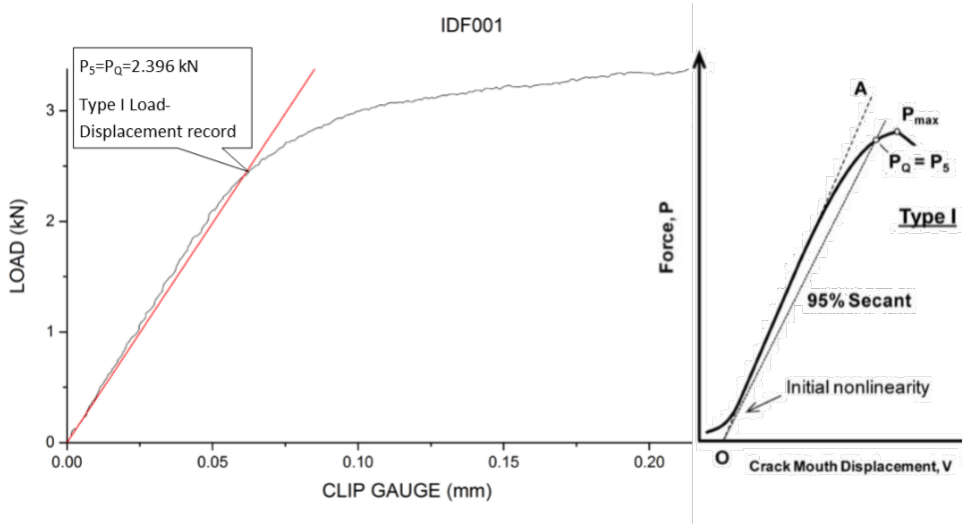

Figure 3.10: Detail of Figure 3.9. Type one Load-Displacement record from ASTM E399 standards [150].

The specimens that were used generated graphs that exhibit type one Load-Displacement record [150]. From these graphs the area under a curve is also calculated in order to obtain J as indicated by the ASTM standards and illustrated in the following figure (Figure 3.11).

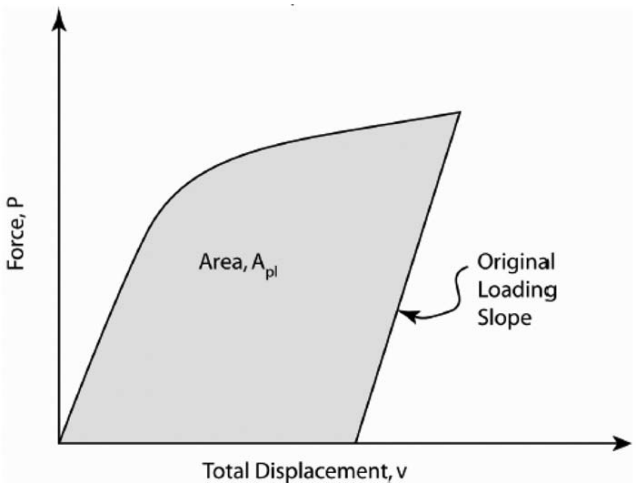

Figure 3.11: Area under the curve calculation [151].

In order to better compare the amount of HAZ and FZ in each sample used, the area at the FZ and the area of the HAZ were estimated. The method of the calculation included the separation of the two areas using photo editing software (Adobe Photoshop CS5) and then the area of the elements (pixels) that represent the surface the area of each zone (FZ, HAZ) was measured (Figure 3.12). The separation of the areas was carried out using the quick selection tool of the software which selects areas with similar colour patterns under the guidance of the user. This allows clear selection of the areas of interest with a relatively high accuracy. After the selection and separation of the two areas was done the pictures were cropped in order to keep only the areas of interest and then turned into a black and white picture.

Figure 3.12: Separation of FZ surface from the whole fracture surface.

To measure the area of each pixel the number of pixels that represent a known length was measured and then divided by the number of pixels. This way, length represented by each pixel was estimated to 0.004 mm and its area 1.6 x 10^{-5} mm^2. By

multiplying the area of one pixel with the number of pixels that represent specific areas can provide with a pretty accurate estimation of the area represented. In order to measure the area a small windows application was developed so that the processed images could be used to measure the number of pixels in the area (Figure 3.13).

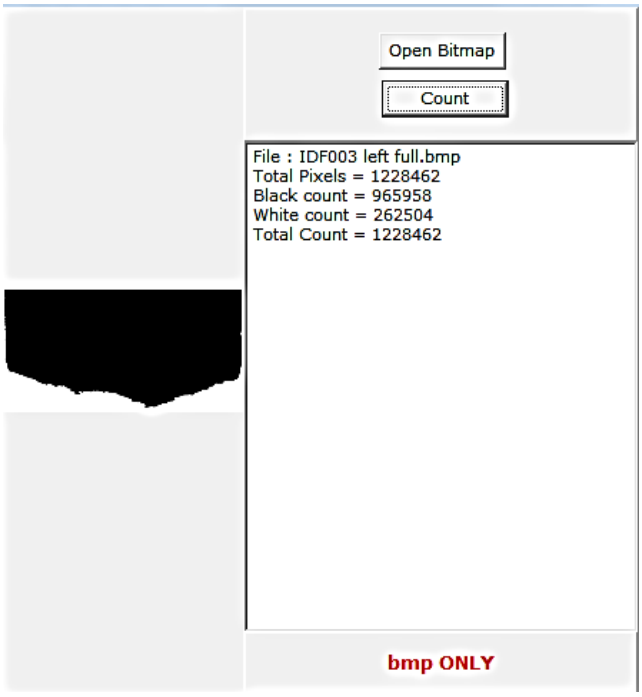

Figure 3.13: Pixel measurements for area estimation.

3.2 Weldability tests

For the weldability testing the Varestraint and Trans-Varestraint tests were used. For the Varestraint tests a small scale rig was used. The small scale tests have been used previously in conjunction with synchrotron X-rays in order to study the phenomenon of hot cracking using EN1A, S303 and mild carbon steel [39]. The rig consists of the following main parts (Figure 3.14): stable mount for a welding torch; two actuators, one for moving the sample in order for a welding bead to be deposited and one for applying the bend; the sample holder that carries bar shaped specimens with an 8 x 8 mm with a length of 300 mm. The holder also has incorporated a bending block of 30 mm radius.

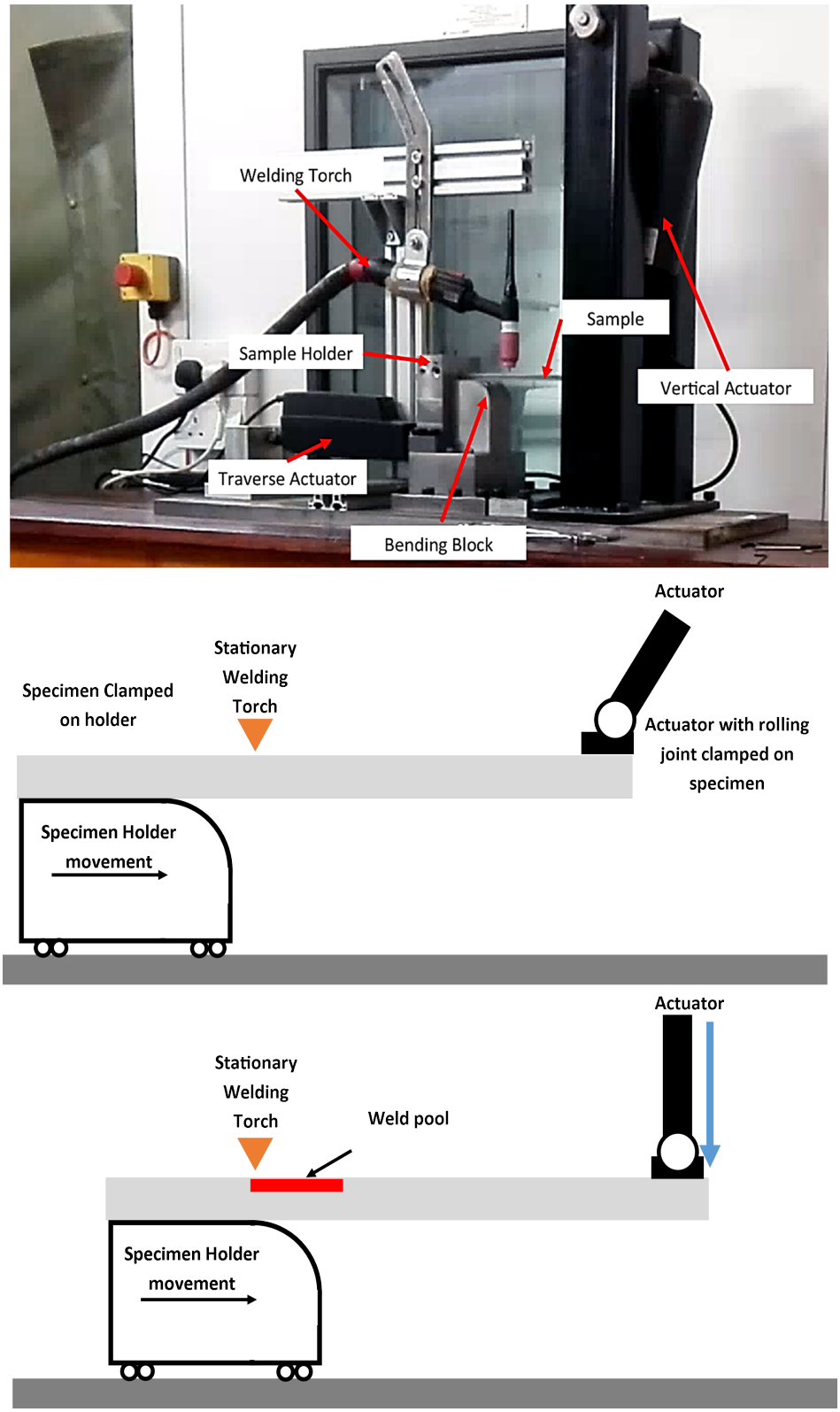

Figure 3.14: Small scale Varestraint rig.

An industrial scale custom made Trans-Varestraint rig (Figure 3.15) was used in the present study. The rig consists of a base on which the formers are placed. The

specimen rests on the former with the moving actuators, powered by a hydraulics unit, positioned on either side. The welding torch is suspended from a traversing system that moves at a specified speed that is fixed during the experiment.

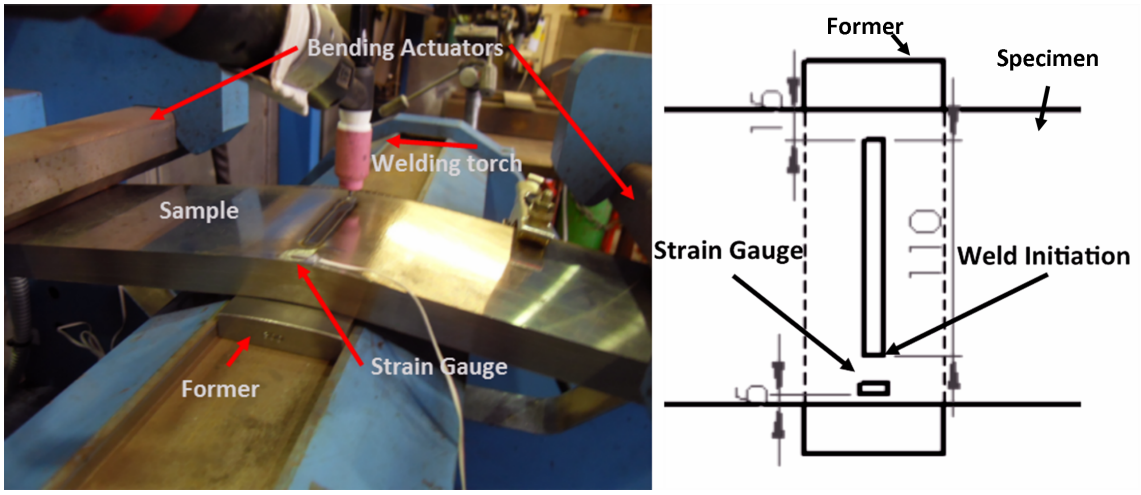

Figure 3.15: Experimental setup for industrial scale Trans-Varestraint rig.

Both experimental setups aim towards assessing and quantifying hot cracking susceptibility of materials. However both setups are not standardized and have limitations on the way the experiments are carried out. Ideally both experimental setups should have comparable results and similar methods for conducting these experiments. However, the small scale rig uses a cantilever approach in order to bend small square bar specimens over a former of a fixed radius. The industrial scale rig uses a different setup that has the capability of bending thick plates in a similar way a three point bend test does using different formers.

3.2.1 New method for conducting the Varestraint and Trans-Varestraint testing.

In Section 3.2 the current state of the Varestraint and Trans Varestraint tests has been described and some significant drawbacks have been highlighted. In order to create a standardized testing methodology the following aspects must be addressed:

- Repeatability must be ensured by the use of a standard setup. The primary parameter that affects solidification cracking in these tests is the strain applied

on the weld, which is determined by the radius of the formers used according to Equation 3.

- Standard discrete former radii, using either a selection table or selection graphs (e.g. Figure 3.16), could be used to ensure the application of the desired strain, according to the thickness of the specimen [138].

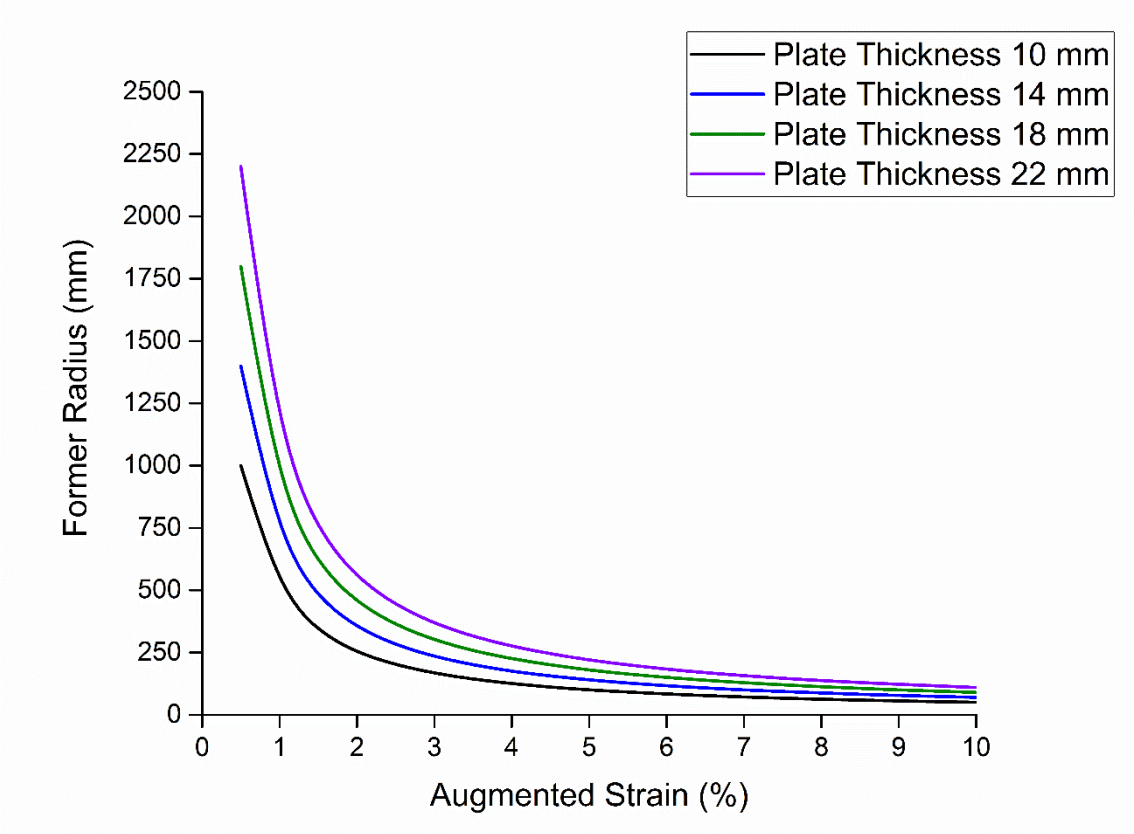

Figure 3.16: Selection of former radius according to desired augmented strain and plate thickness using Equation 3.

- The required bending stroke that results in the required strain shall be defined. Published research has not yet defined this relationship. Tests have instead been carried out with a variety of formers, welding techniques and strain rates [69, 124, 138, 152, 153].

- Appropriate measure for hot cracking susceptibility shall be identified and defined.

In order to obtain a method for conducting these experiments that will be repeatable and produce reliable results an important parameter must be defined. It has been shown by literature that the strain applied on the solidification front is of critical importance. For this reason the behaviour of thick plates, that are the main subject of this study, were examined by simulating their bend on a former as they do in the industrial scale rig. By simulating in the most rudimentary way this relatively simple setup the stresses and strains applied can be estimated.

An Abaqus CAE simulation of the bending of the plate was generated using a standard/explicit model with both elastic and plastic properties for the material. For the deformation of the plate a specific displacement was used. This was calculated by an equation that will be analysed in this section. The properties of X65 steel were obtained from API-5L standards. X65 has a yield strength in the range of 448-600 MPa and its tensile strength is in the range of 531-758 MPa. The number 65 in the X65 designation corresponds to its yield strength in psi which is 448 MPa (65000 psi).

The initial results of the simulations showed the following. As the actuators push the ends of the plate in order to apply the strain the plate plastically deforms to the shape of the former and created a plastic hinge along the centreline of the plate. This plastic deformation is localized in an area around the centreline of the bend. Furthermore, because of the thickness of the plate and that it is not restrained edge effects deform the edges of the plate and cause them to lift from the former. This also increases the strain on the edges. The results of the simulations were also compared and analysed with the experimental results and they will be discussed in the discussion section of the thesis.

Nevertheless, because of the plastic hinge formation the plate is shaped according to the former radius and the rest of the plate remains straight forming a tangent to the former radius (Figure 3.17). The issue is that the strain applied in the centreline is changing constantly as the plate bends. This revealed the issue that exists and described on the application of the strain in these experiments. The fact that the samples are thick plates of steel and that a plastic hinge is forming prevents the bowing of the plate. This phenomenon is expected to be accentuated during the

weldability experiments due to the increased temperature caused by the welding process along the centreline of the specimen.

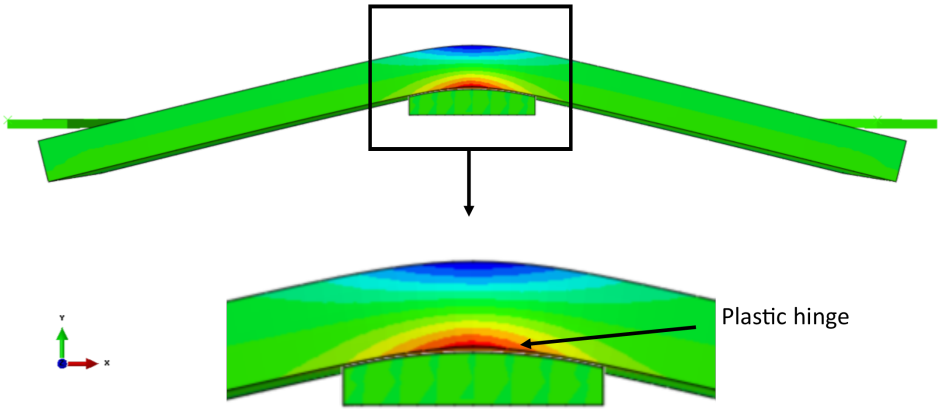

Figure 3.17: Abaqus simulation of bending an X65 plate around a former. Red and blue regions highlight the edges of the plate that are deformed due to the edge effects while bending the plate.

With a setup like this it appears that each test can have tree possible outcomes strain wise. The specimens will either be under bent, over bent, or fully bent (Figure 3.18). If the specimen is under bent the strain applied on the centreline will be less than desired. If the specimen is over bent the strain will be more than desired. In order to ensure that the strain applied matches the target strain the bend must form a tangent to the surface of the former.

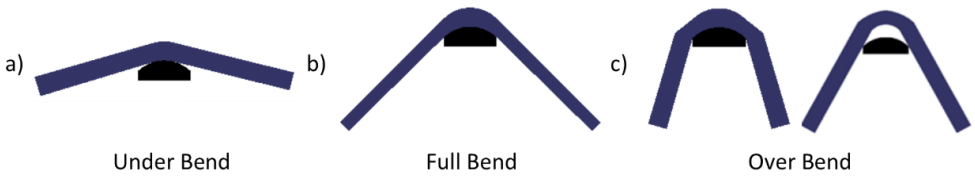

Figure 3.18: Types of bends a) under bend which leads to under straining b) desired bend c) over bend over straining.

To determine the required stroke to be used, a geometrical approach was utilised. Since strain is a geometrical parameter, the basic parts of the test were used as

a basis for the development of a solution (Figure 3.19). The test has a similar geometric arrangement to a three point bend test with a former of a specific radius that ensures that the centreline of the specimen is bent to a specific radius in order for the target strain to be applied.

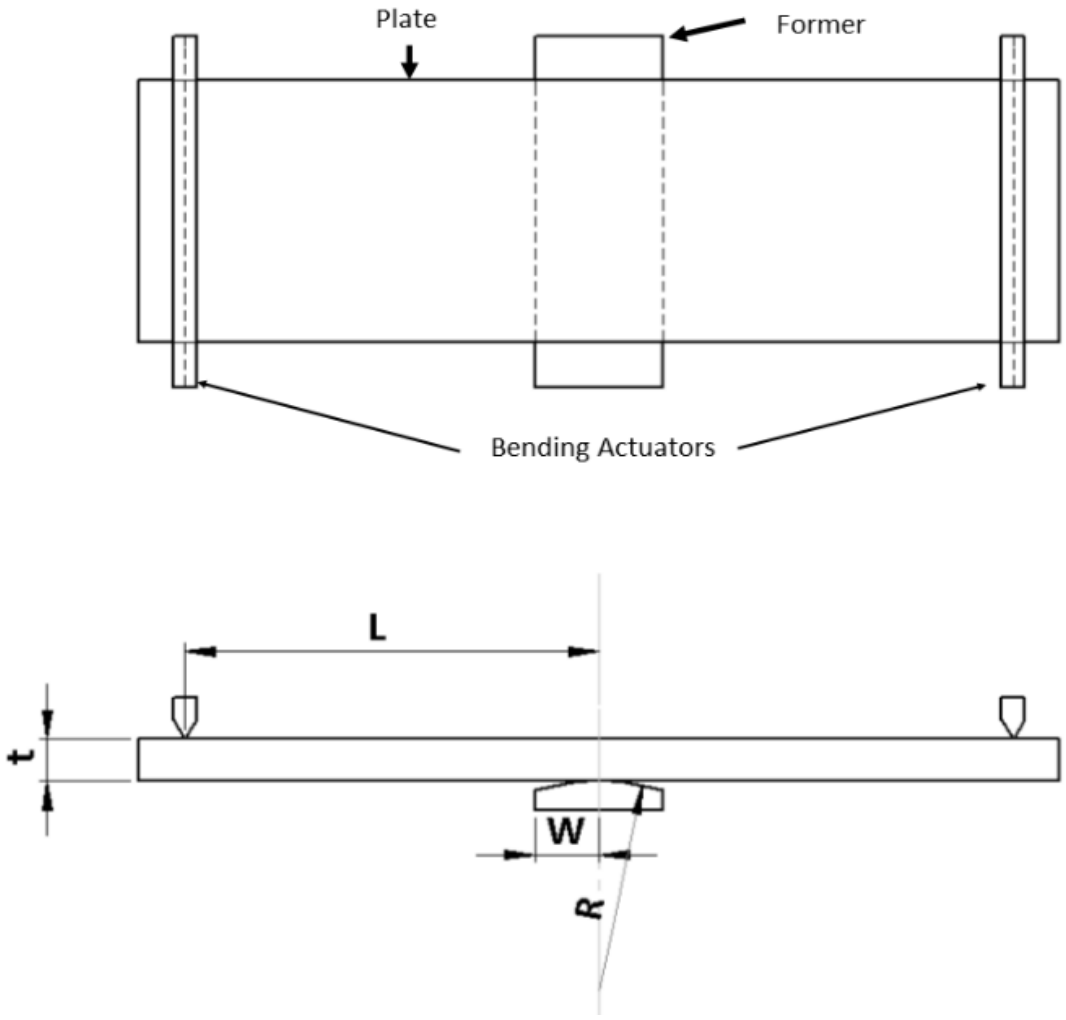

Figure 3.19: Basic geometrical characteristics of a Trans-Varestraint test (where L = Bending span; t = Specimen thickness; R = Former radius; W = Former half-width).

To improve reliability and repeatability, the length of bending stroke (labelled 'S' in Figure 3.20) must be precisely controlled. The bending stroke must be sufficient to ensure that the specimen will utilise the full surface of the former and will always be in contact with it.

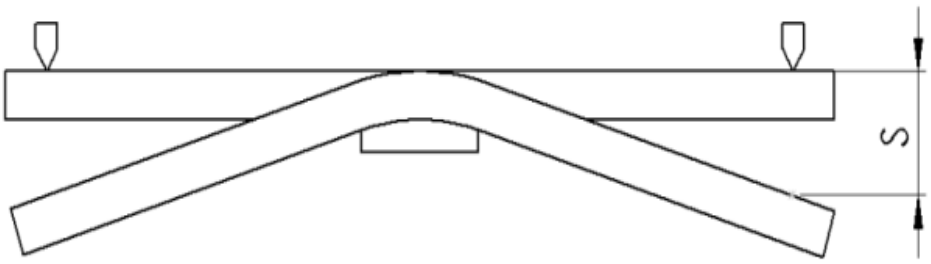

Figure 3.20: The length that needs to be identified is the length of the bend stroke (S).

The bending stroke may be derived from one half of the bending setup, setting the maximum bend as the bend where the plate will follow a tangent line from the edge of the former. Figure 3.21 illustrates the relevant geometry, where:

AA': is the bending span between former centreline and actuator (L)

CC': is half-width of the former (W)

DC' and DA: is the radius of the former (R)

A'B': is the length of the stroke (S)

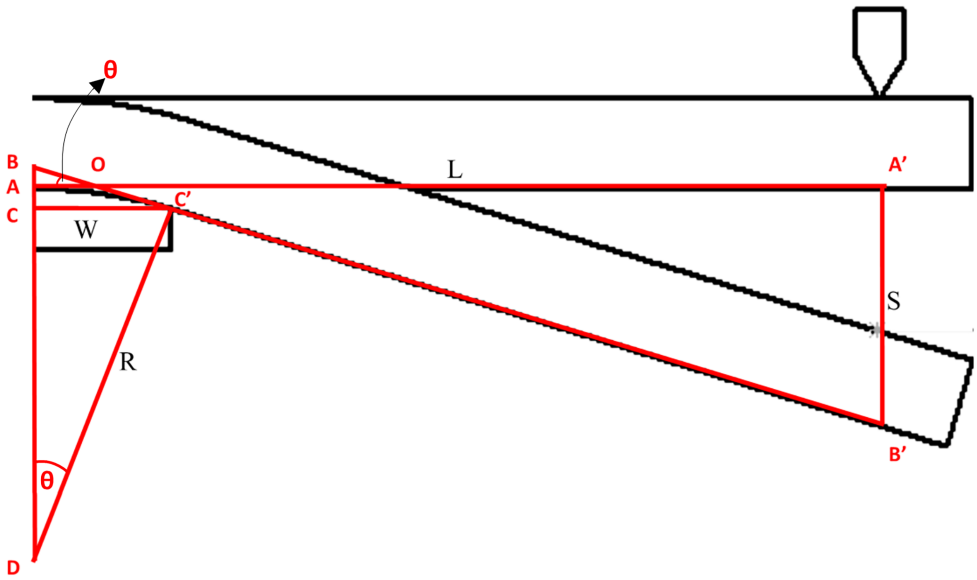

Figure 3.21: Relevant geometry of bending setup.

From Figure 3.21 it can be seen that triangles AOB and A'OB' are similar. Adding

to that the angle formed between the sides AO and BO of the triangle AOB (referred to as from now on) is the same as the angle that is formed by the sides DC' and DC from the triangle DCC'. This means that all the trigonometric numbers in that are the result of these angles in these triangles will be the same. For this reason we have the following.

For the triangle DCC':

$$\sin\theta = \frac{W}{R} \tag{6}$$

$$\cos\theta = \frac{\sqrt{R^2 - W^2}}{R} \tag{7}$$

$$\tan\theta = \frac{W}{\sqrt{R^2 - W^2}} \tag{8}$$

As triangles AOB and A'OB' are similar:

$$\frac{A'B'}{AB} = \frac{A'O}{AO} = \frac{B'O}{BO} \tag{9}$$

$$A'O = \frac{A'B'}{\tan\theta} \tag{10}$$

$$AO = \frac{AB}{\tan\theta} \tag{11}$$

A'O and AO are the length L and A'B' is the stroke length S. So by adding these Equations (10) + (11) we get.

$$L = \frac{A'B'}{\tan\theta} + \frac{AB}{\tan\theta} \ \rightarrow \tag{12}$$

$$S = L\tan\theta - AB \tag{13}$$

For the triangle DBC'

$$\cos\theta = \frac{DC'}{DB} \ \rightarrow \tag{14}$$

$$\cos\theta = \frac{R}{R + AB} \ \rightarrow \tag{15}$$

$$AB = \frac{R^2}{\sqrt{R^2 - W^2}} - R \tag{16}$$

By substituting (16) to (13) we get

$$S = \frac{LW}{\sqrt{R^2 - W^2}} - \frac{R^2}{\sqrt{R^2 - W^2}} + R \ \rightarrow \tag{17}$$

$$S = \frac{LW - R^2}{\sqrt{R^2 - W^2}} + R \tag{18}$$

Equation (20) enables tests to be better defined and controllable. Each experiment has a defined bending stroke that needs to be applied in order to introduce specific strain on the centreline of the setup.

For the Trans-Varestraint test the weld bead should be applied at the centreline of the specimen. At the start of the welding procedure the energy that is introduced is used to form the weld pool. This process is different energy-wise compared to the process after the weld pool is created and the weld bead is steadily deposited on the material. During the second stage the heat transfer is stable and usually where big samples are used is considered a quasi-steady state. The bend should be applied on the sample during this stable state. Each test has three phases (Figure 3.22). At time zero (point I) the welding process initiates and the welding bead starts being applied on the specimen at a fixed speed. Time two (point II) is when the bend will be applied and it is defined by the welding speed and the length from point I to point II (Equation (19)). This is identified by the term tII which indicates the time it takes the welding torch to cover the disstance from point I to point II.

$$t_{II} = \frac{Distance\ between\ points\ I\ and\ II}{Welding\ Speed} \tag{19}$$

After bending at point II the welding process continues so that the solidification cracks have enough space to develop without being re-melted by the welding torch. Recent research has estimated that solidification cracks propagate at a speed between 2-3 mm/s [81]. Therefore, for a weld bead of depth 2-3 mm and a welding speed of 3mm/s the welding process should continue for at least 1 second after the bend. When point III is reached the welding process stops.

For the Varestraint test the setup and execution is the same with only two differences. The welding bead is applied perpendicular to the centreline of the

sample. The bend must occur when the molten material is present at the centreline of the bend in order to ensure that the maximum strain will be applied to the solidification front.

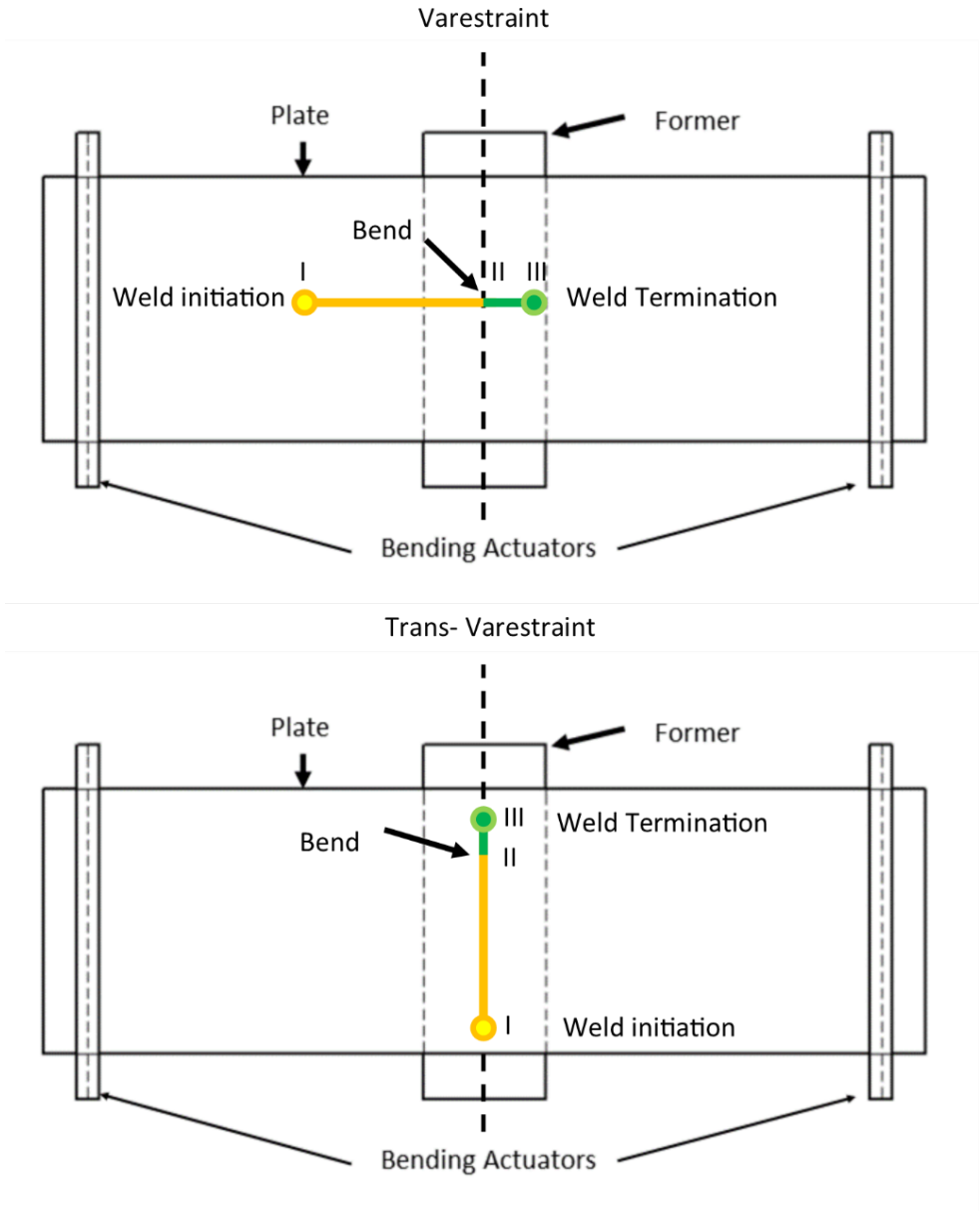

Figure 3.22: Trans-Varestraint test setup.

3.2.2 Small scale weldability tests

The experimental procedure for the small scale Varestraint test is the following. The specimen is mounted on the rig and the actuators are set to their initial position. The welding process initiates and the traverse actuator starts moving the

specimen in order to deposit the weld on it. Towards the end of the welding process the bending actuator bends the specimen and then the welding process and the experiment is finished. Because the rig does not have an interchangeable former the experiments were carried out in the following way. To apply a different strains for each experimental set the bending stroke was varied. Because the actuators can be controlled with the computer (on the scale of ms) after the upgrade, the amount of time that the actuator would bend the specimen could be accurately controlled. For this reason the tests were carried out using the same former but different stroke lengths. Tungsten inert gas (TIG) welding was used with: welding speed, 2.6 mm/s; amperage, 98-112 A; voltage, 10 V; and reversed polarity (-ve). Each test was 15 seconds long. The process was as follows. Welding was initiated at the start of each test and continued for 15 seconds when it was terminated. After 12 seconds from the initiation of the test the bend was applied to the specimen.

Table 3.2: Specimen list for Varestraint experiments organized according to stroke length applied

Time of Stroke (ms)	Stroke Length (mm)	Specimens
100	13.5	VA1001,VA1002,VA1003
200	27.0	VA2001,VA2002,VA2003
300	40.5	VA3001,VA3002,VA3003
400	54.0	VA4001,VA4002,VA4003
500	67.5	VA5001,VA5002,VA5003
600	81.0	VA6001,VA6002,VA6003
700	94.5	VA7001,VA7002,VA7003

3.2.3 Industrial scale weldability tests

The specimens used for the tests were plates of X65 with dimensions of 500 x 150 x 24 mm. To validate the method described a series of eight tests was conducted with target augmented strains between 2 – 11%. Eight different formers were manufactured (Table 3.3) to control the radius of the bend, with radii determined

by the equation for augmented strain (Equation 3).

Table 3.3: Radii of bending formers, stroke length and specimen codes according to augmented strain for X65 steel.

Augmented Strain (%)	Former Radius (mm)	Stroke Length (mm)	Specimens
2	600	14	TVA 2.1, TVA 2.2, TVA 2.3
3	400	20	TVA 3.1, TVA 3.2
4	300	27	TVA 4.1, TVA 4.2, TVA 4.3
6	200	40	TVA 6.1, TVA 6.2, TVA 6.3
8	150	54	TVA 8.1, TVA 8.2, TVA 8.3
9	133	61	TVA 9.1, TVA 9.2
10	120	69	TVA 10.1, TVA 10.2, TVA 10.3
11	109	76	TVA 11.1, TVA 11.2

A strain gauge was set 10 mm from the long edge of the plate near the initiation point of the welding process (as seen in Figure 3.15). The strain gauge was 20 mm away from the initiation point of the weld. Considering that the welding process generates heat and strain gauges are sensitive to temperature changes a number of things were examined during the experimental process. First of all it was assumed that since the welding procedure is not stable when it initiates, the welding torch moves 3.5 mm/s away from the strain gauge and the plate has a significant thickness that facilitates heat conduction the temperature on the strain gauge would not increase at levels that would affect the measurements. Furthermore, the moment that the plate would bend the weld pool would be 100 mm away from the strain gauge. This assumption was further supported by both experimental data and FEA simulation of the bending of the plates. The following figure (Figure 3.23) illustrates this and the FEA results will be presented in the results section.

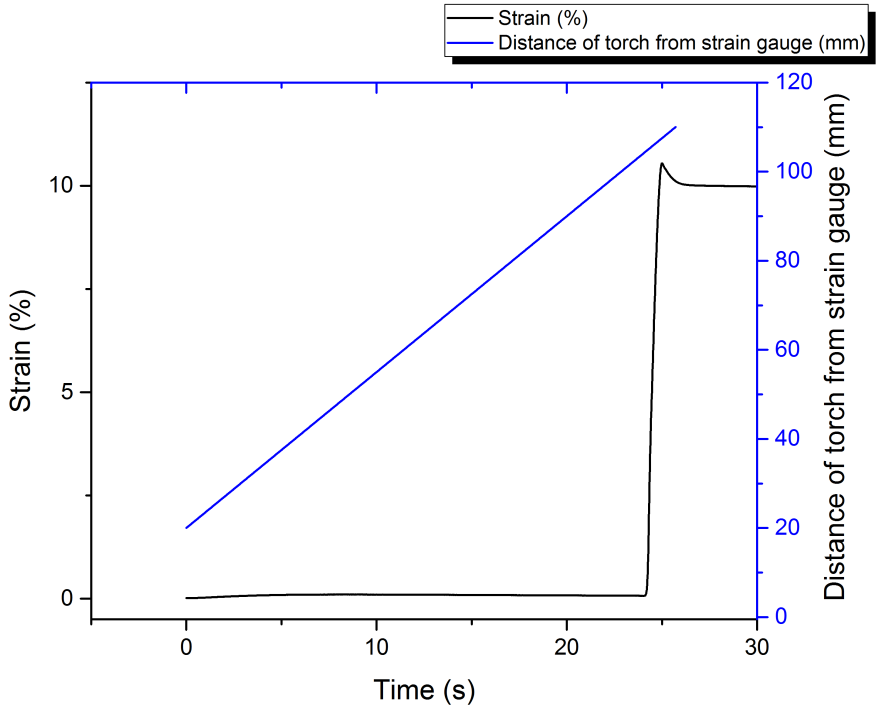

Figure 3.23: Strain gauge measurements while welding process is active. Blue line indicates the distance the welding torch has from the strain gauge.

Using the method, described in Section 3.2.1, tests for the required combinations of strain and stroke length were carried out (Table 3.3). Tungsten inert gas (TIG) welding was used with: welding speed, 3.5 mm/s; amperage, 225 A; voltage, 12 V; and reversed polarity (-ve). Each test was 25 seconds long. Welding was initiated at the start of each test, 30 mm from the long edge of the plate and continued for 25 seconds when it was terminated. The bending process was initiated at 23 seconds. This allows for the process to reach a steady state and to leave some space for the welding process to continue.

One specimen was bent without welding in order to verify that the strain applied, using the described method, was the intended strain. For that experiment, data was obtained from 4 strain gauges placed on the plate (Figure 3.24).

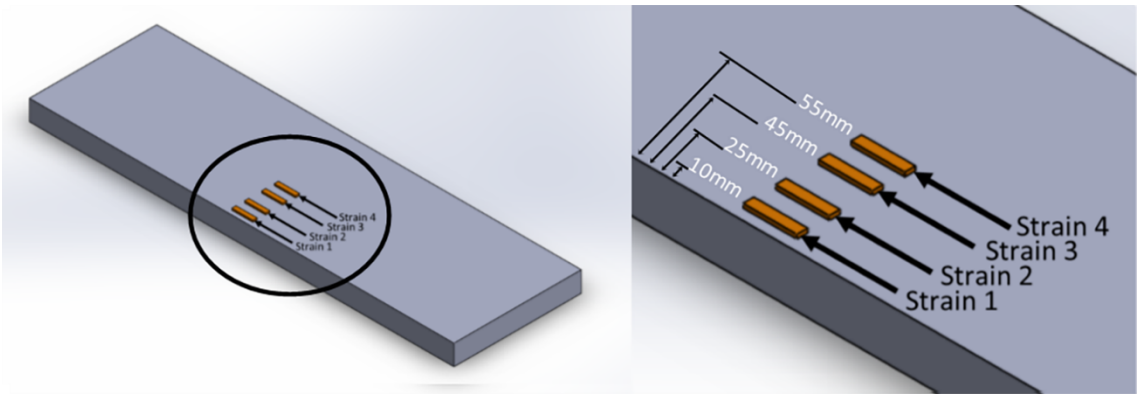

Figure 3.24: Strain gauge positions on plate.

This test was carried out because it was not possible to place strain gauges near the point where the cracks would appear during the test because they would not survive the welding temperatures. Given that the test includes a welding process it was only possible to include one strain gauge at the edge of the plate. The industrial Trans-Varestraint tests were also carried out on EN3B steel in order to obtain a dataset for comparison to the one obtained from the X65 steel. EN3B was chosen because it is known to be susceptible in hot cracking.

3.3 Post processing of weldability tests – Hot crack characterization

After the tests were carried out the specimens were photographed and examined using the Inspex HD 1080 stereo microscope in order to record the cracks as described in Section 2.3.2 (Figure 2.9). After all the required measurements were carried out and recorded two more tests were carried out on the specimens and samples extracted from them.

3.3.1 Liquid Dye penetrant (NDT)

Non-destructive testing (NDT) is a wide group of analysis techniques that is commonly used to test weld joints [74]. NDT is an integral part for industry

because when products are manufactured it is important to identify faults during production that will lead to failure. This identification of defects must take place without compromising or damaging the product [154]. The field of NDT has been extensively researched. At this point of time more than two hundred distinct NDT methods can be identified [155]. NDT for assessing weld quality is a common practice in the oil and gas industry [156, 157]. Non-destructive testing using liquid dye penetrants was carried out on selected samples from each experimental set (Table 3.3). For the tests the following consumables were used:

- MR CHEMIE MR® 68 C Penetrant red and fluorescent
- MR CHEMIE MR® 85 Remover
- MR CHEMIE MR® 70 Developer white

For the testing ASTM 1417 – 99 was used as a guide [158]. The process was carried out on all samples. Briefly the process can be described as follows. Use the remover to clean the surface well with a clean cloth. Wait for the remover to dry out completely (5-10 minutes). Shake the penetrant spray well, apply it on the weld and wait for 10 minutes. Remove the excess penetrant with a cloth and apply remover to the cloth in order to clean well. After cleaning apply the developer by spraying towards one direction only and then wait for the indications to appear.

3.3.2 X-ray computer tomography

X-ray CT (XRCT) has been used to identify defects, pores, cracks in materials with success [159–161]. In order to obtain more information on the hot cracks that have been generated from the weldability tests XRCT was carried out. The working principal of XRCT can be described as follows. The setup consists of an X-ray source that generates the X-rays. The X-rays pass through the samples but as the beams interact with matter they either get scattered or absorbed by it depending on the properties of the material. This results in only a percentage of the beams reaching the detector. In order to generate a three dimensional model of the sample

the sample rotates and multiple projections are obtained. This results in multiple images of the sample at different orientation. These images are used in order to reconstruct a three dimensional representation of the scanned sample.

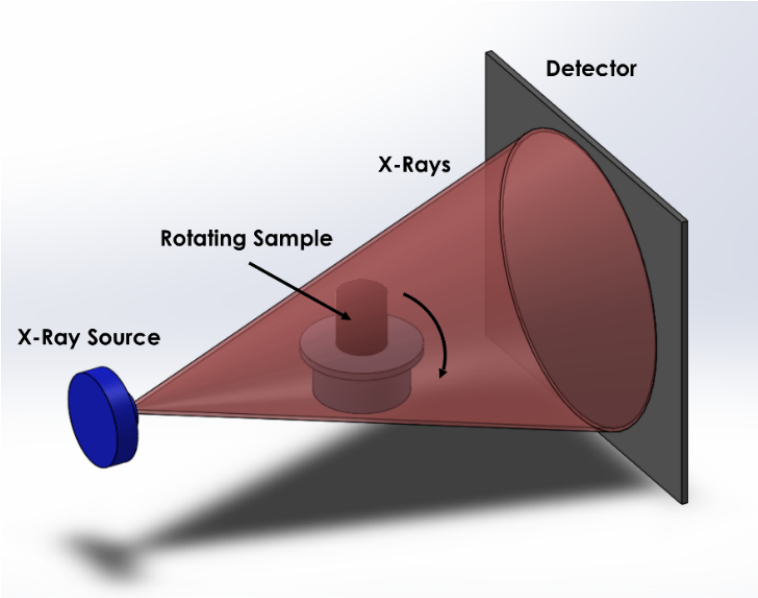

Figure 3.25: Working principal of X-ray computed tomography.

Samples were selected and specimens were sectioned in order to perform XRCT scans for three-dimensional sub-surface crack imaging and measurement. From each group of tests one sample was selected to be sectioned in order to observe how the cracks evolve at different levels of strains. Samples were sectioned to a size of a maximum thickness of 10 mm because of the limitations that X-rays have in penetrating steel [162]. As the volume in which cracks develop is limited to a specific point of the welds, extracting small enough samples, for XRCT, is feasible. A Nikon Metris X-TEK XT H 225 CT scanner was used with a rotating tungsten target and a 1 mm copper filter. The beam had an accelerating voltage of 150 kV and a current of 170 A. 1500 projections, each with a 2 s exposure, were acquired during each scan with the option to minimize ring artefacts enabled. Reconstruction of the scans was carried out using Nikon CT Pro 3D software. For the measurements and identification of the cracks on the specimens VGSTUDIO MAX 3.0 software was used.

3.3.3 Fractography

After XRCT examination the specimens were prepared in order for the cracks to be examined using an SEM (Quanta 650 FEG SEM). In order to open up the cracks without damaging them the following process was followed. The specimens were cut using precision cutting equipment along the centreline of the weld (Figure 3.26).

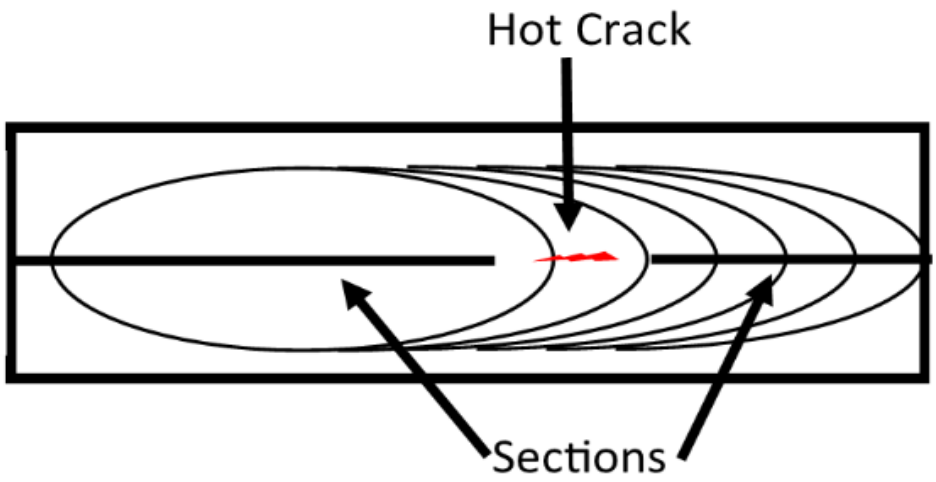

Figure 3.26: Sections on Trans-Varestraint specimen in order to expose the hot cracks.

The cut was carried out without the use of cooling in order to avoid contamination of the hot cracks. The cuts stopped 2-3 mm before the area of interest from both sides of the cracks. Following this preparation the specimens were quenched in liquid nitrogen and broken open. As a result the cracks were opened and were put in the SEM and examined using a voltage of 20 kV and spot sizes between 5.0-6.0.

3.4 Summary

Initially the material was characterized using metallographic inspection of the weld joint, hardness measurements and CTOD fracture toughness measurements. Following the characterization, a new method was introduced for carrying out the Varestraint and Trans-Varestraint tests which has a goal of the improved control of augmented strain applied during these tests. The method is based on the fact

when using a former with a specific radius the stroke length affects the strain applied on the sample. This means that if the radius of the former must dictate the strain applied there must be a specific stroke length that will apply the desired strain. In order to validate the method it was used in small scale Varestraint tests and industrial scale Trans-Varestraint tests. After the tests were carried out the samples were examined using NDT methods and then by XRCT in order to better measure, quantify and study the hot cracks generated by these tests. Finally the samples were prepared to open up the cracks generated from the experiments in order to be examined using a FEG SEM.

Chapter 4

Small Scale Varestraint Rig Upgrades

In this chapter the updates that were carried out on the small scale Varestraint rig will be described. Initially the state that the rig was received will be described and then the proposed upgrades will be presented.

4.1 Initial state of the rig

The small scale Varestraint rig that was used was designed for a previous study [39], as already mentioned, in order to be used in conjunction with synchrotron X-rays for the study of hot cracking. The rig was powered by a 12 V battery and the movement of the actuators was controlled using switches. This setup was used successfully but the following drawbacks were identified during the examination of the rig. The battery adds significant weight to the rig which is in its entirety made of steel and weighs 100 kg. Furthermore by controlling the rig using switches the possibility of errors occurring is increased plus depending on the operator the amount of time the actuators will move will vary. In order to improve the control of the experiments and the rig overall some alterations/upgrades were carried out. The rig utilized the following setup for its control. The commercial accessories and components in Table 4.1 were used.

Table 4.1: List of commercial accessories used in the small scale Varestraint rig

Part	Product Name	Product Code	Maximum Force	Supply Voltage	MAX Current	QTY
Traverse Actuator	LINAK LA12	121000-10401201	Push 750N Pull 750N	12VDC	4.6A	X1
Vertical Actuator	LINAK LA36	365F75-10150A20	Push 500N Pull 500N	12VDC	26A	X1
Actuator Control Switches	LINAK Marquardt – Rocker Switch	TR-1939.3314-00				X2
DC Motor Controller	LINAK TR-EM-288			10-35VDC	30A	X1
DC Motor Controller Programmer	LINAK TR-EM-236					X1

For that original setup of the rig the programmer is used to setup the controller that drives the actuators. Once the controller is programmed (speed of the actuators is set), the user uses the switches to primarily control the traverse actuator to push the sample into the desired position and to apply the weld. Then the traverse actuator is turned off and the second switch is used for the vertical actuator to bend the specimen. Since all the components that are used can work using a supply of 12 VDC a car battery is used to power the system.

4.2 Proposed upgrades

From what has been described, a significant number of improvements can be implemented in order to improve the performance of the rig. The improvements can be divided in three main categories.

- Power supply upgrade
- Control upgrade

- Data logging upgrade

Each category can be further divided in different levels/steps of upgrading that will be analysed further. At this point it must be stated that the amount of upgrades and their levels that can be achieved in the scope of this research varies and it depends mainly on the amount of weigh that will be put on them. Adding to that, given that the researchers' main field of work and specialisation is not in embedded systems and digital control, the changes will lead to improvements on the one hand but it is sure that there will be room for further improvements in the future.

4.3 Power Supply Upgrade

Using a battery to power this kind of equipment may provide with sufficient power to use the equipment but the power source cannot be easily monitored and controlled. Electronic equipment in general is sensitive to non-normalised power inputs and usually require regulated power inputs in order to perform accurately and reliably. Adding to that the cost of replacing a battery is significant and the use of a proper power supply will reduce both the cost of running the rig and its total weight.

The way the power supply of the rig can be improved is described in the following figure (Figure 4.1). The upgrade at this point can be achieved in two different levels. The first level is the most direct one and the one actually used for this project. Replacing the battery with an appropriate power supply that can drive all components of the rig safely and regulated. This will also provide with a basic level of protection in order to avoid problems with the power causing faults to the components.

The second level is the use of a more sophisticated power supply that can provide with multiple power lines that can supply multiple circuits with different voltage and ampere parameters. This will provide with better control of the power supply of the equipment plus it will provide with additional power lines that can be used in the future for other parts if needed.

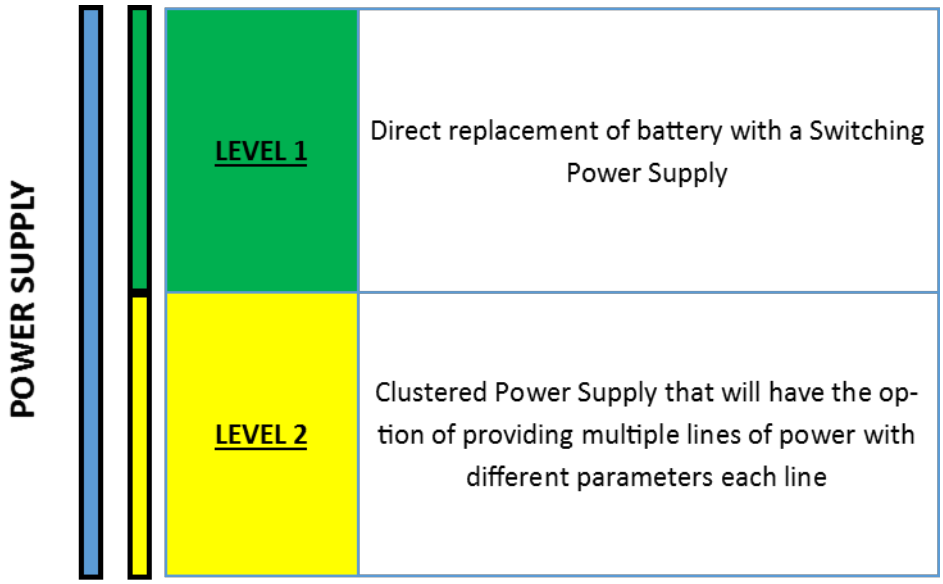

Figure 4.1: Power supply upgrade in levels.

4.4 Control Upgrade

The use of switches to control the movement of the actuators is sufficient but not fully controllable. There is no way for a person to accurately control the actuators and make them move in the exact same conditions every time. Thus leading to differences on the timing when the switches are pressed to move the actuators. Adding to that accidents may occur if the user presses the wrong switch at any point.

These accidents may just cause a loss of specimens but they can also lead to damages on the actuators that will prevent the rig from functioning. Controlling the rig using a PC or a laptop will increase the repeatability of the experiments and the control of the rig will be improved overall. The following figure (Figure 4.2) describes the ways that the control of the rig can be improved.

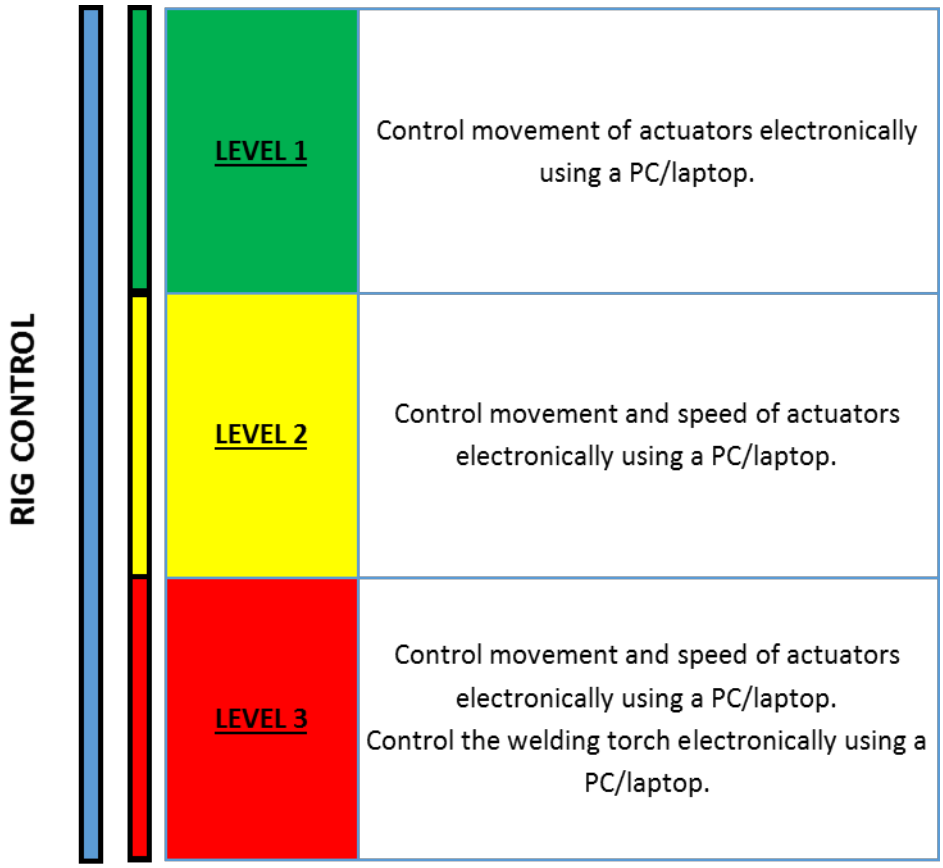

Figure 4.2: Rig control upgrade in levels.

These upgrades have been implemented at LEVEL 1 and provided with a significant control of the rig. There can be further improvements in the future that may increase the productivity and the amount of results that can be extracted by the Varestrain rig further.

4.5 Data Logging Upgrade

Given that a computer will be involved in the control of the rig the option of logging data electronically is becoming available. The amount and the quality of the data that can be recorded will improve the data output of the experimental procedure. Adding to that, it will provide with the opportunity of more intensive design of experiment with increased data output from the rig.

The amount of data and their quality is proportional to the amount of control the

computer has on the rig. Additionally, the amount of sensors and measurement points the equipment has in total also adds to the data. The only data that were recorded from these experiments were data that were extracted from post experimental examination of the samples or in the case of in-situ experiments the data that were extracted from those experiments.

The only data that the user can get are the parameters that are already set in the controller of the speed and the time (in seconds primarily, millimetres secondarily) that the user is calculating and recording when the experiment is conducted. The way the data logging can be upgraded and the levels that can be achieved are described in the following figure (Figure 4.3). For this project the data logging was implemented at LEVEL 1.

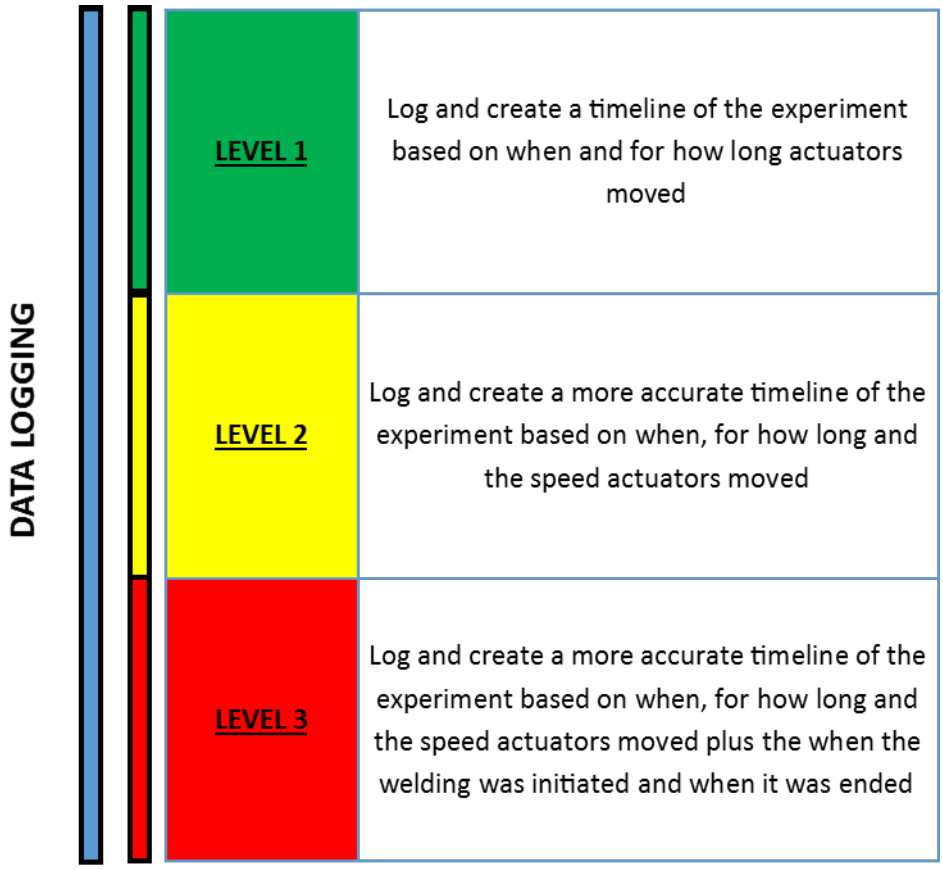

Figure 4.3: Data logging upgrade in levels.

4.6 Technical details of the upgrades

In order to upgrade the experimental setup, in this study the following changes were carried out in order to facilitate the integration of a computer with the rig. Table 4.2 shows the components used.

Table 4.2: Components needed for the upgrade

Component	Product Code	Operating or Output Voltage	Output Current
Micro-controller board	Arduino Nano	7-12V	
Switching power Supply	PSP-600-12	12V	50A
DIP Series Reed Relay	D1A051D00	5V	1A

The updates of the control are described in Figure 4.4. The battery has been replaced by a more reliable power supply. The role of the switches that controlled the actuators is substituted by the control unit that was introduced and used to send signals to the actuator drivers in order to move the actuators.

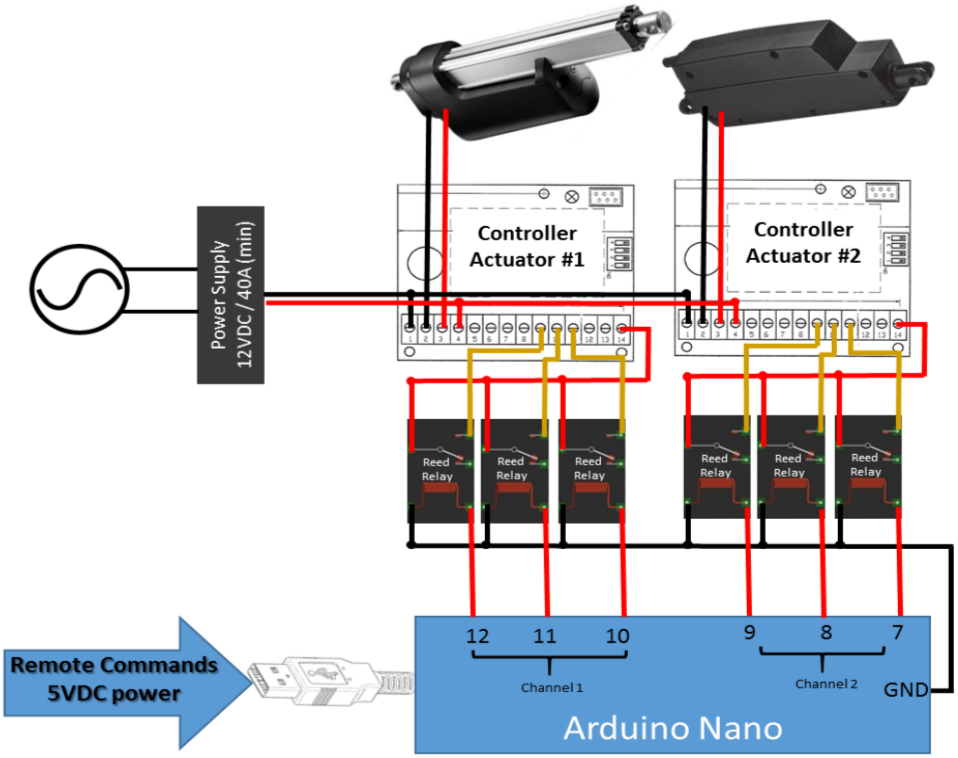

Figure 4.4: Schematic of the upgraded setup for the small scale Varestraint rig

This setup was separated into two sections. One section was the control section and the second was the power section. As Figure 4.5 shows, the Arduino Nano and the relays are housed in a box that also has LED indications about the movement of the actuators. This is connected to the power section that takes as input the commands of the control sections (just like the switches used to do) and the output is the movement of the actuators. This allows for increased control of the actuators since the time that the actuators will move forward and backward is controlled by the Arduino digitally.

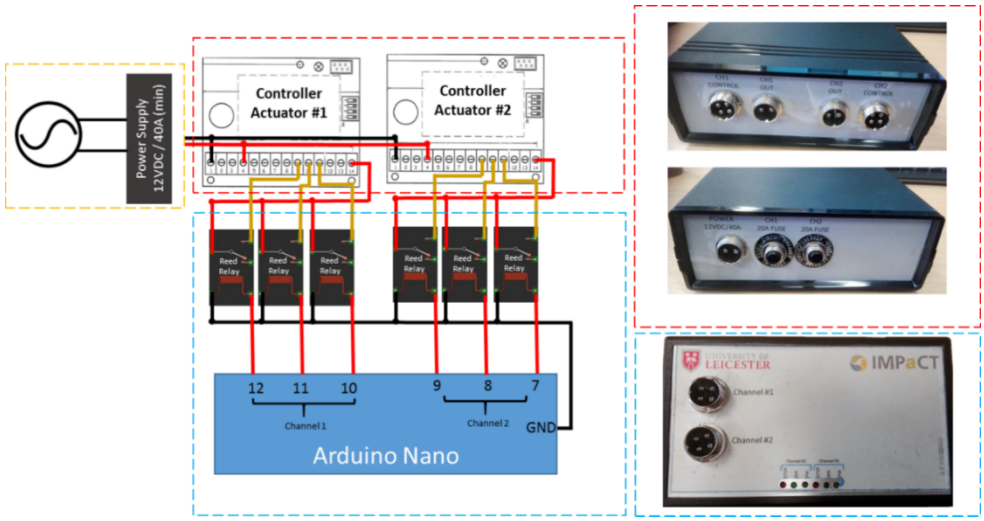

Figure 4.5: Control section (blue dashed lines) and power section (red dashed lines) of the small scale Varestraint rig setup.

4.7 Implementation

The upgrade of the Varestraint experimental rig can occur in multiple stages. At this point it must be made clear that not all the possible upgrades will be implemented for this project. This is due to the amount of time and research required to achieve these upgrades and the fact that the scientific field that this project is based on is materials science and not embedded systems or digital control. Despite these limitations the introduction of a low level automatic control of the experimental rig will certainly lay the foundation for further improvements in the future. For these reasons all the upgrades were carried out to Level 1. The first step that was realised was to solve the powering issue of the rig. A switching power supply replaced the current setup that required a battery to power the rig. Continuing, the electronic components were used to replace the switches that were used in order to control the movement of the actuators (not their speed). For this upgrade a printed circuit board was designed in order to accommodate the electronic components described previously. During the circuit board design the software that will control the components, the DC motor controller and will create logs of the process was developed. Phase one of the upgrades that will cover the level 1 that is discussed previously will be considered completed after the completion of the testing of the rig after these steps have been

implemented. After the completion of phase one the basic control of the rig will be achieved. This will be considered the groundwork for future upgrades. The future upgrades can include the following. Digital control of the speed of the actuators. This will increase the level of upgrades to level 2 for the control and logging parts of the equipment. It will also provide with even better control and more data to be obtained from the rig. After these phases the possibilities of upgrades and improvements spreads in many fields. For example thermocouples or other sensors can be introduced to the rig and use an updated interface to get more data from the experiment. Another possible upgrade is to also control the use of the welding torch (ON/OFF) from the computer to eliminate the need for the user to control when the weld starts and stops. Adding to that sensors that provide feedback from the actuators can be added in order to avoid overloading them or even to calculate the force that the bending actuator applies on the specimens.

4.8 Summary

When conducting an experiment the control of the parameters of the experiment is essential. Adding to that the amount of data that can be extracted from an experimental process is also essential. This means that when an experimental process is being developed it is critical for the process to be designed to produce as much data as possible in order for them to be studied and analysed. The experimental Varestraint rig that was designed to study the hot cracking susceptibility of steels and has already been used in combination with a synchrotron light source has produced a significant amount of date. Its use is based mainly on manually manipulating welds and specimens and the focus was the collaboration with synchrotron light sources. This leads to data being extracted mainly from the x-ray scans and the post examination of the samples. But the parameters and data that occur from the setup itself are minimal. The possibility of upgrading the equipment and laying the groundwork for further improvements for future upgrades was discussed. The focus at this point it to implement a basic level of digital control to the rig in order for the experimental

parameters to be better controlled and possibly provide with some usable data for further analysis. This can be achieved by introducing some electronic components that will provide the user with the option to control the rig using a PC/laptop and record the timeline of the experiment in a consistent and repeatable manner.

Chapter 5

Experimental Data

This section will present the experimental data obtained using the methods described in the previous chapter. The section will initiate with the general characterization of the API-5L X65 steel and proceed to the weldability tests that have been carried out.

5.1 Characterization of API-5L X65 pipe sample

5.1.1 Microscopic Examination

Both optical and scanning electron microscopy was carried out in all regions of the weld joint, from which a composite image was made. Figure 5.1 shows all the regions of the welding joint. From left to right the regions are the base metal (BM), the recrystallization zone (RZ), the heat affected zone (HAZ), the coarse grained heat affected zone (CG-HAZ) and the fusion zone (FZ).

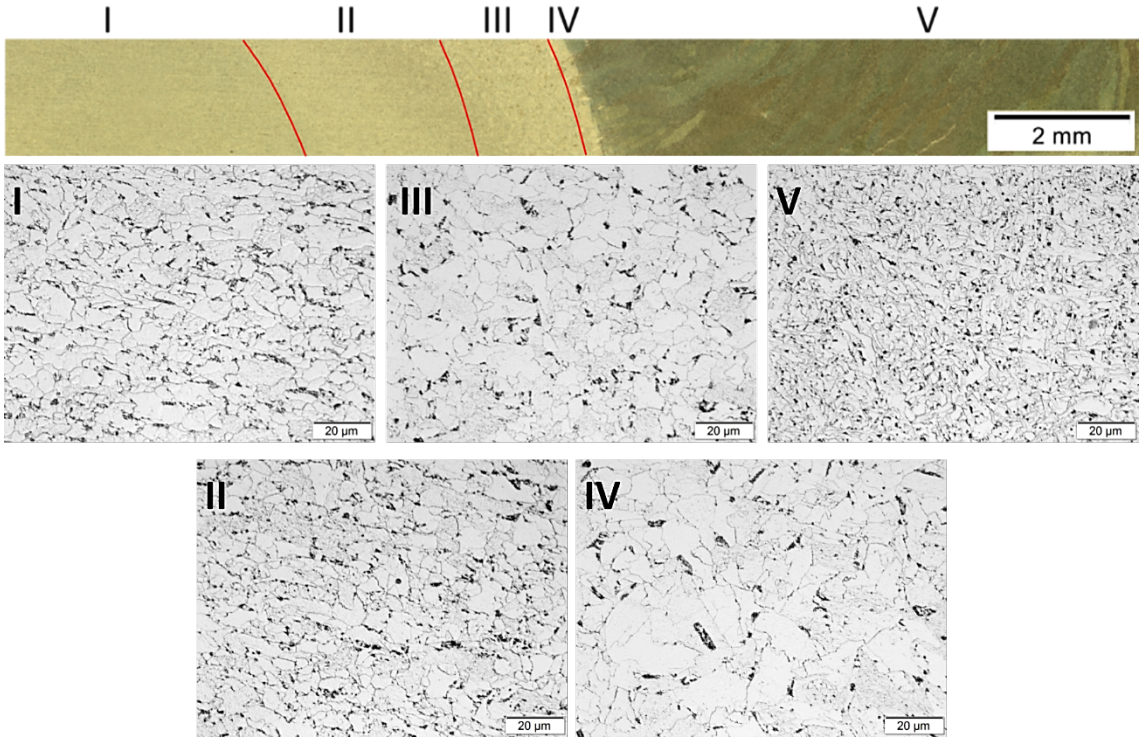

Figure 5.1: SAW weld Joint of X65 steel (optical microscope) I) Base Metal (BM) II) Recrystallization Zone (RZ) III) Heat Affected Zone (HAZ) IV) Coarse Grained HAZ (CG-HAZ) V) Fusion Zone (FZ)

Analysis of the FZ (Figure 5.2) revealed columnar grains with a specific orientation towards the heat source. The microstructure of the region is predominantly acicular ferrite (AF).

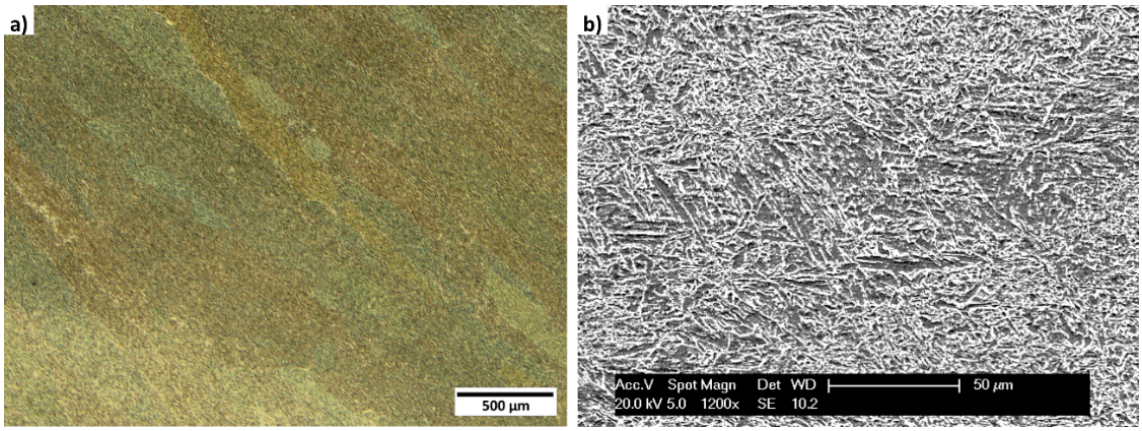

Figure 5.2: Microscopy of FZ a) columnar grains oriented towards the heat source. b) acicular ferrite dominated structure with small regions of polygonal ferrite.

Closer examination of the FZ (Figure 5.3) confirmed that the structure is mainly AF with some polygonal ferrite phases also present.

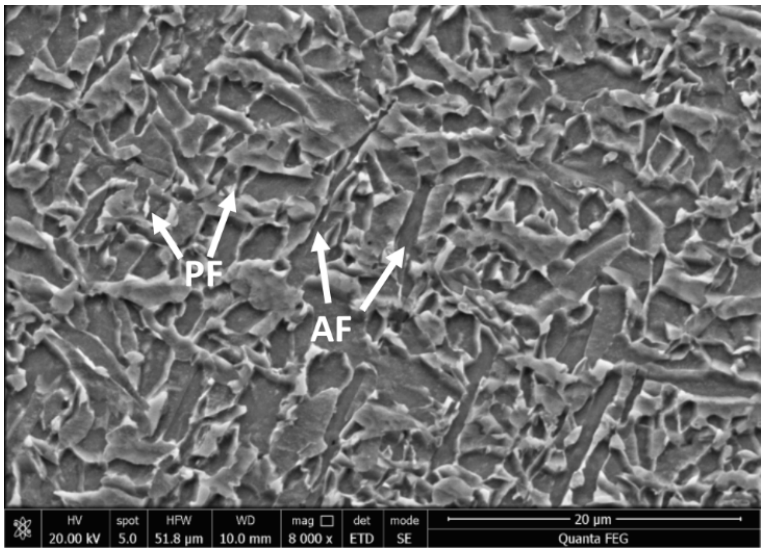

Figure 5.3: SEM image showing the acicular ferrite dominated structure of the FZ with some polygonal ferrite present.

By examining the BM on both sides of the weld, areas that contain predominately ferrite(Figure 5.4)

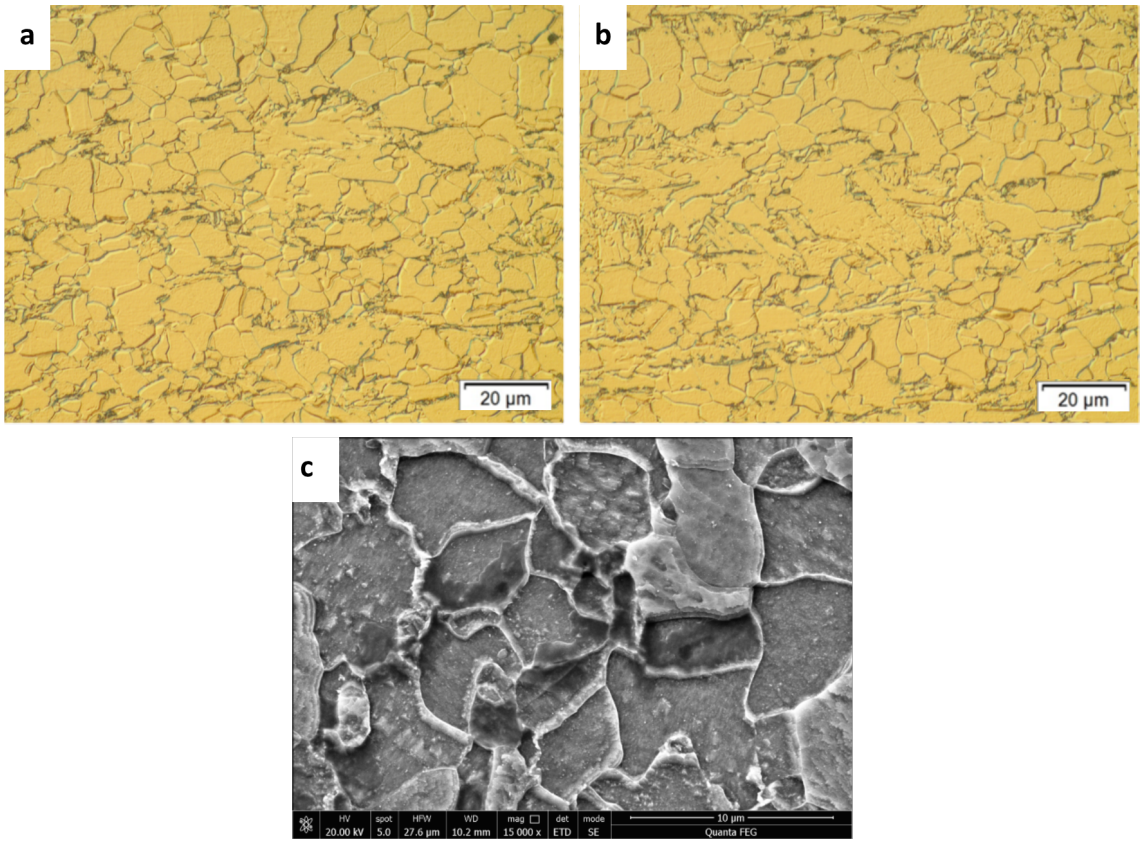

Figure 5.4: a) BM left of the FZ b) BM right of the FZ c) SEM image of ferritic structure.

The grain size measurements were carried out according to the ASTM E112-12 Standard test method for determining average grain size. The method used was a general intercept procedure at a magnification of 1000x as shown in the following figure (Figure 5.5).

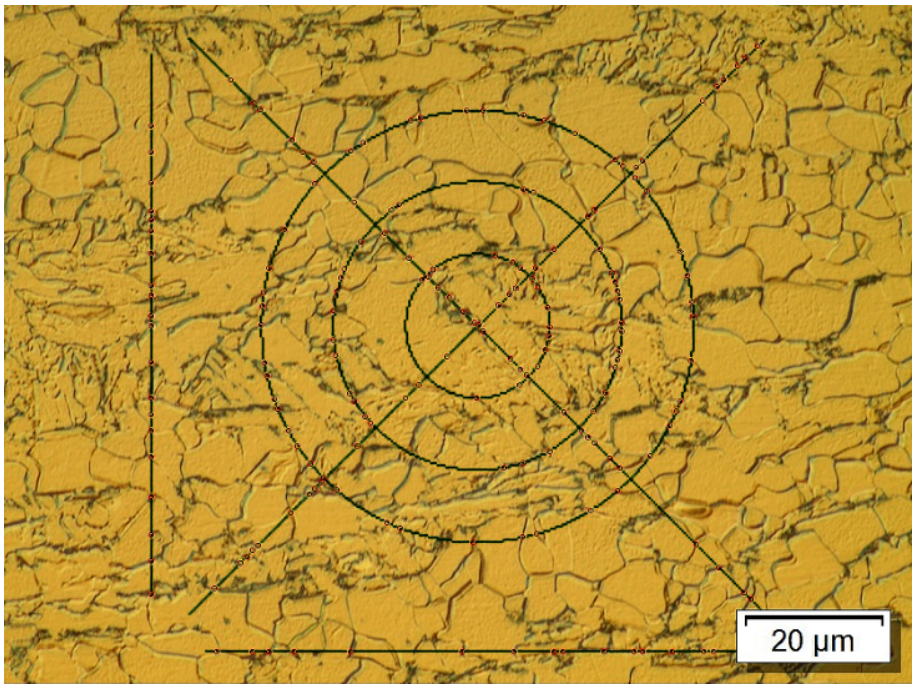

Figure 5.5: Intercept pattern for a field.

Measurements were carried out on the base metal (BM), on eight (8) sites on the right side of the FZ and nine (9) sites on the left of the weld zone. Standards state that in order for the grain size measurements to be valid the relative accuracy (RA) of the measurements must be below 10%. This value indicates the percentage of variation between measurements. The measurements on both sides of the FZ had an RA below 10%. Both sides of the BM have the same grain size of ASTM G 12.5 (4.7 µm ± 0.4). Nevertheless there are some small differences between the two sides of the weld in the BM as shown in the following graph. (Figure 5.6). It appears like the average intercept length on one side of the weld is slightly below the other. Despite that difference both sides of the BM are classified at ASTM G 12.5.

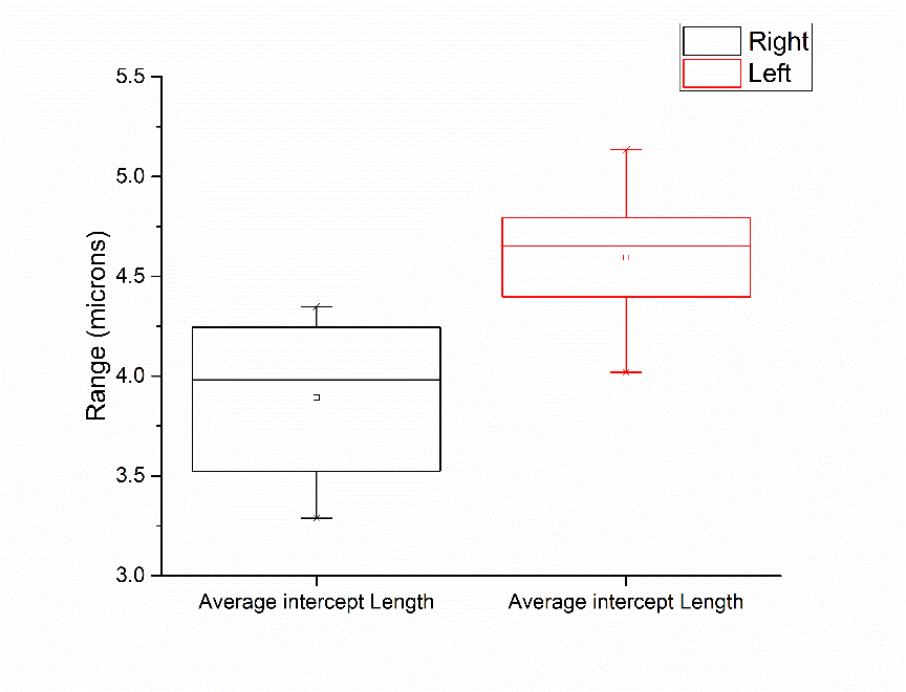

Figure 5.6: Graph illustrating the intercept length measurements and the differences between left and right areas of the FZ.

5.1.2 Hardness testing

As described previously (Section 3.1.2), hardness measurements were carried out. Before measurements were carried out the hardness tester used was calibrated and a correction curve generated in order to adjust the indication that the hardness tester was providing. The following figure (Figure 5.7) indicated that at the range of hardness between 400 HV02/3923 MPa and 600 HV02/5884 MPa there is a slight deviation of the measurements from the nominal values. Nevertheless, according to ASTM standards the values are repeatable and these deviations can be corrected.

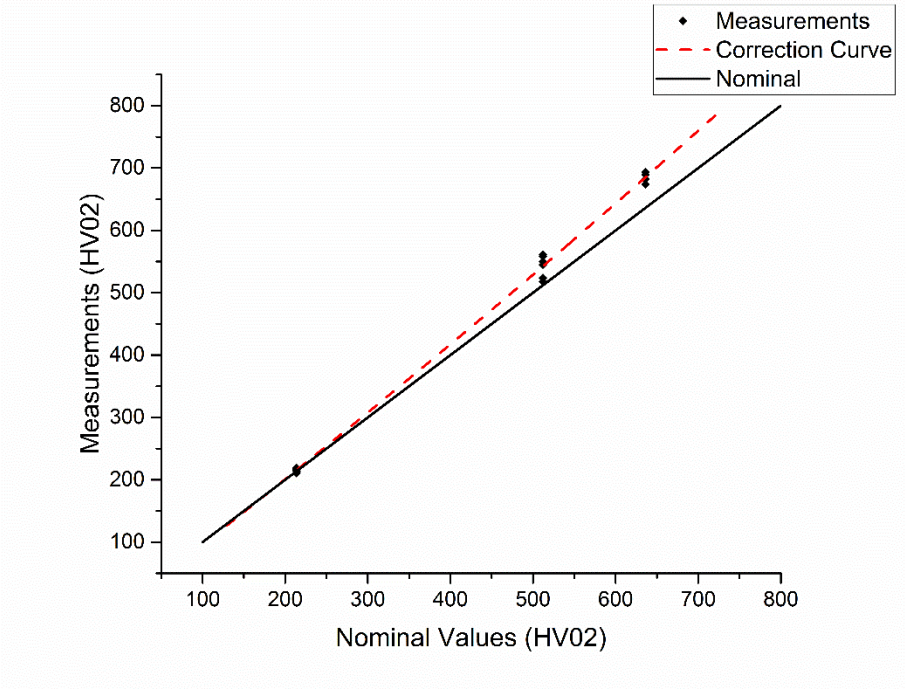

Figure 5.7: Correction curve for Tukon hardness tester.

A hardness map of the weld joint was obtained using this hardness tester. The test block (Figure 5.8) had a surface with dimensions of 78.50 x 18.80 mm and a thickness of 14.75 mm. A matrix of HV02 measurements was obtained with 28 rows and 350 columns resulting in 9800 hardness measurements.

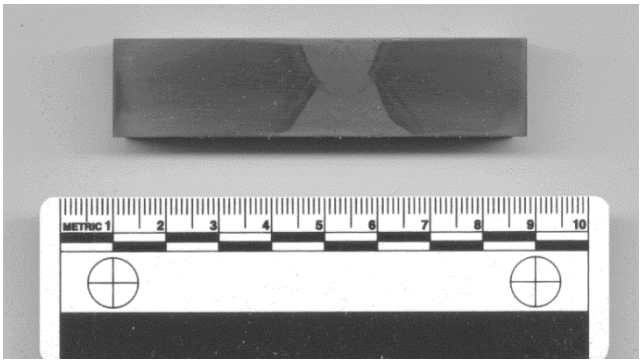

Figure 5.8: Test block used for hardness maps.

The hardness measurements presented (Figure 5.9), showed a clear difference in hardness that corresponds to the main areas of the weld (FZ, HAZ, BM). Hardness of the FZ has an average of 235.3 HV02 ± 7.4. BM has an average hardness of 198.4 HV02 ± 5.9 and the heat affected zone has an average of 179.8 HV02 ± 4.9. This

figure also indicates that the heat affected zone of the weld joint is not completely symmetrical as far as hardness is concerned.

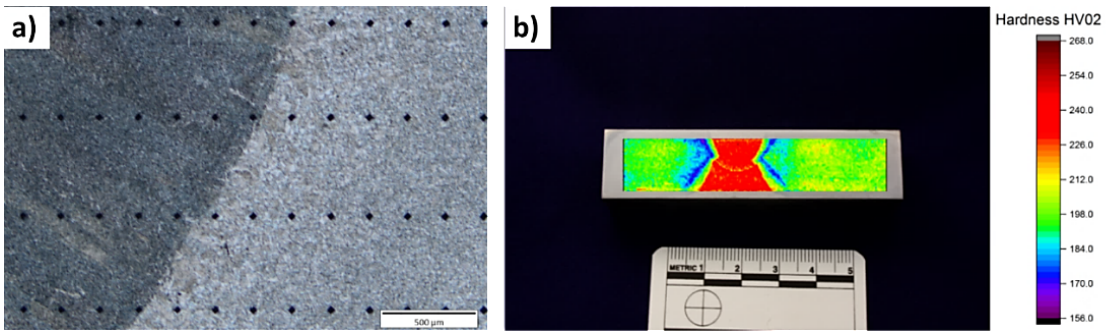

Figure 5.9: a) Microscopic image of hardness measurements b) hardness map on sample

By examining the map closer it becomes clearer that the hardness distribution on the weld joint is not symmetrical but the key areas of the weld joint can be identified as shown in the following figure (Figure 5.10).

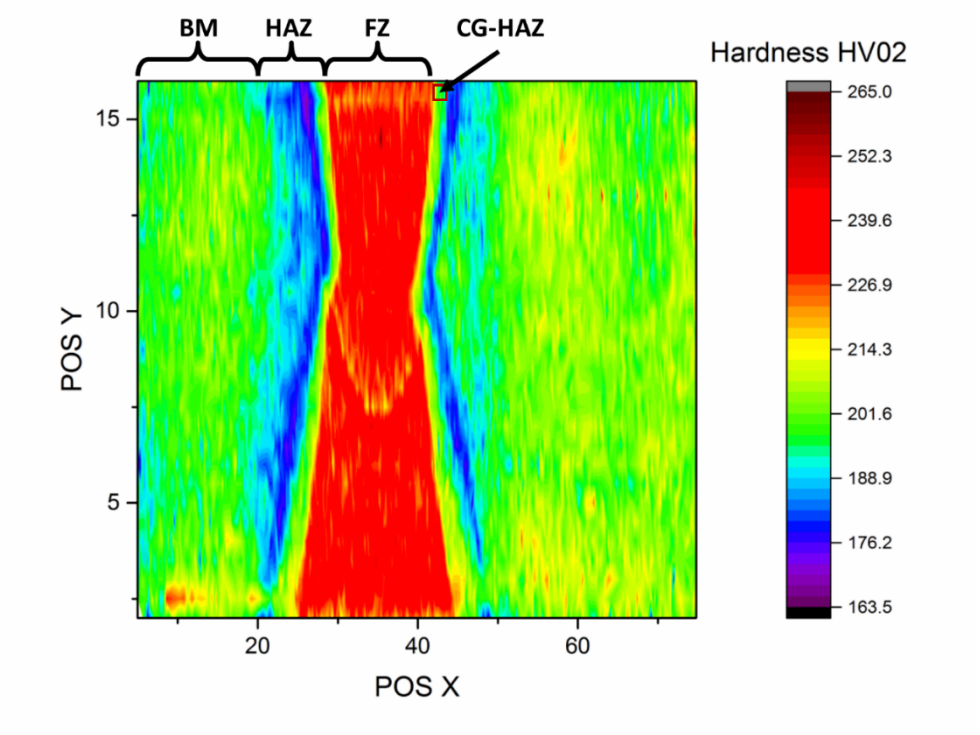

Figure 5.10: Hardness map and correlation with the zones created during welding.

5.1.3 Fracture toughness CTOD

Samples were subjected to a three point bent test to measure their fracture toughness. The results of the tests are presented at Table 7.1 (Appendix A). At this point it must be noted that the expected properties of K_{IC} could not be obtained because the size of the specimens did not comply with the ASTM standards so the value that the experiment did provide was not the K_{IC} value but the K_Q value. This is primarily because as it is mentioned on the ASTM E399- 09 standards in paragraph 9.1.3 in order to be able to calculate K_{IC} the ratio of P_{max}/P_Q must not exceed 1.10 in order for the test to be considered a valid K_{IC} test [158, 163]. The average ratio of P_{max}/P_Q for the experiments that were carried out was 2.09.

In order to meet the requirements of the standards and obtain a valid K_{IC} value the specimen must be bigger. In the specific situation where there is a need to measure the fracture toughness in specimens taken from a pipe where the notch contains 50% HAZ and 50% FZ this is not possible. This leads to elastic-plastic fracture toughness results. Another check that must be carried out is that crack lengths are measured so that each individual measurement is within the limits α_0 - 0.05B $< \alpha_0 < \alpha_0 + 0.05$B. Tables 7.2, 7.3 (Appendix A) include the crack length measurements that were taken and their limits. It is shown that on the IDF003 the first crack length is barely out of the limits.

The experimental results obtained were compared with previous results on the same type of specimens [39]. Previous tests were carried out with the notch placed 100% in the fusion zone. Results showed that the fracture toughness of 50% HAZ 50% FZ specimens is lower than the fracture toughness of the 100% FZ specimens (Figure 5.11).

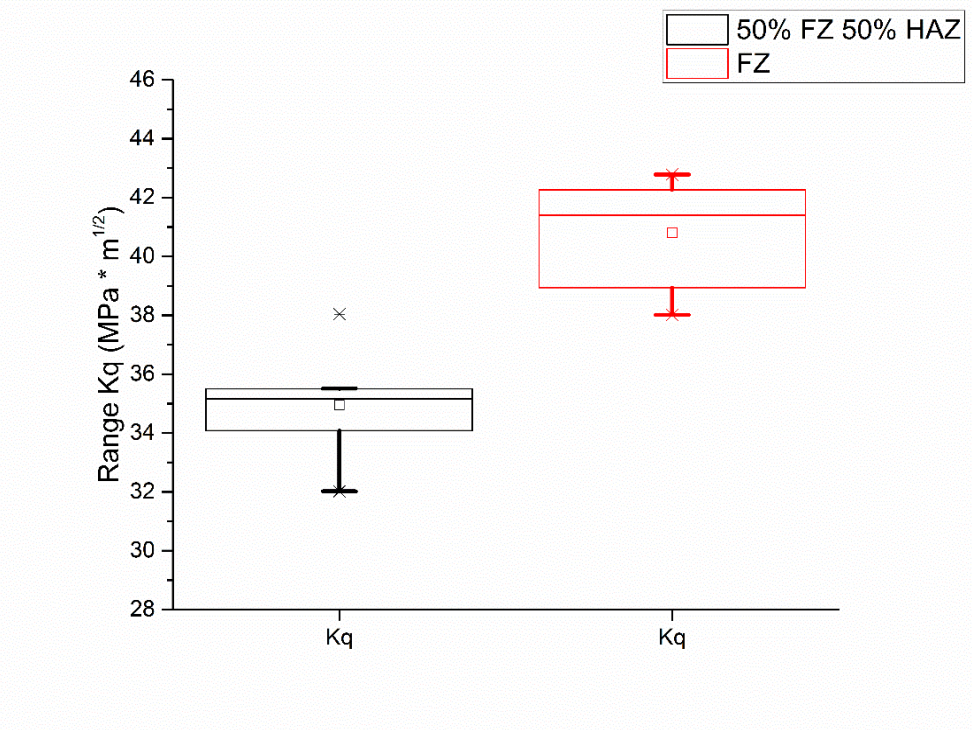

Figure 5.11: Fracture toughness values (RED) 100% FZ work carried out by Lee Aucott [39], (BLACK) 50% HAZ 50% FZ.

After the testing was complete the specimens were broken and the crack length was measured according to ASTM E1820-09 standards. This was done in order to get the data needed to calculate basic values of parameters for the fracture toughness. In order to separate the crack length caused by the test and the crack that was caused from the breaking of the specimens the specimens were dipped in liquid nitrogen before they were broken in order to force a brittle fracture.

By examining all the specimens macroscopically two basic observations can be made. The first one is that the surface of the specimens examined does not have exactly 50% FZ and 50% HAZ. Measurements that make that clear are illustrated in the following figure (Figure 5.12).

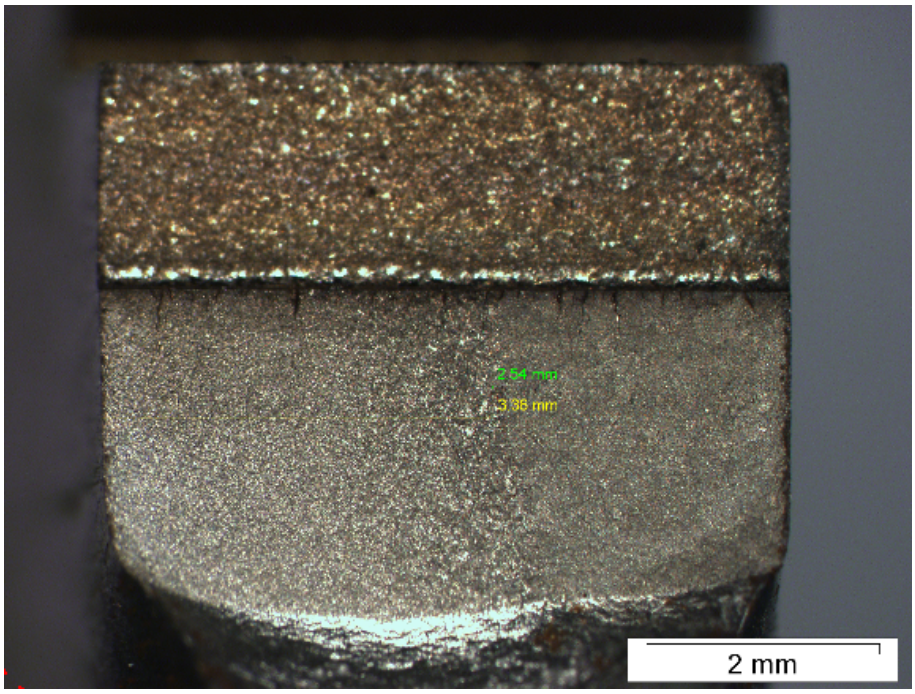

Figure 5.12: Length measurements comparing HAZ and FZ on the fracture surface.

The following table (Table 5.1) contains the results of these measurements and the diagram following this table (Figure 5.13) shows the comparison between the two areas.

Table 5.1: Area estimations for fracture toughness specimens

	IDF (Inner Diameter of Fusion)				ODF (Outer Diameter of Fusion)			
	001	**002**	**003**	**004**	**001**	**002**	**003**	**003**
Whole Surface area (mm2)	15.7	15.4	15.1	15.9	14.4	14.0	16.8	11.3
FZ Area (mm2)	5.9	9.1	7.4	13.1	6.3	7.6	6.7	5.9
HAZ Area (mm2)	9.8	6.2	7.6	2.8	8.0	6.3	10.1	5.3
Percentage of FZ area (%)	37.54	59.32	49.52	82.36	44.15	54.62	39.99	52.68
Percentage of HAZ area (%)	62.46	40.68	50.48	17.64	55.85	45.38	60.01	47.32

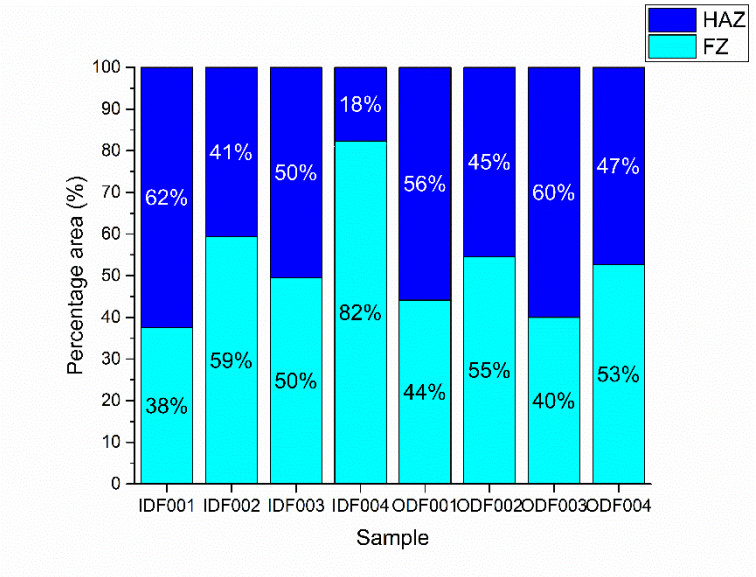

Figure 5.13: Comparison between FZ and HAZ areas.

The second observation has to do with the fracture surfaces themselves. As it is shown in the following figure (Figure 5.14) the fatigue crack length differs between

the FZ and HAZ. It seems that the fatigue crack length of the areas of HAZ is longer than the length of the FZ.

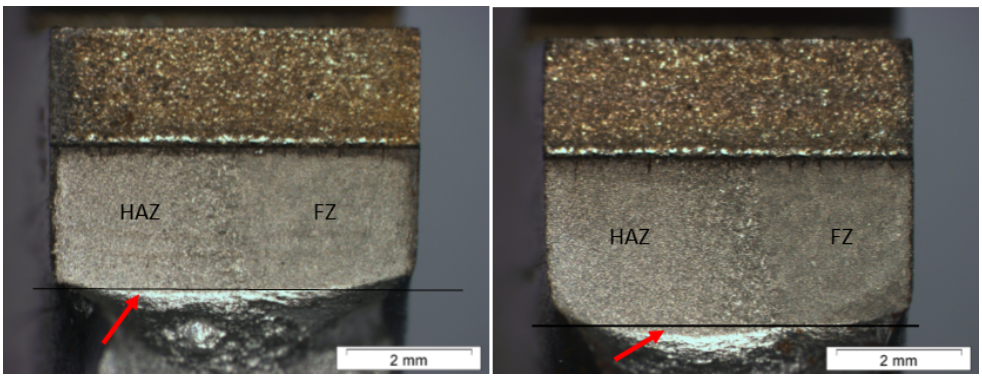

Figure 5.14: Difference in crack length between FZ and HAZ.

SEM examination of the fracture toughness specimens revealed that the fracture surface differs within the same specimen. As shown in Figure 5.15 the interface between the FZ and HAZ is visible and the morphology of the fracture differs between them. Both areas present with a ductile fracture but the FZ has very small and uniform dimples compared to the HAZ which has larger and deeper dimples.

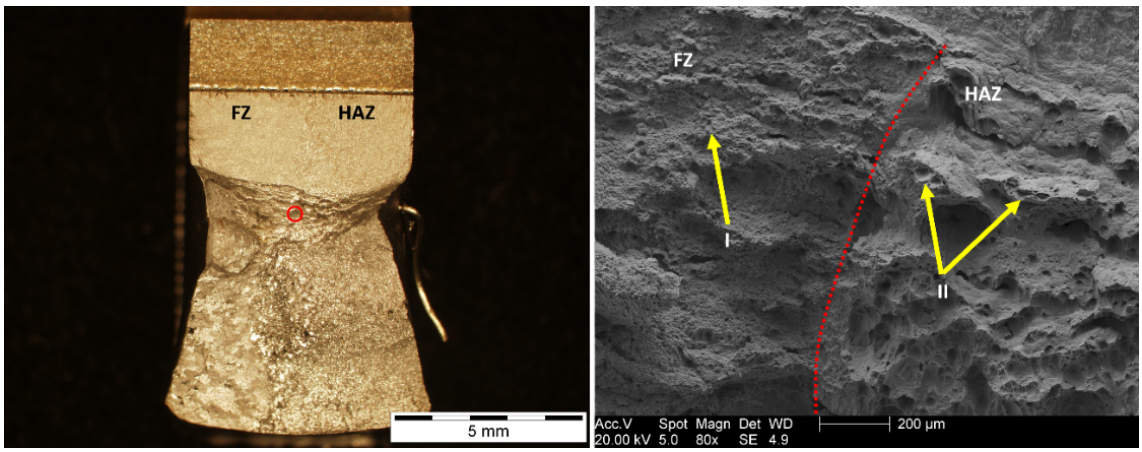

Figure 5.15: Interface between fusion zone and heat affected zone in fractured specimen (I: Ductile fracture in FZ with a fine morphology and small dimples, II: ductile in HAZ with larger dimples) interface between the two zones indicated by red dotted line.

5.2 Weldability Tests

5.2.1 Small Scale Weldability tests

X65 steel samples were subjected to a small scale Varestraint test as described in Section 3.2.2. The tests were carried out as designed with only the addition of one extra sample at the following sets.

- At stroke length 54.0 mm (VA4004)
- At stroke length 94.5 mm (VA7004)

The reason for these additions was because one of the original three specimens for each set was slightly over-bend. A general view of the welded samples is shown in the following figure (Figure 5.16).

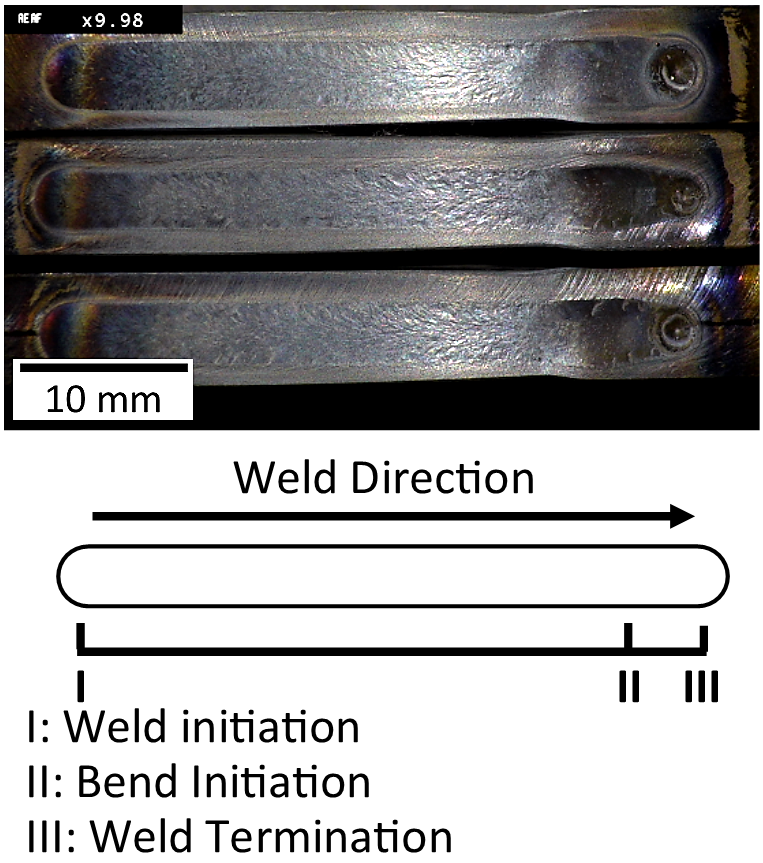

Figure 5.16: Small scale Varestraint specimens set of VA600 and a schematic outline of the experimental procedure.

Samples were examined under a stereoscope and measurements of MCL and MCD were taken as shown in the following figure (Figure 5.17). As the figure shows the MCL was measured for each crack present along the axis of the crack. On the other hand MCD was measured along the centreline axis for each crack.

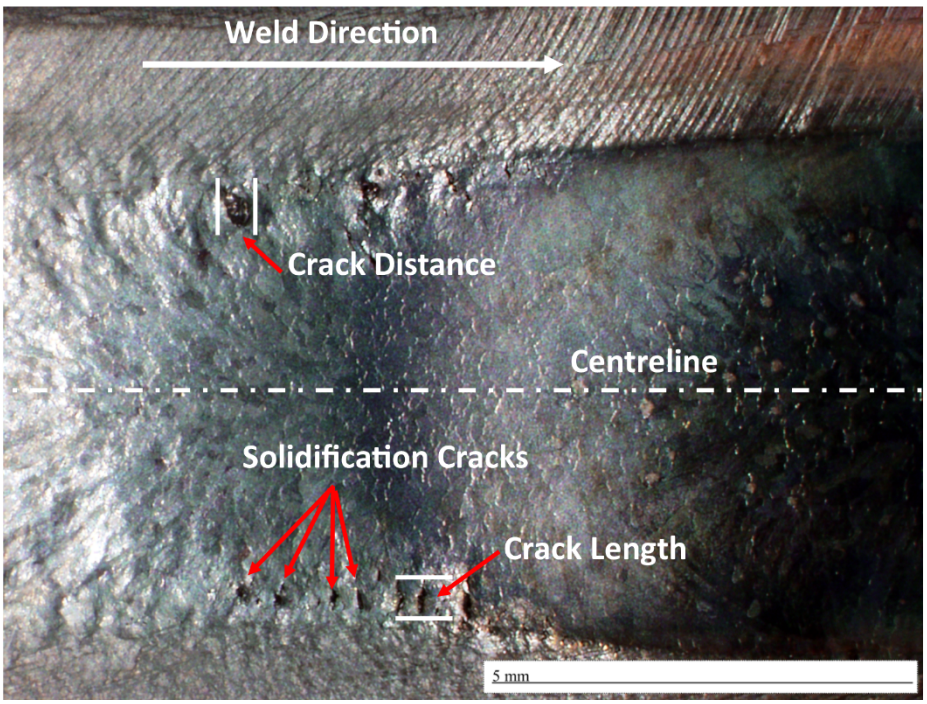

Figure 5.17: Solidification cracks on X65 sample. (VA7002: Stroke length 94.4mm)

After all the measurements from all the specimens were recorded the TCL was calculated and plotted in a graph of TCL vs stroke length (Figure 5.18). The results showed that as the stroke increases the TCL also increases and does not show any indications of reaching a saturation point. This is shown by the red indicative line in the graph.

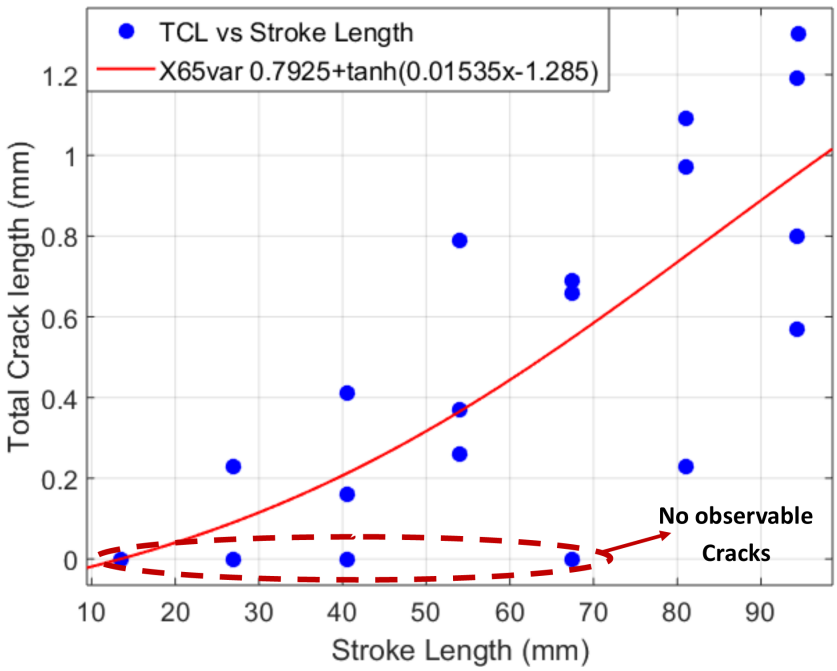

Figure 5.18: Total Crack Length vs Stroke Length of all Varestraint test specimens. Red line shows that the trend of the TCL does not exhibit any saturation point.

Measurements of MCD of the same specimens were plotted against the stroke length in order to view the evolution of the MCD as stroke increases. The results (Figure 5.19) provided indications of a possible threshold and saturation points like the one described in Figure 2.11 in Section 2.3.2. However the shape of the line that describes the evolution of MCD does not clearly have the shape described in Figure 2.11. Nevertheless because the maximum stroke length of the experimental setup was 94.5 mm the possible actual saturation point could not be clearly identified. It can only be assumed that the experiment approaches some saturation point given the limited amount of liquid metal during the process.

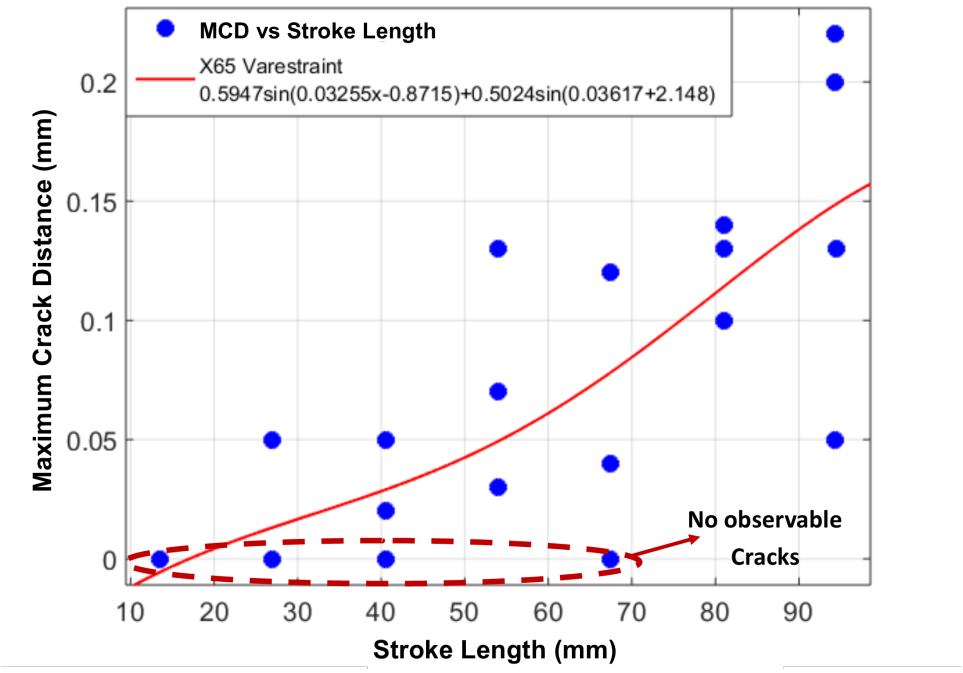

Figure 5.19: Maximum Crack Distance vs stroke length of all Varestraint test specimens. Red line shows that the trend of MCD exhibits a possible saturation point.

At this point it must be noted that for all the experimental data obtained, multiple fitting methods were tried in order to examine if the evolution of the crack lengths fit the theoretical one (Figure 2.11). There is not currently a mathematical model in order to attempt to fit the data obtained to it. The following tables (5.2, 5.3) show that the small scale varestraint test results do not seem to be able to provide with an accurate enough model that reflects the evolution of hot cracks.

From the parameters shown in the tables it is clear that MCD is a more reliable parameter to observe for these tests. This is evident by comparing the sum squared error (SSE) performance between MCD and TCL. MCD has a significantly less SSE value from TCL regardless the fitting equation used. Nevertheless, both TCL and MCD fittings have low R-Square and adjusted R-Square values which are indicating low accuracy.

Table 5.2: TCL vs Stroke Length for the small scale Varestraint test

Fit Type	SSE	R-Square	Adj R-sq
a*sin(b*x+c)	1.426	0.639	0.533
a+tanh(b*x+c)	1.427	0.639	0.603
a*x+b	1.467	0.629	0.611
a*exp(b*x)	1.504	0.619	0.601
a+atan(a*x+b)	1.576	0.601	0.582

Table 5.3: MCD vs Stroke Length for the small scale Varestraint test

Fit Type	SSE	R-Square	Adj R-sq
a*sin(b*x+c)	0.039	0.610	0.495
a*exp(b*x)	0.040	0.601	0.582
a*x+b	0.041	0.587	0.567
a+atan(a*x+b)	0.041	0.586	0.566
a+tanh(b*x+c)	0.100	0.000	-0.100

5.2.2 Industrial Scale weldability tests

X65 and EN3B samples were tested using the industrial scale rig as described previously in Section 3.2.3. The experiments were carried out as designed. General view of the X65 samples is shown in the following figure (Figure 5.20).

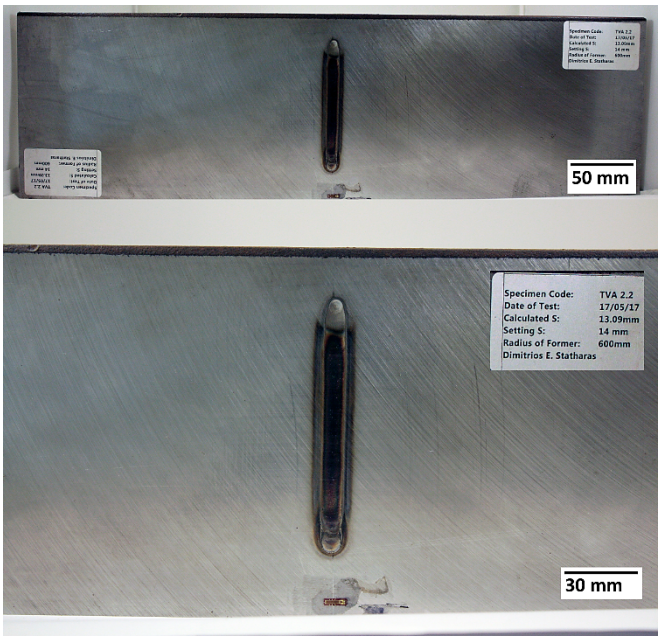

Figure 5.20: General view of Trans-Varestraint specimen (X65 steel).

Samples were examined under a stereoscope and the MCL and TCL values were recorded. The following figure shows how crack lengths and crack distances were measured. This shows that indeed for the Trans-Varestraint tests the MCD is equal to MCL.

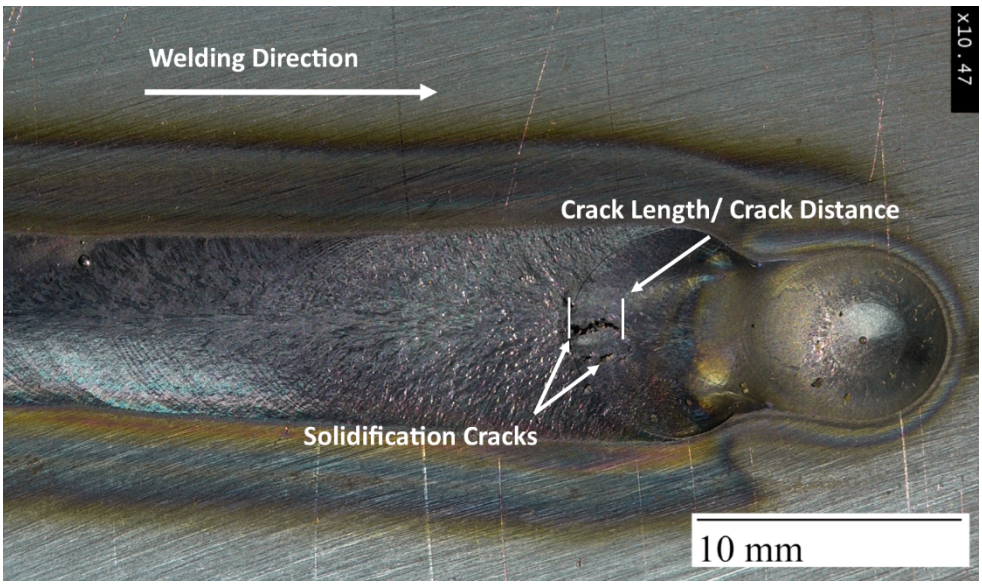

Figure 5.21: Solidification cracks on X65 sample. (TVA 10.2: augmented strain applied 10%.

Measurements were carried out on all of the samples and the TCL was plotted against the augmented strain as shown in Figure 5.22. Results show that EN3B

steel produces an amount of crack lengths higher than the X65 overall. This is clear from the fact that X65 presents a TCL of below 1 mm at 4% where EN3B reaches a crack length of almost 6 mm. Adding to that EN3B presents cracks at lower augmented strains than X65.

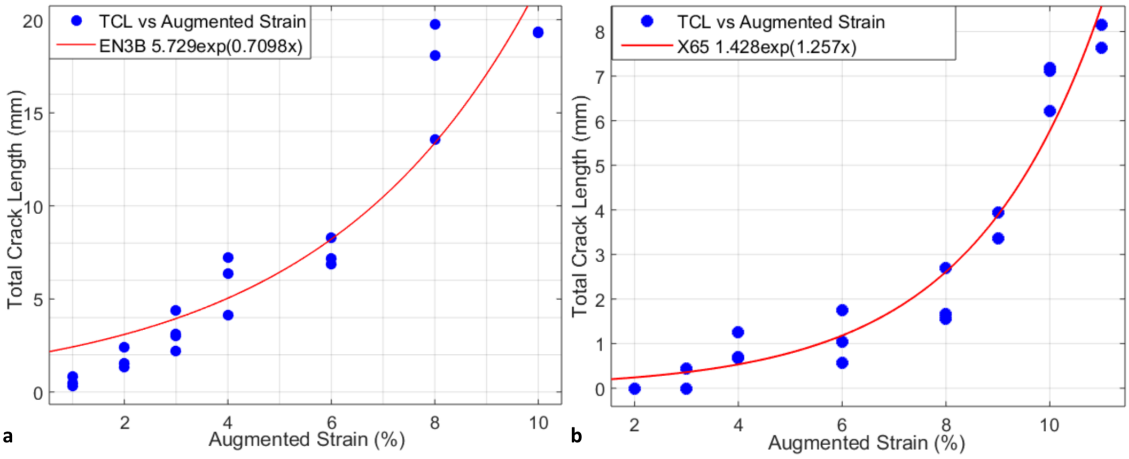

Figure 5.22: TCL vs augmented strain for Trans-Varestraint tests a) EN3B b) X65, red line indicating the evolution of the crack lengths as augmented strain increases.

As with the small scale experiments the same methods were used to find a fit that corresponds to the evolution of the TCL of the hot cracks of the materials. The following tables (5.4, 5.5) show the different types of fit and their parameters.

By comparing these tables it is clear that for the Trans-Varestraint test the R-Square and its adjusted values are good but the SSE values for the EN3B experiments are significantly higher than the X65. Both of them though are significantly high.

Table 5.4: TCL vs Augmented strain for the industrial scale Trans-Varestraint test for EN3B steel

Fit Type	SSE	R-Square	Adj R-sq
a*sin(b*x+c)	44.523	0.951	0.935
a*x+b	77.714	0.915	0.910
a*exp(b*x)	106.610	0.883	0.877
a+atan(a*x+b)	610.730	0.330	0.295
a+tanh(b*x+c)	709.279	0.222	0.136

Table 5.5: TCL vs Augmented strain for the industrial scale Trans-Varestraint test for X65 steel

Fit Type	SSE	R-Square	Adj R-sq
a*sin(b*x+c)	5.723	0.965	0.953
a*exp(b*x)	8.948	0.945	0.942
a*x+b	33.434	0.795	0.784
a+atan(a*x+b)	55.954	0.657	0.639
a+tanh(b*x+c)	99.505	0.390	0.322

EN3B Trans-Varestraint tests were carried out up to the augmented strain of 10% because at this strain the weld bead of the material failed completely and in a way that measuring a length of hot cracks was difficult as seen in the following figure.

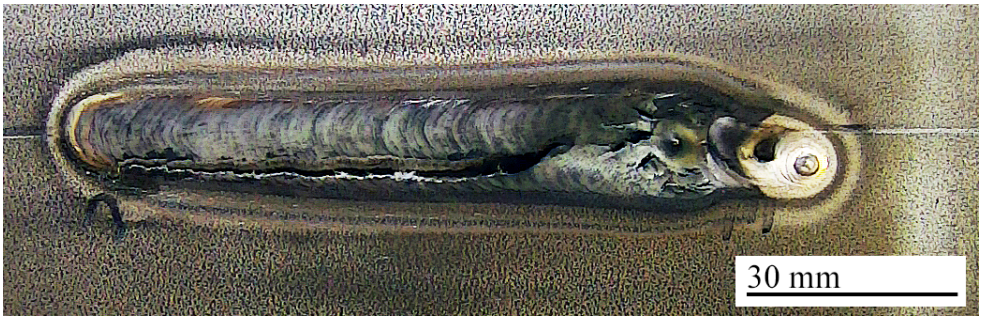

Figure 5.23: EN3B Trans-Varestraint sample strained at 10%.

MCL measurements were recorded and plotted against the augmented strain as shown in the following figure (Figure 5.24). Results from the MCL measurements also indicate that the EN3B steel is more susceptible to hot cracking than X65 since it produces higher crack lengths at lower augmented strains. An important finding from these results is that both materials behave as expected according to what was discussed in Section 2.3.2 and presented in Figure 2.11.

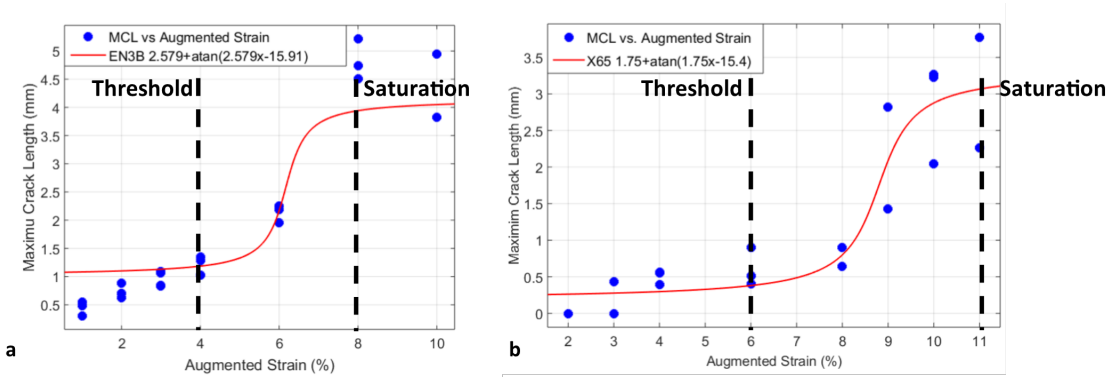

Figure 5.24: MCL vs augmented strain for Trans-Varestraint tests a) EN3B b) X65, red line indicating the evolution of the crack lengths as augmented strain increases.

The fitting methods that were used for all the other experimental sets were also used for the MCL measurements. The following tables (5.6, 5.7) show the comparison between the EN3B results and X65 results. Compared to previous sets of results these results present with better SSE and R values and appear to be more reliable and comparable. It is critical to be noted that these are approximated fits that are used to evaluate the experimental results. The fits presented could be significantly improved but this is not the aim of this thesis.

Table 5.6: MCL vs Augmented strain for the industrial scale Trans-Varestraint test for EN3B steel

Fit Type	SSE	R-Square	Adj R-sq
a*sin(b*x+c)	1.454	0.973	0.964
a+atan(a*x+b)	5.396	0.901	0.896
a*x+b	6.972	0.872	0.865
a*exp(b*x)	9.247	0.830	0.822
a+tanh(b*x+c)	13.992	0.743	0.715

Table 5.7: MCL vs Augmented strain for the industrial scale Trans-Varestraint test for X65 steel

Fit Type	SSE	R-Square	Adj R-sq
a+atan(a*x+b)	3.891	0.867	0.860
a*sin(b*x+c)	4.288	0.854	0.805
a+tanh(b*x+c)	5.230	0.821	0.801
a*exp(b*x)	5.468	0.813	0.803
a*x+b	8.050	0.725	0.710

5.2.3 Measurement of applied strain during Trans-Varestraint test

During the Trans-Varestraint testing of X65 steel the strain gauge measurements were consistently higher than the desired applied strain. Since the strain gauges though were not placed exactly at the position where the weld bead was and the cracks were generated a test where multiple strain gauges were placed on a plate was carried out (Figure 5.25). This test was carried out because it was not possible to place strain gauges (because of the heat of the weld) close to the point where the cracks would appear during the test. For the welding tests, only one strain gauge could be placed and the position was as close to the weld as was tolerable given the heat.

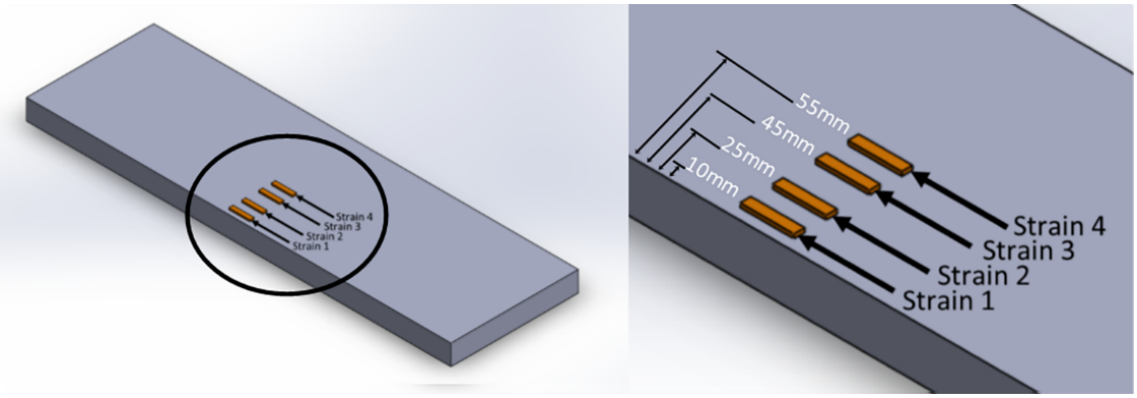

Figure 5.25: Strain gauge positions on plate for the experiment where the bend is applied without welding.

The results of the cold bend experiments (Figure 5.26) demonstrate the importance of control of the stroke length during Trans-Varestraint experiments. The maximum strain recorded was always greater than the intended strain. The strain near the edge was greater because of the near edge effects (Poisson's ratio) during bending that allowed for the plate to contract in those regions. The cold bend test indicated that further from the edge of the specimen the strain decreased. Additionally, particularly in the edge region an overshoot from the desirable stroke was observed. This was followed by a spring-back that occurred when the force ceased to be applied due to the elastic component of the strain in the plate at the end of the bend.

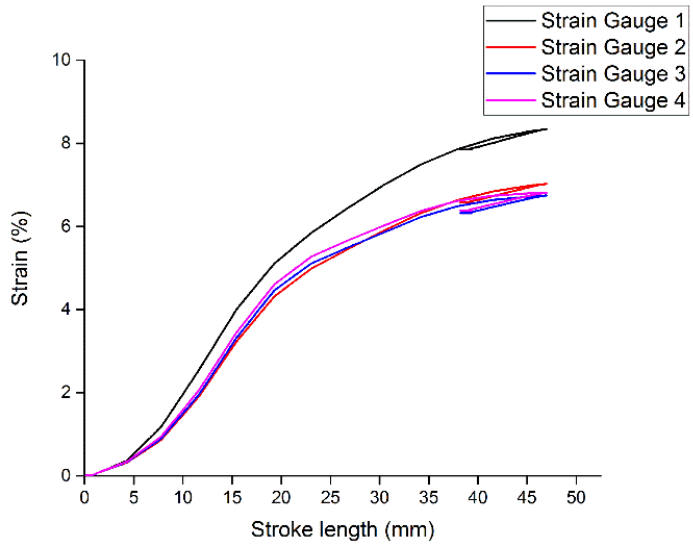

Figure 5.26: Strain development during cold bending of plate at 6% target augmented strain.

By examining the results further towards the centre of the plate where the welding process is taking place and where cracks are generated, the strain is significantly lower (near strain gauge 3 as seen in Figure 5.26). The results also indicate that the use of the equation, which has been suggested for this method, will provide with a stroke length that will ensure that the required strain will be applied on the centreline of the plate. In this case the desired strain was 6% and the stroke length calculated was 39 mm.

5.3 Post processing of weldability tests

5.3.1 Liquid Dye Penetration Tests (NDT)

Liquid dye penetration tests were carried out in all specimens in order to identify cracks on specimens that could not be identified using a stereoscope. The non-destructive testing for the small scale experiments was carried out in all of the specimens as shown in the following figure (Figure 5.27).

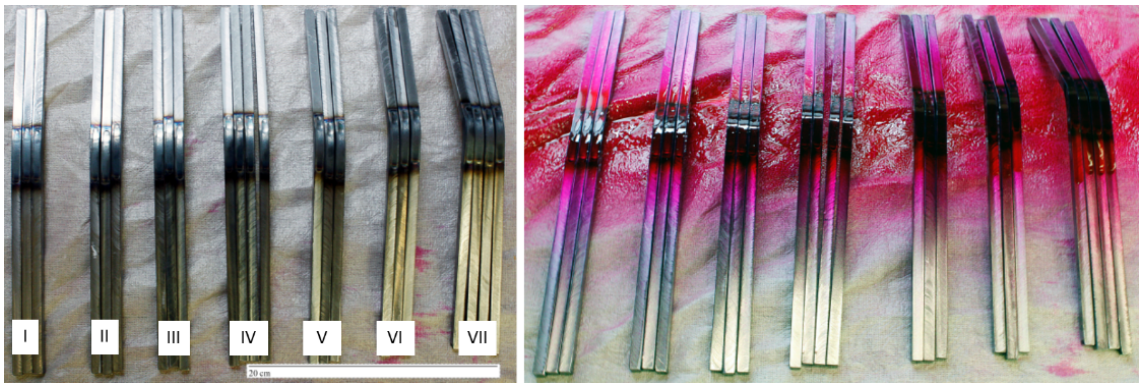

Figure 5.27: Varestraint samples during NDT testing I: VA100 II: VA200 III: VA300 IV: VA400 V: VA500 VI: VA600 VII: VA700.

NDT showed indications of cracks from specimens III to VII as shown in Figure 5.28.

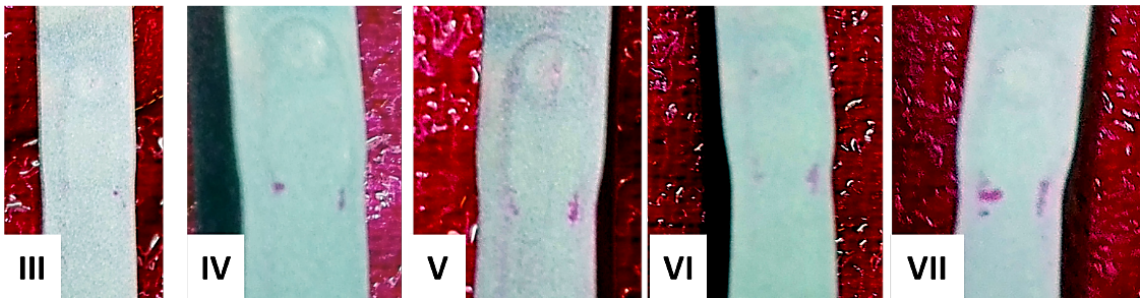

Figure 5.28: Indications of cracks from specimens III to VII.

NDT indications on the small scale Varestraint samples show that the location of the hot cracks generated from the experiments are not at the exact same location on all of the specimen and indeed in some samples cracks are generated only on one side of the weld. The specimens with a stroke length of 27 mm provided with indications

demonstrating how critical the position of the solidification path is in comparison with the bending position. In Figure 5.29 it can be seen that in one sample the bend occurred after the weld solidified. As a result no cracks were generated on this sample. The results of the NDT examination in combination with the results of the crack length measurements on these samples indicated that for the small scale experiments the position of the solidification front at the time of the bend is critical.

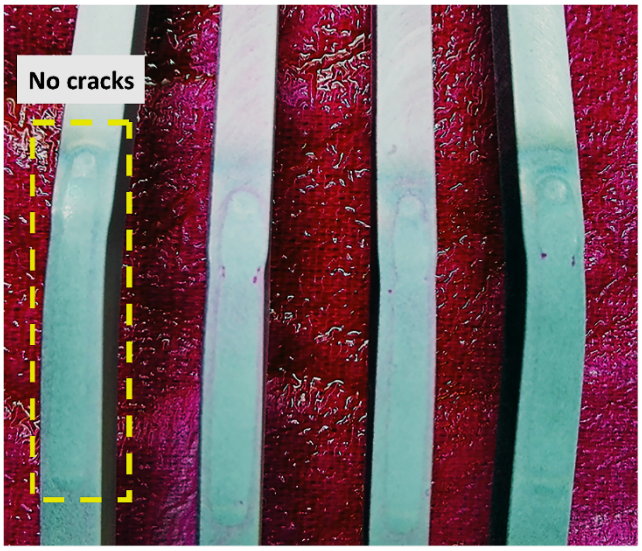

Figure 5.29: Varestraint samples where one sample (indicated with yellow broken line) does not have any cracks present.

NDT was carried out on all of the industrial scale Trans-Varestraint experiments as well. The tests were focused on the specimens that 2 % augmented strain was applied since during the stereoscopic examination no cracks could be identified. NDT gave indications of cracks on these specimens as seen in Figure 5.30.

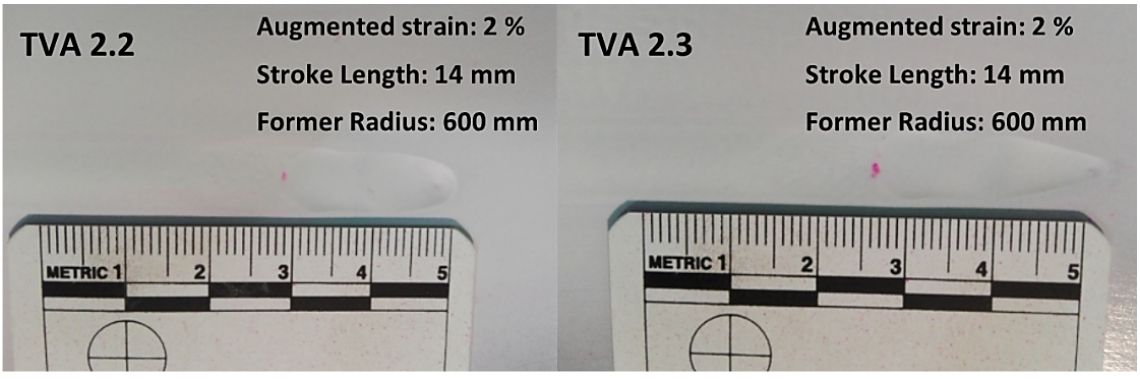

Figure 5.30: TVA 2.2 and TVA 2.3 (X65 steel) NDT showing indications of cracking defects at the limit of the 'mushy zone' were cracks are expected to initiate from.

NDT on the Trans-Varestraint samples showed that the defects during these tests are formed mainly along the centreline of the weld. This makes the crack positions easier to spot and identify when compared to the cracks generated during the Varestraint tests on small samples. As expected the biggest cracks during these tests develop along the centreline of the samples and further away from the centreline smaller (secondary) cracks are be developing.

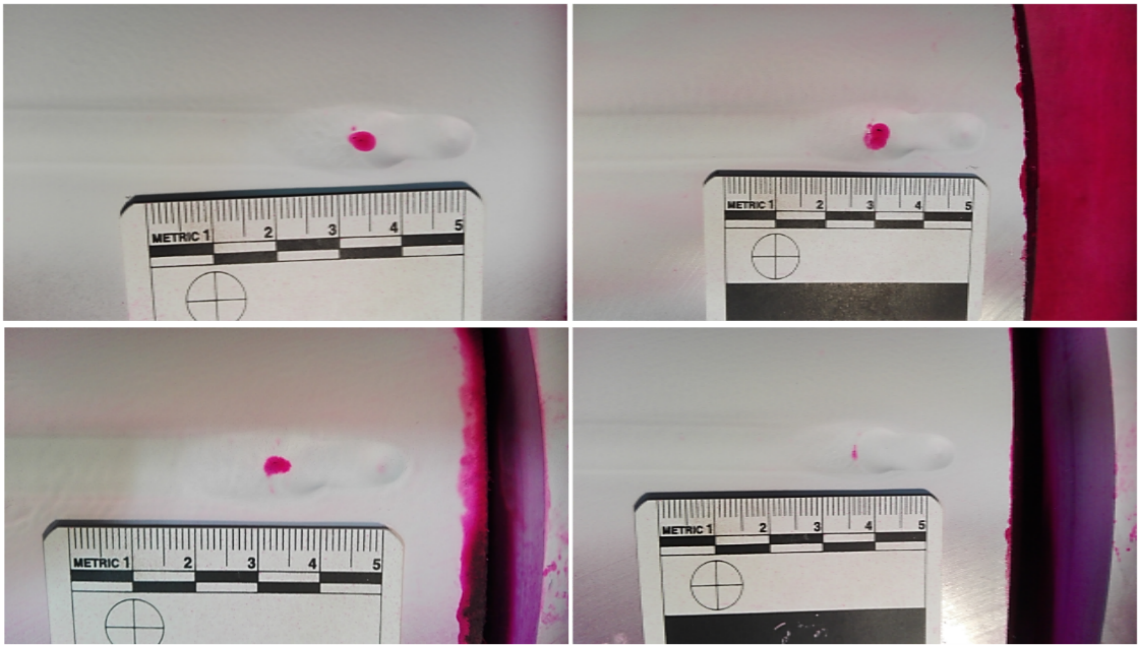

Figure 5.31: Indications of defects during NDT (X65 steel) on various Trans-Varestraint samples.

In order to further examine the cracks generated from both the Varestraint and Trans-Varestraint tests samples were extracted from the specimens in order to be examined using XRCT.

5.3.2 X-Ray Computed Tomography (XRCT)

Specimens from both types of tests were extracted and examined using XRCT as described in Section 3.3.2. XRCT on the small scale experiments provided with accurate representations of the samples and highlighted the cracks as seen in the following figure (Figure 5.32).

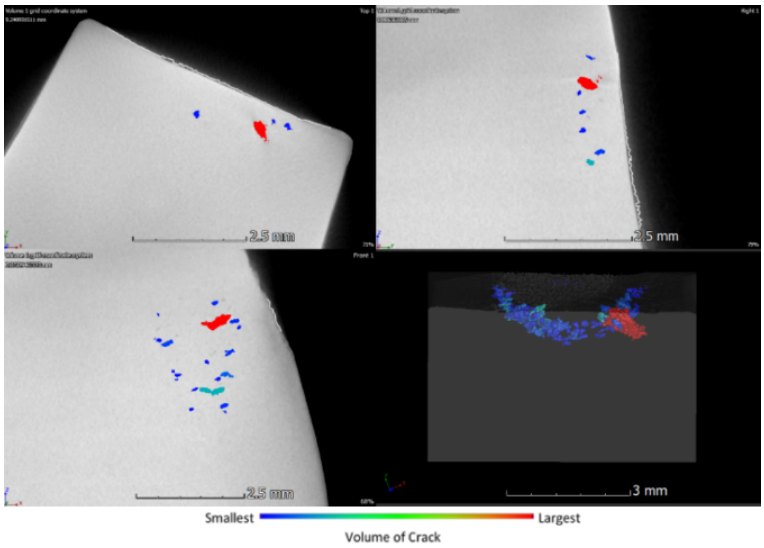

Figure 5.32: XRCT overview of small scale Varestraint sample (VA700.2).

Using the XRCT capabilities it is also possible to compare cracks on specimens where different levels of augmented strain were applied. The following figure (Figure 5.33) compares small scale Varestraint samples with different stroke lengths applied. By comparing these samples it can be seen that when the cracking is fully developed it follows the solidification front and can be used to identify the maximum depth of the weld bead and measure the maximum depth of the cracks. In this case it can be seen that the first cracks that are formed are positioned on the one side of the weld bead and at a depth that is smaller than the actual weld depth. Additionally, the XRCT shows that even at low strains where cracks might not be observed at the surface of the material subsurface cracks may be present.

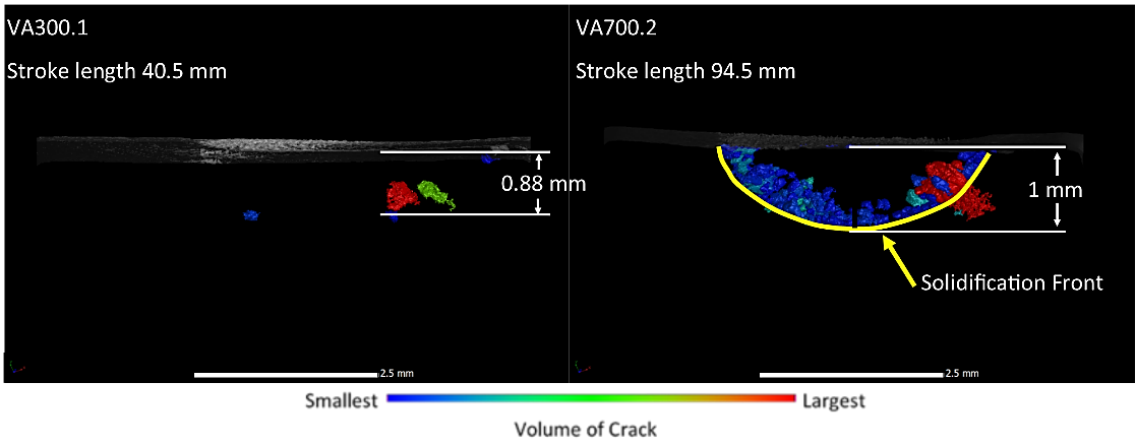

Figure 5.33: Comparison of VA300.1 vs VA700.2 showing different stages of crack generation and propagation.

The following figure (Figure 5.34), shows the XRCT scan on the EN3B sample from the Trans-Varestraint experiment where 2% of strain was applied on the specimen.

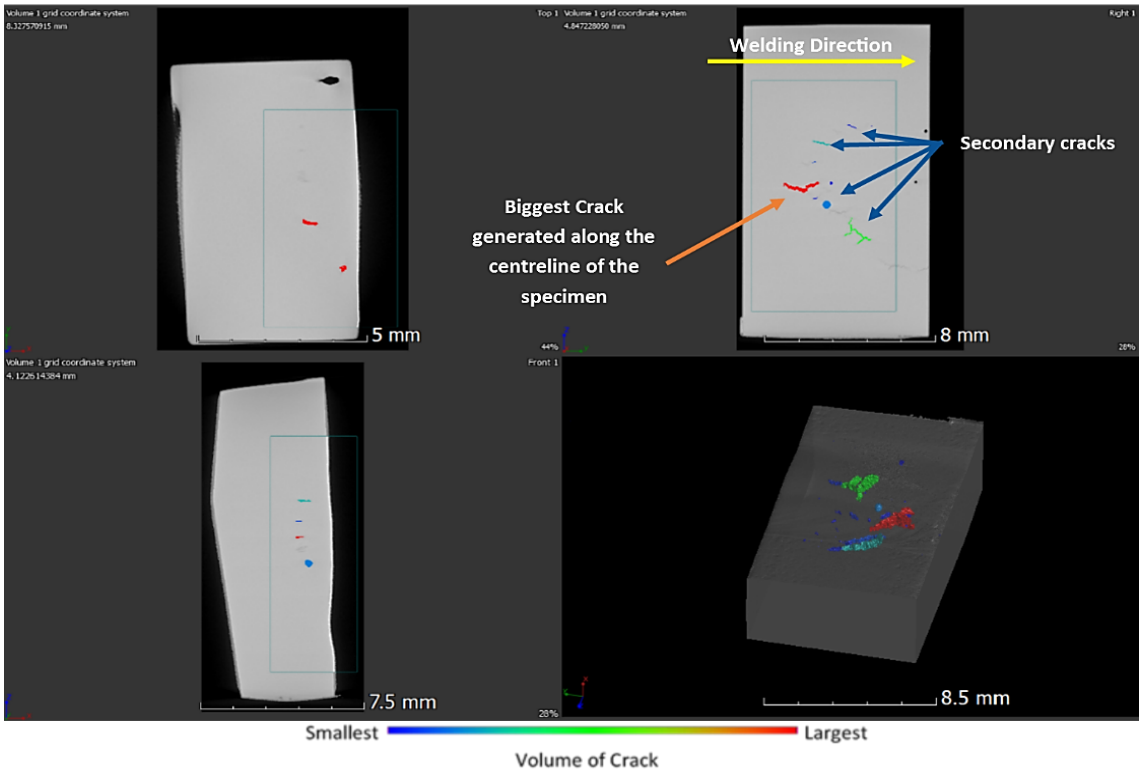

Figure 5.34: XRCT scan of TVA 2.1 (2% augmented strain, EN3B) steel.

Initial indications from XRCT on X65 Trans-Varestraint specimens showed that hot cracking develops from the solidification front as shown in the following figure (Figure 5.35) of TVA 11.1.

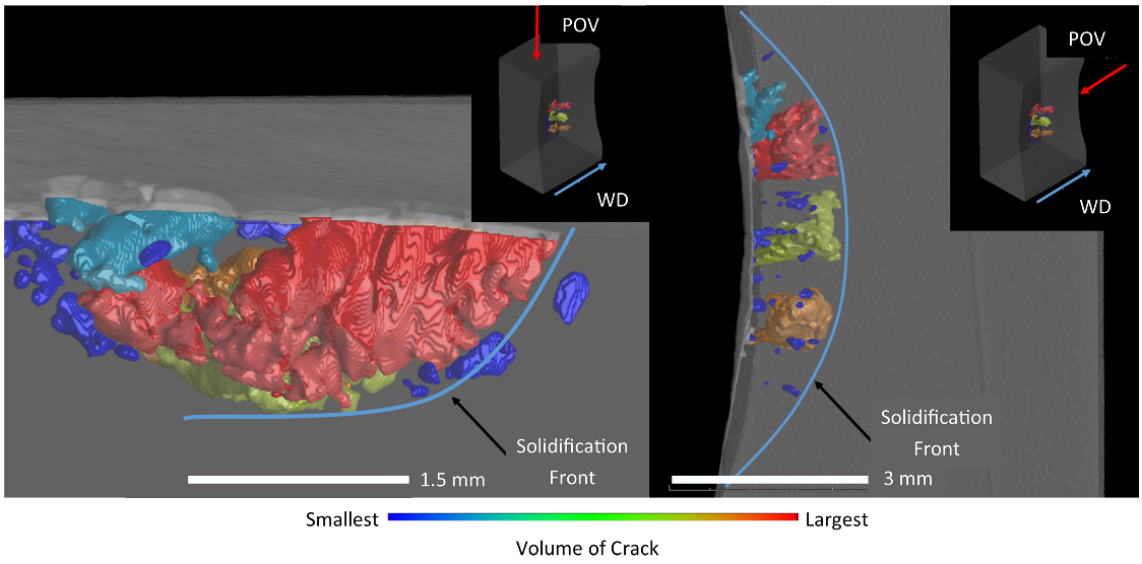

Figure 5.35: Specimen TVA 11.1 (X65) (augmented strain: 11%) crack pattern follows solidification front of weld (WD = Welding Direction, POV = Point of View).

The maximum crack depth was recorded for all the specimens that were scanned. The scans revealed that even when 2% strain was applied (and no cracks were observed in the surface of the weld) sub-surface cracks were present. All the cracks measured had the same maximum crack depth, approximately 1.4 mm from the weld surface, except in the 2% strained specimen, where the crack depth was approximately 0.9 mm (Figure 5.36).

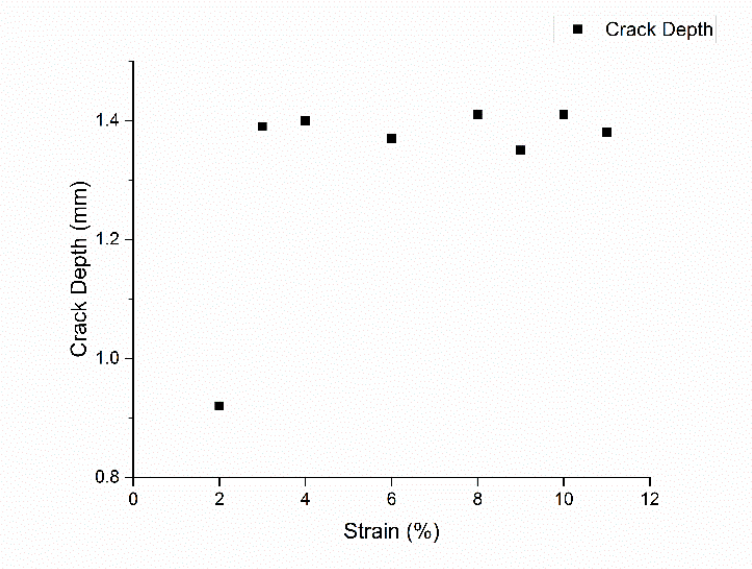

Figure 5.36: Maximum crack depth for Trans-Varestraint test specimens (X65).

These results demonstrate that hot cracks initiate below the surface and, once a maximum depth is reached, the amount of strain imposed will not affect it. By comparing the cracks developed in a high strain specimen compared to a low strain specimen (TVA10.1 and TVA2.1, Figure 5.37) it was observed that cracks tend to initiate on the solidification front where its angle relative to the surface is 45°.

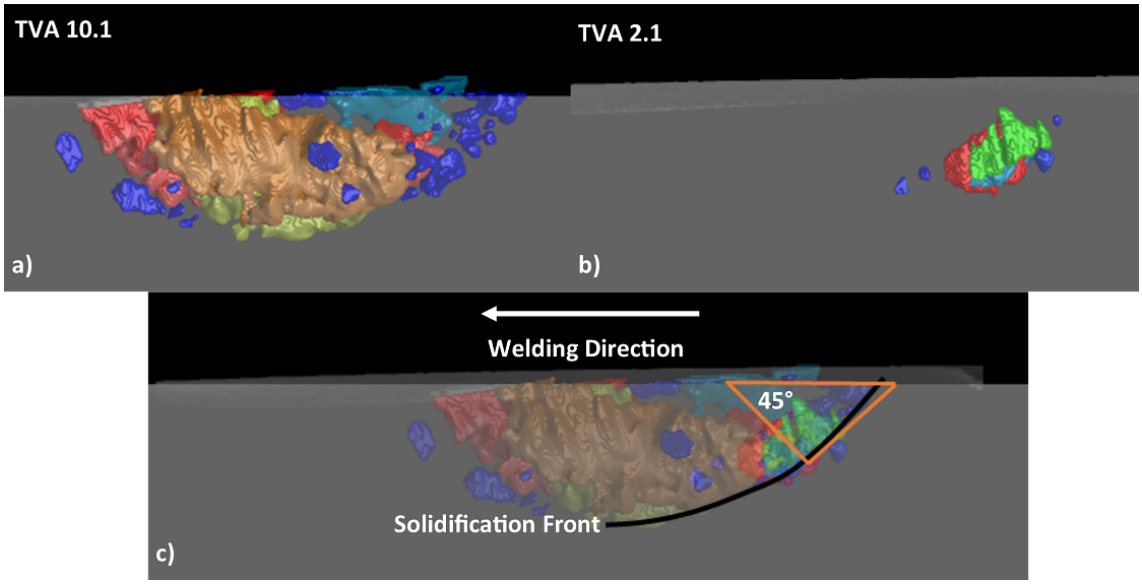

Figure 5.37: Comparison of hot cracks: a) 10% strain specimen; b) 2% strain specimen; c) overlay of the two specimens, illustrating that cracks initiate on the solidification front where its angle with the surface of the specimen is 45°.

The same observation was made at the Varestraint test samples VA300.1 and VA700.2 as shown Figure 5.38.

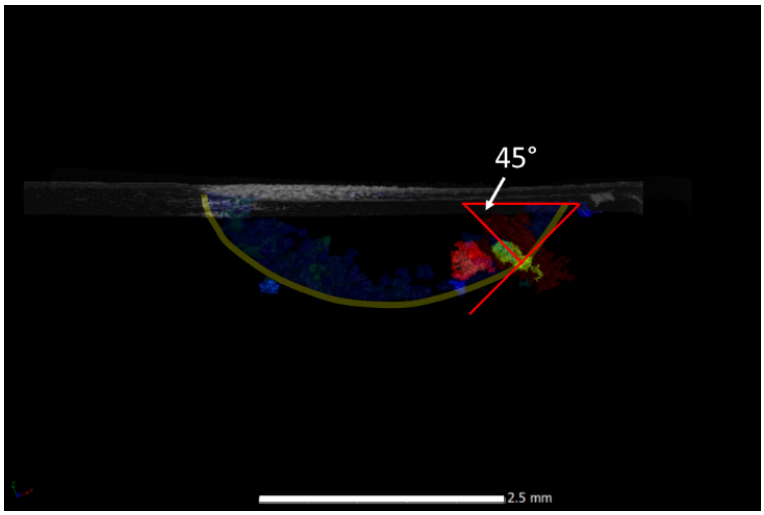

Figure 5.38: Overlay of the two specimens (VA300.1 and VA 700.2), illustrating that cracks initiate on the solidification front where its angle with the surface of the specimen is 45°.

5.3.3 Fractography of hot cracks

In order to examine further the XRCT findings from the Trans-Varestraint specimens fractography was carried out in hot cracks generated from the experiments as shown in Figure 5.39.

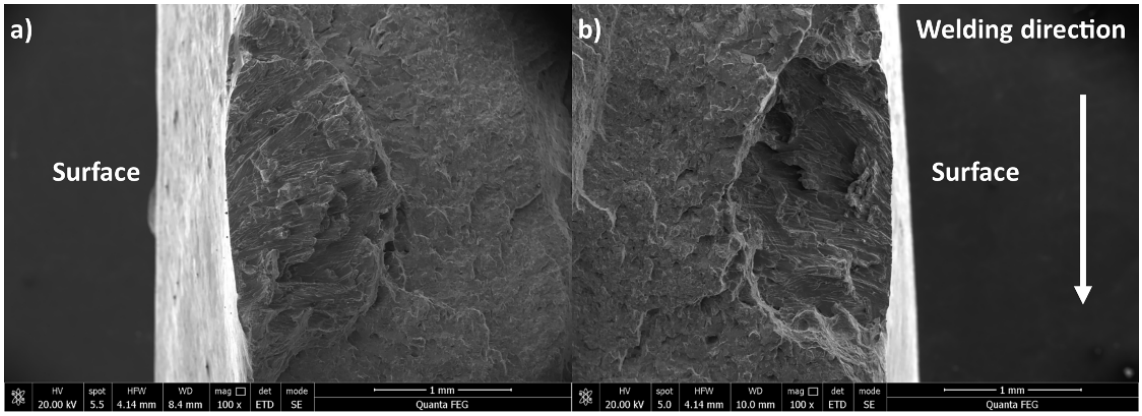

Figure 5.39: Low magnification images of both sides of a hot crack from a TVA specimen (TVA 10.1, augmented strain 10%).

By focusing on the inter-dendritic stage 3 fracture, which originates from the crack initiation point that was identified by the XRCT scans, it was observed that the dendrites have a preference in orientation that forms a 45° angle with the surface of the sample (Figure 5.40). By following these structures to their origin, the depth

measured was approximately 0.9 mm. This indicates that there is a connection between the initiation point of the cracks and the angle that is formed by the solidification front and the surface of the weld.

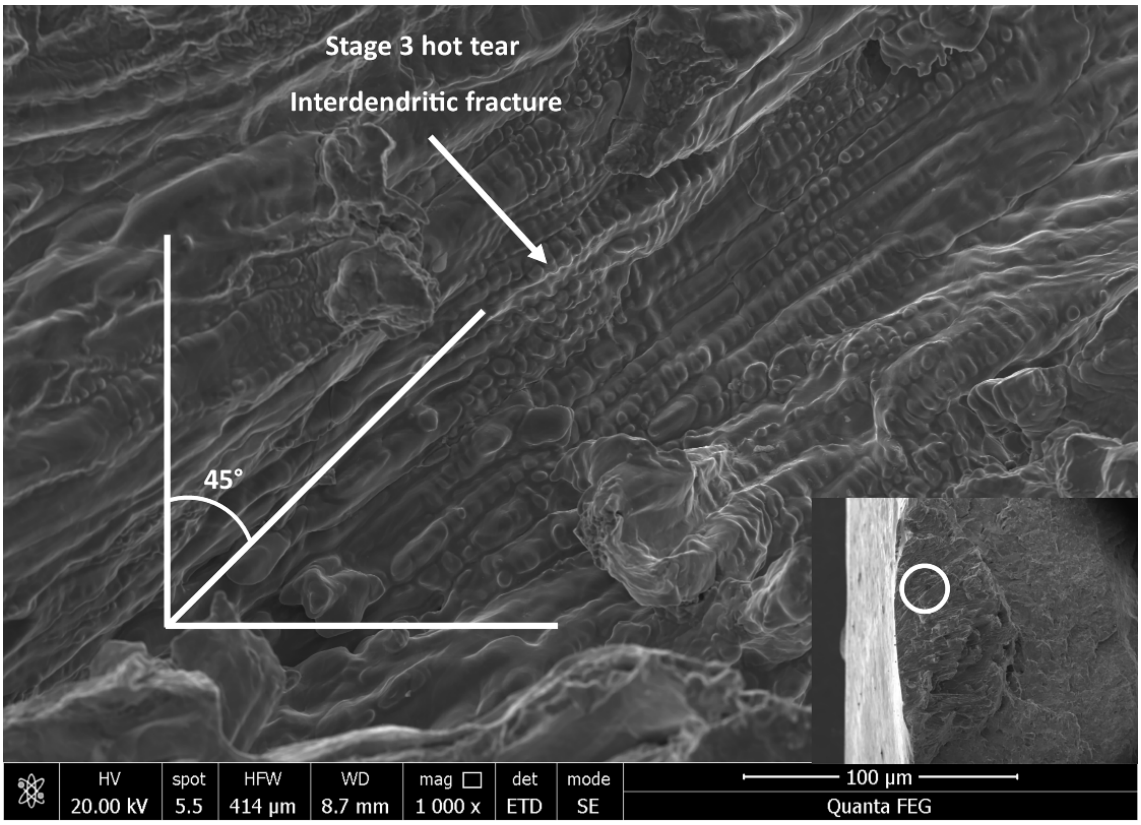

Figure 5.40: Stage 3 hot cracking near the surface of the weld pool indicating clear preference in the orientation of the dendrites at an angle of 45° with the surface of the weld.

5.4 Summary

This chapter presented the main results of the study that was carried out. Metallographic examination of X65 steel revealed that its structure is mainly ferritic with regions of degenerate pearlite in the base metal and mainly acicular ferrite in the fusion zone. What was also clear during the metallographic examination was the CG-HAZ where enlarged grains were observed.

Hardness testing of the weld joint showed how the distribution of hardness corresponds to the welding resulting regions. Fracture toughness of samples that consisted of 50% HAZ and 50% FZ indicated that the toughness on the interface of

the weld is lower than the one in the FZ. Additionally despite the challenges in obtaining samples that consisted of 50% HAZ and 50% FZ the experiments were carried out successfully.

Small scale Varestraint tests were carried out on X65 and the results showed that the average MCD at a stroke length of 94.5 mm was 0.15 mm and that the evolution of the MCD as the stroke length was increased follows the expected theoretical trend of MCD vs augmented strain. The Trans-Varestraint tests were carried out on X65 and EN3B steel in order to obtain comparable results and validate the proposed method. The results clearly indicated that EN3B is more susceptible to hot cracking than X65. EN3B constantly presents a MCL higher than that for X65 at lower augmented strains. 0.5 mm MCL at 1% augmented strain versus 0.25 mm MCL at 3% strain respectively.

Tests were carried out without performing a weld on a plate with multiple strain gauges on the centreline in order to validate further the method proposed. The results showed that in the area where the cracks appear the strain applied is the desired augmented strain. The specimens that were used for the Varestraint and the Trans-Varestraint tests were examined using NDT (Liquid Dye Penetration) mainly to observe if there are defects on the weld beads that could not be observed using the stereoscope.

The results showed that in the Trans-Varestraint samples of X65 steel where no cracks were observed stereoscopically some indications were observed during NDT. Specimens were extracted from the samples and the examination using XRCT showed that indeed even if cracks are not observed on the surface of the weld subsurface cracks may be present. An interesting finding of the XRCT is that it appears that cracks initiate at a point where the solidification path of the material forms a 45° angle with the surface of the weld.

These indications were reinforced by the fractography of the hot cracks where the orientation of the grains that lead to the expected initiation point indeed form a 45° angle with the surface of the weld. In the following chapter the experimental results will be analysed and discussed in order to further understand the importance

of these findings, how they can be used in future research and to further improve the Varestraint and Trans-Varestraint tests.

Chapter 6

Discussion

The experimental procedures and results presented were focused on two main parts. The first one was the characterization of API-5L X65 steel. The second one was the study of hot cracking susceptibility and its mechanisms using mainly X65 steel.

6.1 Characterization of the material

API-5L X65 steel is an HSLA steel that is commonly used in offshore pipelines. The microstructure of the material was examined using a submerged arc welded (SAW) pipe part. The microstructure is mainly ferritic with some degenerate pearlite present in the base metal. By approaching the interface of the weld the CG-HAZ was clearly identified and the FZ was mainly acicular ferrite. During the grain size measurements it was observed that the grain size of the material according to ASTM was G 12.5 (average diameter 4.7 μm). Because the grain size measurements were carried out on both sides of the weld a difference was observed though between the left side and the right side of the specimens. It appears that the grain size measurement on the left side of the material are consistently slightly higher than the right. However, this difference is not significant enough to affect the categorization of the material. The material can still be categorized as an extremely fine grained material. By taking under consideration the way the part is manufactured, which is described in Sections 1.3.1 and 2.1 a cause for this

difference can potentially be identified. As the UOE process has described, after the welding of the pipe is carried out the expansion process is carried out in order for the pipe to obtain its desired size. If, during this process the pressure applied by the tool is slightly uneven and distributed along the surface of the pipe non-uniformly, it can potentially lead to differences like this. Given that the differences observed in the grain size do not cause a change in the overall grain size of the material these slight differences may also be as a result of residual stresses.

Hardness tests of the weld joint provided some interesting results. One of the most important ones was the fact that it appears that the HAZ on the one side of the specimen covers a bigger area compared to the HAZ on the other side of the specimen. Given that the welding process that is used during the welding of the pipe is taking place in multiple stages this difference can theoretically be explained. If the heat input in the weld joint is not absolutely centred then one side of the material will receive a greater amount of heat thus creating a slightly bigger HAZ. However this there is no evidence to support if this difference affects or not the performance of the material.

CTOD fracture toughness experiments were proven challenging as the aim of the tests was to measure the fracture toughness directly on the interface of the weld. Therefore, it was required that the specimens contained 50% HAZ and 50% FZ in their notch. In order to achieve this multiple accurate measurements needed to be carried out in order to enable precise extraction of the specimens. The other reason was the dimensional restrictions set by the ASTM standards in order to obtain a K_{IC} value. Due to size restrictions and demands of 50% HAZ 50% FZ the size of the specimens could not meet the ASTM requirements for K_{IC} measurements. Nevertheless the experiments could provide with a K_q value that allows the materials toughness to be evaluated. As far as the success of the experiments to measure the fracture toughness in a 50% HAZ 50% FZ notch the experiments can be considered successful since the average percentage of HAZ vs FZ area across the specimens was 52% vs 48% respectively. Comparative results between the 100% FZ fracture toughness tests that have been carried out on the same material indicate that the fracture toughness of the interface of the welds is lower than the FZ (34.9 MPa $m^{1/2}$

vs 40.7 MPa $m^{1/2}$). This drop of fracture toughness has also been observed in X80 steel as mentioned in the literature review Section 2.1.

The SEM examination of the fracture toughness specimens provided with a clear contrast between the way cracks manifest in the FZ versus the HAZ. The examination indicated that the FZ fractured surfaces presented a more uniform ductile fracture which is expected when the microstructure of the material at that point consists of acicular ferrite which provides with high mechanical properties and limits the slip distance of dislocations. On the other hand the HAZ, which at this scale and that close to the FZ is for the most part CG-HAZ, consists of a lower strength matrix with enlarged grains that allows for large dimples to form. As a result the fractured area of the specimen is presented with a ductile morphology with the characteristic ductile dimples that are presented at these types of fractures. Overall CTOD fracture toughness tests can provide with critical information that is required for the applications that steels like X65 are used for in the oil and gas industry and specifically the off-shore ones. Nevertheless, it has been proven challenging to obtain specimens directly from the interface that contain 50% FZ and 50% HAZ. During this study the specimens had to be carefully extracted and the directions for their extraction were specific. In order to repeat an experiment focused on the interface of welds the focus should be on the extraction of the specimens.

6.2 Weldability tests

6.2.1 Experimental procedure of the small scale Varestraint tests

The presented method was applied for a set of small scale Varestraint experiments and industrial scale Trans-Varestraint experiments. The small scale apparatus had some limitations as far as applying the proposed method is concerned. Firstly, the setup did not allow for an interchangeable former of different radius to be used according to the desired strain. Secondly, the setup was not designed to work

similarly to a three point bend test as the method proposed expects. Nevertheless by taking into consideration that the former that was part of the rig had a radius of 30 mm and the specimen thickness was 8 mm it had the capability of applying a maximum of 13% strain on the specimens (Equation(3)) . Before the upgrade of the equipment the control of the stroke length was not possible because the actuators were controlled manually by the use of switches.

The upgrades carried out for this study provided with the required control of the stroke length. This allowed the imposition of different levels of strain on the specimens during the experiments. This was achieved by not bending to the full stroke length available during all experiments but by bending at different lengths in order to apply different strains. The strain amount could not be measured using strain gauges in this setup for two reasons. Because the specimens are small scale the weld bead covers all the available space where strain gauges could be placed so welding and measuring the strain at the same time was not possible.

The second reason was that the rig is not powerful enough to bend the specimens when they are cold, therefore the placing of strain gauges on a specimen and bending it without welding was not an option. For that reason the results of the experiments were presented as crack lengths versus stroke lengths and not strain percentages. Nevertheless since at different stroke lengths the amount of strain applied will be different the results are in a form that corresponds to the crack length versus augmented strain that is discussed in the literature.

What was observed by examining the results of the small scale tests was the following. The Varestraint tests are sensitive to the position of the weld during the bend. Considering that during Varestraint and Trans-Varestraint experiments the aim is to apply the maximum desired augmented strain on the solidification front of the weld the following occurs. As the following figure shows, in the current setup for the small scale tests the position where the maximum augmented strain is applied is at a different point from the position that the solidification front is during the process (Figure 6.1). Because of the small size of the specimen and the small size of the welding bead the solidification front cannot be more that 5 mm behind the weld torch as was observed from the Varestraint specimens. The issue

at this point is that the position of the potential maximum strain is further away from the solidification front.

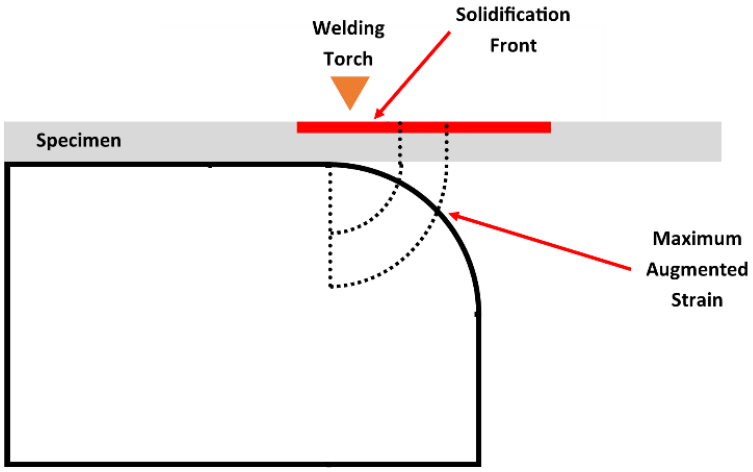

Figure 6.1: Position of the solidification front in relation to the position of the maximum applied augmented strain during the small scale Varestraint experiments.

Another issue is the way the specimen is attached at the bending actuator for the experiment. Because the specimen is placed on the specimen holder and gripped so it moves with the holder in order carry out the welding process the following occurs. At the start of the experiment the bending actuator is attached on the specimen at a specific angle. At the point where the bending process initiated this angle changes to 90° because the specimen moves towards the bending actuator as shown in the following figure (Figure 3.14). This means that if for some reason the specimen in not set on the holder at the exact same position every time the angle between the actuator and the specimen at the time of the bend will be different.

This will result in a different deflection of the specimen resulting to different strain applied. This was made clear during the experiments where the stroke length was 54.0 mm and 94.5 mm. During those experiments the specimens where not attached at exactly the same position as the other experiments and as a result the bends were different and the resulting cracks were also different. There were also cases where the main axis of the bend was sufficiently far from the solidification front which caused no cracks to be generated at all.

6.2.2 Small scale Varestraint experiments

The issues discussed can also explain the fact that the MCD measurements for the Varestraint tests have a relatively big spread in values. Both Varestraint and Trans-Varestraint tests have a strong dependence on the application of augmented strain. Therefore, the greater the variation that exists in the augmented strain applied the greater the effect it will have on the results. In addition as will be explained as this section progresses the Varestraint test has less control in the application of augmented strain compared to the Trans-Varestraint test. This argument is also reinforced when considering the following. The aim of the test is to apply the desired augmented strain on the solidification front. This means that during the bending process the solidification front must be at the position where the maximum strain is applied.

This leads to the logical conclusion that in order to have that kind of positional control of the solidification front the shape, size and position of the weld must be known accurately prior the experimentation. This is information that is not readily available for all weldable materials and all welding processes. Bearing in mind that any testing procedure which has as an aim to export significant results without extreme pre-testing, the requirement of this level of information prior to experimentation reduces the functionality and usefulness of the experiment overall.

Furthermore, experimental procedures of that scale for the Varestraint experiments produce small welding beads which in turn, if the material is not susceptible to cracking, produce small defects which increase the variation of results due to the difficulty of accurately measuring the crack lengths. This means that in order to perform small scale Varestraint experiments and extract reliable results there is a necessity for a significant number of specimens that will improve the accuracy of the experiments.

6.2.3 Industrial scale Trans-Varestraint tests

The Trans-Varestraint experiments were carried out by applying the method described in Section 3.2.1. The experiments were carried out using X65 and EN3B steels in order to obtain comparable results and to further validate the method. The results of both experimental sets on X65 and EN3B that have been presented show the following characteristics. Compared to the results of the Varestraint tests the Trans-Varestraint results show less variation. By comparing the Trans-Varestraint results between X65 and EN3B it is evident that EN3B is more susceptible to hot cracking than X65 since the overall crack length across the span of augmented strains is higher than X65 and because EN3B presents cracks at lower augmented strains than X65.

The industrial scale tests also allowed for strain measurements to be carried out. These measurements were carried out during the first set of experiments in order to ensure that the stroke lengths that are provided by Equation 20 previously presented, will be the ones that will be actually applied during the experiment. Because the strain measurements could not be taken from the position where the weld will take place strain gauges were placed at the edge of the plate as previously described. The initial results of these measurements were consistently higher than the ones the experimental design demanded. For this reason an experiment where multiple strain gauges were placed on a plate were carried out in order to get a profile of strain that is applied during the bending. These measurements showed indeed that at distances of 40 to 50 mm from the edge of the plate where the actual welding bead is during the tests the strain applied is the one expected from the experimental design.

The only deviation that occurred during the industrial scale experiments from the experimental design was the fact that the experimental rig was slightly, but repeatedly, over shooting the desired stroke length during the bending process and also there was a spring back after the bend was applied due to the elastic properties of the steel. These deviations occurred for the following reasons. The Trans-Varestraint rig, used in this study, was designed to apply the maximum possible stroke length during the test and hold the plate at that position to

eliminate spring back.

However, the method presented requires different stroke lengths to allow for the variation of the applied strain. Under these conditions the hydraulics unit would not hold the actuators in place and so a small amount of spring back was inevitable. Additionally, due to the inertia of the rig the target stroke was systematically exceeded. Despite these limitations, the method was still controllable and repeatable since both the spring back and overshoot were consistent in each experiment (Figure 6.2). Specifically, these were found to be -1.11 $\pm$ 1.3 mm and 6.62 $\pm$ 1.16 mm respectively, which can therefore be compensated for in future experiments.

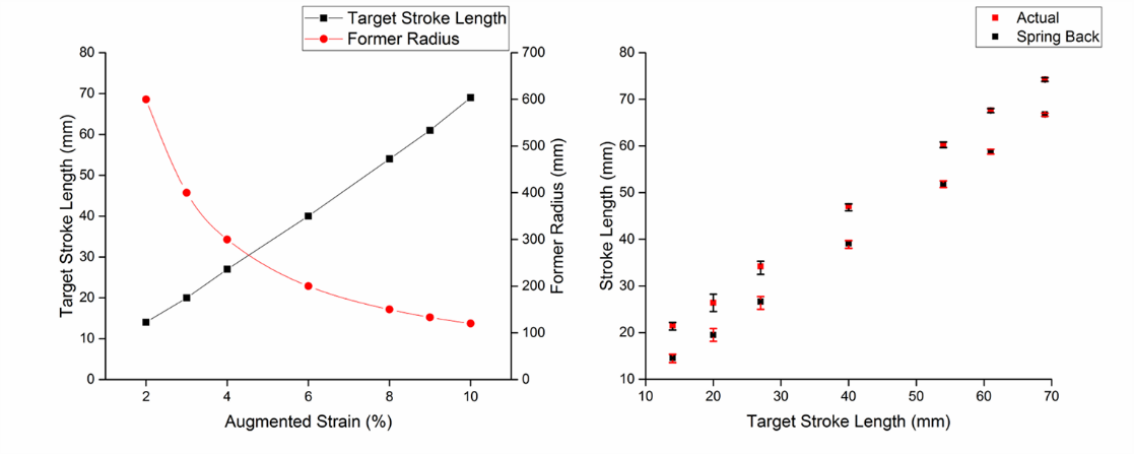

Figure 6.2: Comparison of stroke lengths for each experiment.

As far as augmented strain application is concerned the Trans-Varestraint experiments exhibited stability. The resulting cracks had a smaller variation than the Varestraint tests and the results of MCL versus augmented strain were as the literature suggested it should be. Another positive aspect of the tests was the fact that even if the bend process would initiate at a slightly different time than the one designed the augmented strain applied on the solidification front was the same because the weld bead was applied on the centreline of the sample so the solidification front was always at the same relative position to the centreline of the sample.

6.3 Post processing of the weldability tests

Post processing of the weldability experiments provided with insight into multiple sections of the hot cracking phenomenon. Initially the NDT tests showed that even when cracks cannot be identified by inspection of the samples with a stereoscope does not mean that some minor defects might not be present. An example of this was the X65 experiments where at the specimens where 2% strain was applied and cracks were not observed during stereoscopic examinations. NDT revealed indications of defects in the weld at the position where hot cracks were expected to manifest.

The examination that provided with further input though was the XRCT scans of the Varestraint and Trans-Varestraint samples. The initial observation of the samples was that the hot cracks that were caused from the experiments are indeed generated on the solidification front. This was made clearer at the specimens where high augmented strains were imposed and cracks of significant size were present. Adding to that, by measuring the maximum depth of cracks it was revealed that when the cracks are initiated, they are manifesting from a depth that is lower than the maximum depth of the solidification front. Specifically the maximum crack depth for the X65 specimens showed that at 2% augmented strain where cracks do not quite reach the surface of the weld their depth is lower than all the rest measurements. This difference in crack depth was also observed in the Varestraint samples. The cracks for the experiments where the stroke length was 40.5 mm were at a lower depth (0.88 mm) compared to the ones of 90.5 mm stroke length (1.00 mm) as seen in Figure 4-33.

It is argued that, as the tests that have been described have been carried out such that control of the strain is repeatable and reliable, that each specimen can be considered as a snapshot of the various stages of crack initiation and evolution. This means that even if it is known that the cracks initiate below the surface during welding and propagate towards the heat source [124] their initiation appears to not be at the maximum depth possible.

Further examination revealed that during hot cracking, cracks first initiate on the solidification front, where the tangent of the solidifying material makes an angle of

45° with the surface (Figures 5.37, 5.38). This was highlighted by the observation of the sub surface cracks on specimens from both experimental setups. The observation of cracks forming, the tangent of the solidification front that made an angle of 45° to the surface, can be explained as this is the point where the maximum shear stress on the solidifying material exists.

These observations were examined further by examining the cracks of specimens using an SEM microscope for carrying out fractographic examination. Close examination of the hot cracks revealed that indeed solidification of the material happens perpendicular to the solidification front. Additionally, the examination revealed that the dendrites have indeed an orientation of 45° to the surface at the points where the initiation of the cracks are occurring. This is considered noteworthy since there is bound to be, in any solidification front during welding, a range where its angle is at a 45° angle with the surface.

Adding to that, during the Trans-Varestraint and Varestraint tests the strains applied on the solidification front in the middle of the bend are mainly tensile (Figure 6.3). This means that, as solidification is still taking place at the point where the greatest shear stress/strain is being applied, dendrites are being pulled apart creating voids which result in initiation of cracks.

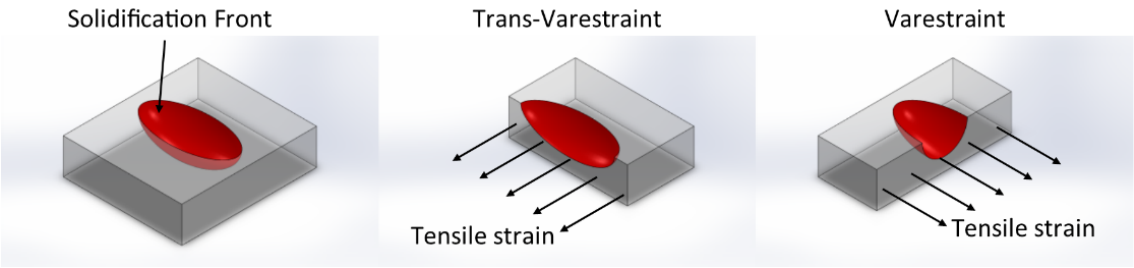

Figure 6.3: Strains applied on the solidification front during Trans-Varestraint and Varestraint tests.

The observation of this crack initiation point is supported by analytical modelling based on Rosenthal's equations [65]. By employing Rosenthal's solution for the temperature gradients for thick plates, a realistic approximation of the welding bead that has been used for the experimental process was achieved. The model (Figure 6.4) illustrates the shape of a weld pool with a maximum depth of 1.40 mm. This

weld pool is like the one created during the Trans-Varestraint experiments. Between the depths of 0.84 mm and 1.09 mm the tangent of the solidification front (light blue) forms a 45° angle with the surface of the weld. Assuming a tensile load on the solidification front the maximum shear stress will be applied at those depths and will generate cracks. Experimental results indicate that the depth of initiation of the cracks is 0.90 mm which is in the range provided by the analytical model.

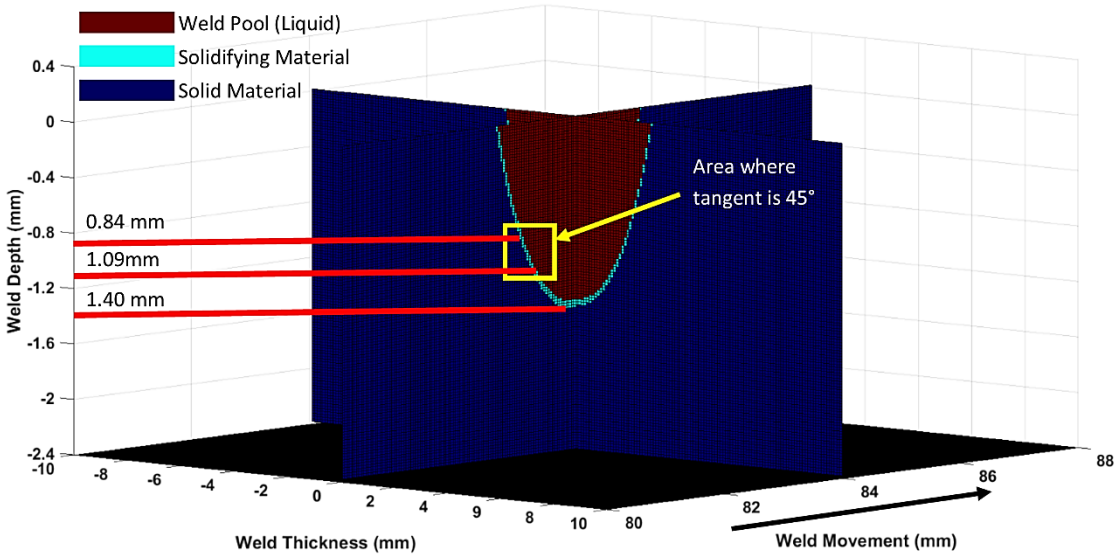

Figure 6.4: MATLAB R2015a solution to an analytical welding model based on Rosenthal's equations indicating the depth where the tangent of the solidification front is 45°.

6.4 General output and evaluation of findings

Cracking phenomena in welds in general have been an important subject of research [139]. Multiple experimental procedures and methods have been employed and used as tools to focus on the study of hot cracking [76, 80, 113, 153, 164, 165]. Additionally, Material properties like toughness, hardness and processes that affect them like heat treatments have been studied in order to investigate their connection to hot cracking [60, 119, 166, 167]. Furthermore, the mechanisms that govern the hot cracking phenomena especially as far as their initiation and growth have also been investigated [39, 81, 168]. Research mentioned here but also presented in the literature review indicated clearly that the hot cracking

phenomena are indeed complicated and the process of quantifying them is important.

Overall both Varestraint and Trans-Varestraint tests produced results that exhibit MCD and MCL development at increasing augmented strain as expected. Adding to that, it can be argued that the evolution of the hot cracking phenomenon has been examined in a greater range that has been presented in the literature. Furthermore, it can be stated that most of the literature has examined the initiation/threshold of hot cracking susceptibility of materials as presented and this study proceeded in examining a greater range of the phenomenon. By comparing the two tests some specific issues are becoming clear. First of all the small scale Varestraint test showed that it is really sensitive to the position of the solidification front during the bending stage of the test compared to the Trans-Varestraint test. This sensitivity is not only limited to small scale experiments like the ones conducted. This is because even if the scale of the test was larger the test would still have the same issues as far as the positioning of the solidification front. On the other hand the Trans-Varestraint test does not have the same issue as far as the solidification front positioning is concerned because the welding bead, and as a consequence the solidification front, is at all times on the centreline of the specimens and the bend.

Adding to that, the Varestraint tests produce small cracks in materials with high resistance to hot cracking susceptibility which makes it harder to identify them and measure them accurately compared to the cracks generated from the Trans-Varestraint test. Another observation is that the spread of the results on a Varestraint test is significantly higher than the Trans-Varestraint test. This can potentially reduce the overall levels of accuracy and repeatability of experiments. One of a few characteristics of standardised and reliable tests is the capability of the test to produce repeatable and reliable results on multiple circumstances. This means that the test must be robust and able to generate results without requiring extreme levels of control. Trans-Varestraint tests compared to the Varestraint tests exhibit this capability and with the method proposed the main driver for hot cracking (augmented strain) can be controlled. As already mentioned in Section 2.3.2 there are five main reasons preventing a standardised approach for

conducting these experiments.

- Lack of an optimal apparatus setup to conduct the experiments with
- Lack of a specific way to apply the augmented strain during the experiment
- Lack of an optimal strain rate that should be used for the experiment
- Lack of specimen specifications
- Lack of specification of welding time.

This study advocates for the use of the three point bending type approach for these tests because it shows increased robustness and control of the experiment overall. For the standardisation of tests, reliability and repeatability must be demonstrated and verified by multiple investigators.

With Varestraint and Trans-Varestraint tests this has not yet been achieved due to the variety of welding procedures and test rigs that have been used in the published literature. These include cantilever, mandrel and three-point bend designs [138, 152, 153, 169, 170]. It is further worth noting that the alignment of the bending plane of the specimen, the axis of any former (if used) and the weld bead (and therefore the solidification front) is also critical as the strain varies significantly away from the bending plane of the specimen. This was verified through both strain gauge data from the cold bend experiment and by simulation, using the CAE software ABAQUS, to replicate the bending process (Figure 6.5).

In summary, previous methods have lacked accurate control of the applied strain to the weld bead. By using formers of a prescribed radius (Equation 3), a controlled stroke length (Equation 20) and consistent time of bend, these factors have been addressed in the present study. Furthermore alternative setups for conducting hot cracking susceptibility assessment experiments appear to not take under consideration that during the bending process the strain applied on the sample is not the same in every position and it depends on the stroke length. This was made clear from the small scale Varestraint experiments where the cantilever approach was utilized for conducting the experiments.

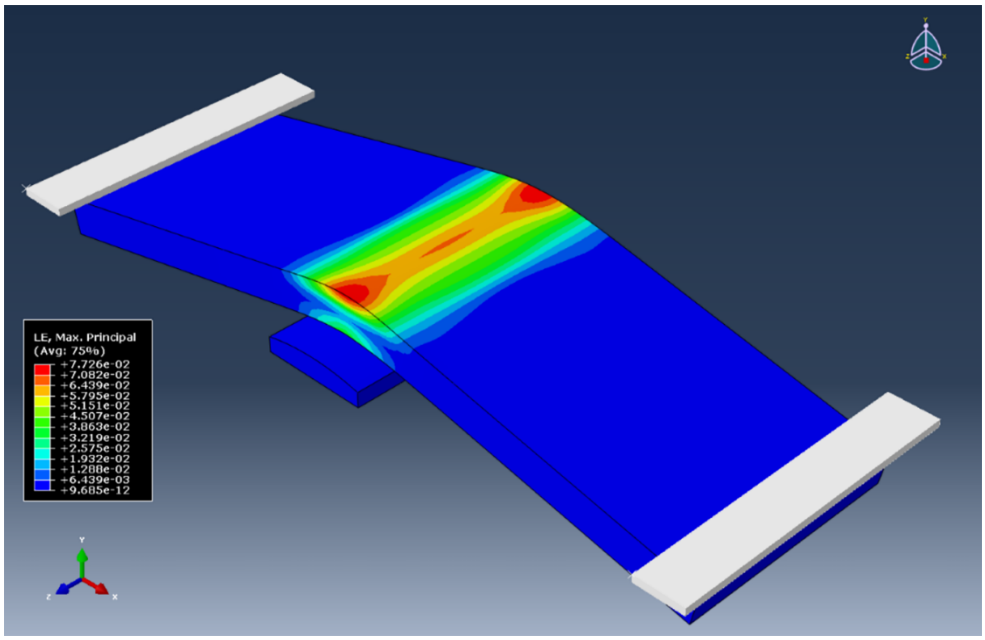

Figure 6.5: ABAQUS results that replicate cold bend test. Strain along the centreline is highest (red/orange) and drops away from the centreline (yellow/green/blue).

The method proposed introduces a solution to the problem of reliable augmented strain application for these experimental procedures and proposes that the Trans-Varestraint experiments are the experiments that are more reliable for testing the hot cracking susceptibility of materials. Strain is the main driver for the evolution of the phenomenon that is studied. By achieving control of the driver an appropriate infrastructure is set for further developments and potentially standardization of the tests.

This way materials can be potentially characterized according to the results of these tests as follows. The materials that present the initial cracking with low MCL at high augmented strains can be characterized as highly weldable materials. On the other hand materials that their initial cracking occurs during the application of low augmented strain and high MCL are measured can be characterized as low weldability materials (Figure 6.6). These differences also appear to apply to the TCL values versus the augmented strain. The only difference is that because the TCL values contain the size of all the cracks on the samples the differences between materials are highly accented compared to the MCL values. The boundaries and limits of this categorization of materials according to their hot cracking susceptibility

can be set after a significant range of materials have been tested using the method proposed.

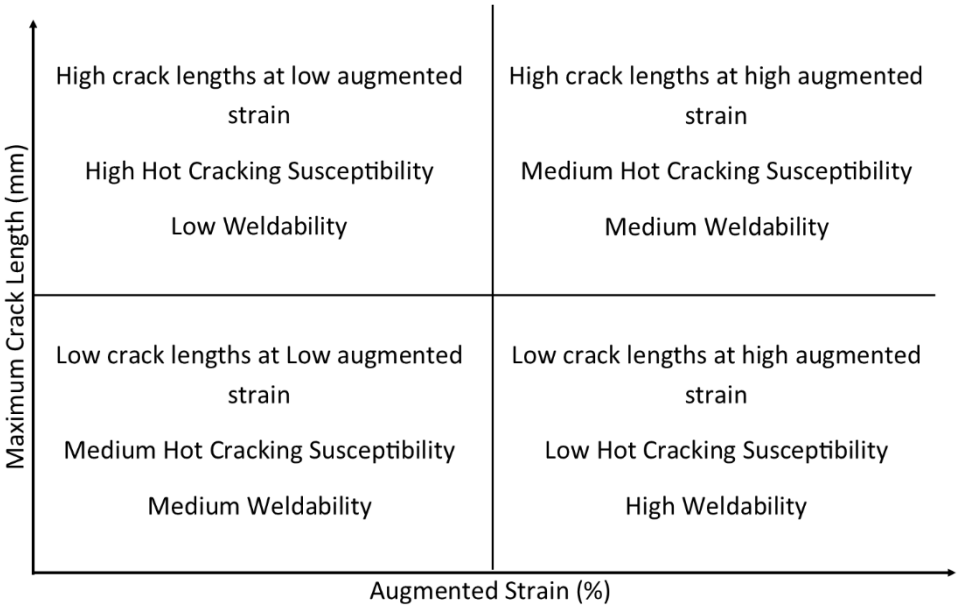

Figure 6.6: Proposed method for assessing hot cracking susceptibility of materials according to their initial crack length vs the augmented strain that caused this crack length.

The MCD results of this study can be used as shown in the following figure (Figure 6.7) to illustrate how a categorization like that would be like.

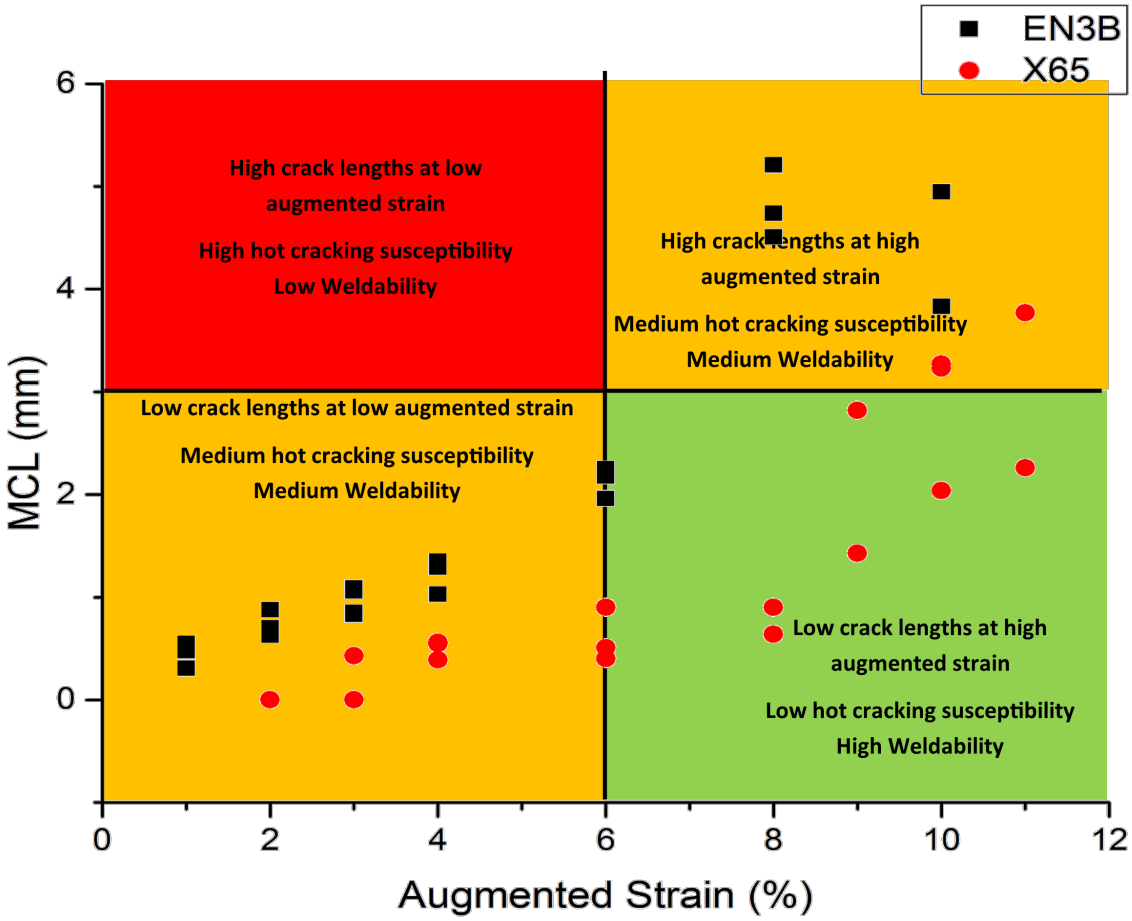

Figure 6.7: MCL results of both EN3B and X65 with the categorization of 6.6 overlayed over them for comparison.

From the experiments that have been carried out a mechanism for hot crack initiation has emerged and is therefore proposed. Along the centreline of the welding bead, dendrites start to form in the direction of the heat source (i.e. the welding torch). During the Trans-Varestraint test the augmented strain results from the combination of the shrinkage strain due to solidification and the mechanical strain imposed by the bending action of the test [124].

The strains applied from the test are tensile perpendicular to the plane in which the axis of the welding bead lies. During this application of strain, welding and solidification is still under development and due to the nature of the shape of the weld pool there is bound to be a section of the solidification front that will create an angle of 45° with the surface of the weld. As solidification is still taking place at the point where the greatest shear stress/strain is being applied, dendrites are

being pulled apart creating voids which result in initiation of cracks.

The results reported also identify a range of 'critical' depths where hot cracks initiate, which correlates with the dendrite growth orientation and maximum shear stress location. These findings may therefore be applied in future welding simulations to predict crack initiation and hot crack susceptibility in a wide range of materials, which would be a valuable predictive tool for both further academic research and industrial application. In the latter case such a standardized testing approach may result in a database of materials with a parameter quantifying their hot cracking susceptibility.

The lack of standards for hot cracking susceptibility prevents reliable evaluation of candidate materials and development of further understanding of the hot cracking phenomenon [119, 139, 164]. The experimental work, reported in this study, demonstrates a method for Trans-Varestraint testing that is more repeatable and reliable than reported in the previous literature. In combination with the results of published research [39, 60, 76, 80, 81, 113, 119, 139, 153, 164–168], the method presented could form the basis of standardized Trans-Varestraint tests.

6.5 Summary

The microstructure of API-5L X65 steel has been examined with no findings indicating deviation from the expected microstructure of the material or the weld joint. The hardness mapping of the weld joint revealed all the characteristic regions of a weld (FZ, HAZ, BM) and the distribution of the hardness was as expected. From the hardness map a minor difference on the size of the HAZ between the two sides of the weld which can be explained by slightly uneven heat input during welding.

The examination of the fracture toughness of the material has been proven challenging because obtaining specimens that contain 50% HAZ and 50% FZ requires intense planning and precise design. Nevertheless for this study the goal has been achieved and the fracture toughness of the fusion boundary has been

measured. Results showed that the fracture toughness on the boundary of the FZ with HAZ is lower than the fracture toughness of the FZ. This drop of fracture toughness sets the boundary of the FZ as a possible location for crack initiation.

As far as the Varestraint and Trans-Varestraint tests are concerned the testing of the samples was carried out according to the experimental design set and their post processing revealed some interesting features. Overall the Trans-Varestraint experiments are considered better overall because they appear to be more stable, controllable and repeatable than the Varestraint tests. Results demonstrated that EN3B is significantly more susceptible to hot cracking than X65 since it constantly presents a MCL higher than that for X65 at lower augmented strains. 0.50 mm MCL at 1% augmented strain versus 0.25 mm MCL at 3% strain respectively. Furthermore the proposed method does indeed impose the desired augmented strain on the samples. This proves that when conducting these experiments the radius of the former and the magnitude of the stroke of the bend are intrinsically connected. As a result experiments using this method will produce accurate, reliable and repeatable results compared to the ones obtained so far.

From the post processing (XRCT and fractography) of the samples some significant results have emerged. First of all the examination showed that hot cracking follows the solidification front of the weld as expected but the cracks initiate at a smaller depth than the depth of the weld. Further examination showed that at these depths where the first cracks occur the orientation of the solidification front forms an angle of 45° degrees with the surface of the weld. This is deemed noteworthy because taking under consideration the fact that the strains applied at the solidification front during the experiments are tensile in nature the angle of the solidification front and the initiation of the cracks coincides with the angle of the maximum shear strain that occurs during tensile loading.

Another result that formed as a result of the study is a categorization system that will improve the categorization of materials according their hot cracking susceptibility. Finally it is argued that, because the presented method appears to provide with significant control of the augmented strain imposed during experimentations, an infrastructure that can be used for the future standardization

of these experiments has been established.

Chapter 7

Conclusions

This study has provided with information and results that lead to multiple conclusions. From the theoretical point of view a clear outline that can be used to define the phenomenon of hot cracking has been introduced. This will allow for clearer definitions because there have been observations of terms being used interchangeably in the literature. For this reason ways of addressing this have already been presented in the literature. This study adds to the literature by using the available information to compile a clearer and more concise way of defining hot cracking defects (Section 2.3, Figure 2.7) and potentially this can be used to define other defects such as warm cracking and cold cracking. In short the definition of cracking defects proposed must address the following stages:

- Macroscopic definition
  - Type of cracking defect
  - Stage of welding that it manifests at
  - Position that it manifests at
  - Subset of defect according to the position it manifests at
- Microscopic definition
  - Conditions that define the subset
  - Morphology of the cracks

– Subset/name according to the morphology

As far as the mechanical properties of the material that have been examined in this study the following occurred.

- Compared to the FZ of the SAW X65 pipes the fracture toughness of the interface between the FZ and the HAZ of the weld joint is lower by 14%. (FZ HAZ Interface 34.9 MPa $m^{1/2}$ vs FZ 40.7 MPa $m^{1/2}$)
- SEM examination of the fracture surfaces of the CTOD specimens showed that interface between the FZ and HAZ is visible and the morphology of the fracture differs between them.
- Hardness measurements of the weld joint indicated that during welding the heat input is not evenly distributed to the rest of the material which cause a minor difference in the shape of the HAZ size on one side of the weld (Figure 5.10). Measurements showed that the hardness of the FZ has an average of 235.3 HV02 ±7.4. BM has an average hardness of 198.4 HV02 ± 5.9 and the heat affected zone has an average of 179.8 HV02 ± 4.9.

As far as the experimental method proposed and the assessment of the hot cracking susceptibility of X65 the following occurred.

- Through this study a new equation has been introduced that can be used in order to improve the reliability and compatibility of both Varestraint and Trans-Varestraint tests for assessing hot cracking susceptibility of materials. This equation defines a specific stroke length that should be applied during the bending of the samples that are undergoing these tests. The equation takes under consideration all the basic geometrical characteristics of the apparatus used for the tests in order to export the stroke length.

$$S = \frac{LW - R^2}{\sqrt{R^2 - W^2}} + R \tag{20}$$

This works under the assumptions that the formers on the used apparatus are interchangeable and calculated by the Equation 3, given for the calculation of the former radius according to the desired augmented strain.

- This study also proposes a graphical solution (Figure 3.16) on selecting former radii according to the thickness of the specimen and the desired augmented strain which is generated by the Equation 3.

- By examining X65 steel and EN3B steel using the method proposed it can be confirmed that EN3B is significantly more susceptible to hot cracking than X65 since it constantly presents a MCL higher than that for X65 at lower augmented strains. 0.5 mm MCL at 1% augmented strain versus 0.25 mm MCL at 3% strain respectively (Figure 5.24).

- Examination of the hot cracks under XRCT and SEM revealed that the orientation of dendrites that originate from the crack initiation points have a 45° angle with the surface of the weld (Figure 5.37, Figure 5.22). This, in combination with an analytical model, revealed the possibility of predicting the initiation sites of hot cracks during welding.

- This study also revealed that the augmented strain applied during the Trans-Varestraint tests can be controlled accurately and reliably (Figure 5.26). This will allow tests that are conducted using experimental setups similar to the one described to be comparable

- This study advocates the use of an experimental setup similar to a three point bend test since it allows for a better control of the location that the augmented strain will be applied to.

- As far as assessing the hot cracking susceptibility of materials this study proposes an evaluation of the materials depending on the size of the hot cracks that first manifest on the material in combination with the augmented strain that they are manifesting at (Figure 6.6). An example for this method of comparing and assessing materials has been presented by comparing X65 vs EN3B.

- Overall as far as the experimental procedures are concerned this study advocated for the use of the Trans-Varestraint tests over the Varestraint tests because the former exhibit better control and increased accuracy in their results compared to the latter.

Through this study it has been shown that the control of the augmented strain for the Varestraint and Trans-Varestraint experiments is feasible. This is an important contribution for the following reasons.

- Hot cracking is a strain driven phenomenon which means in principal that, when testing for it, the control that the experimental procedure provides to its application is paramount.
- By reliably controlling the strain other parameters of the test can be also studied and potentially controlled.
- By reaching a consensus that in order to control the strain as demonstrated, a specific type of apparatus must be used, specimen and welding specifications for conducting the experiments will emerge.
- It is argued that through this study a groundwork for future standardization of tests for assessing hot cracking susceptibility has been set.

On the hot crack nucleation subject this study proposes the following mechanism. Because of the shape of the weld pool there is bound to be a section of the solidification front that will create an angle of 45° with the surface of the weld. The specimen is bent whilst solidification is still taking place. The evidence suggests that at the point where the greatest shear stress/strain is being applied, dendrites are being pulled apart creating voids which create the initiation point for the cracks. This mechanism does not negate other proposed mechanisms but it adds to the existing findings. For example as it has been mentioned Ti(C, N) have been observed to facilitate the nucleation of hot cracks during welding. It is logical to assume that not all Ti(C, N) present in the microstructure of the material will cause the nucleation of cracks but, in combination with the mechanism proposed

by this study will they significantly increase the probability of the initiation of hot cracks.

The information presented in this study provides with some important findings and potential additions to science and the industry in general. Nevertheless the findings of this study can be used for the further development for both the experimental procedures and the hot cracking mechanisms of materials theories. Some potential routes that can be followed have already been presented, such as the examination of the strain rate on the now more stable Varestraint and Trans-Varestraint experimental procedures. Others could potentially be in mathematical modelling of these testing procedures in order to further improve existing models. As always with science and engineering the possibilities are endless and are always present.

Appendix A

Table 7.1: Results of CTOD specimens fracture toughness tests

		Sample Code							
Property	Units	IDF001	IDF002	IDF003	IDF004	ODF001	ODF002	ODF003	ODF004
Kq	MPa * m1/2	33.89	34.27	38.04	34.99	35.33	35.48	32.02	35.51
C.T.O.D.	mm	1.151	0.946	0.972	0.771	1.357	1.461	1.015	1.501
Area Under the Curve	J	15.78	12.92	12.93	10.49	15.32	19.78	13.94	20.07
Plastic J Jpl	J/mm2	1.107	0.903	0.938	0.734	1.305	1.407	0.975	1.448
Elastic J Jel	J/mm2	0.02	0.021	0.023	0.019	0.028	0.03	0.016	0.035
Total J	J/mm2	1.127	0.924	0.961	0.753	1.333	1.437	0.991	1.483
Maximum Load	kN	4.762	4.947	4.764	4.708	5.48	5.58	4.373	5.85
Load at 0.95 Slope	kN	2.396	2.457	2.482	2.497	2.417	2.415	2.291	2.338
Pmax/PQ		1.987	2.013	1.919	1.885	2.267	2.310	1.908	2.502

Table 7.2: Crack measurements

Position	IDF001 Crack Length (mm)	IDF002 Crack Length (mm)	IDF003 Crack Length (mm)	IDF004 Crack Length (mm)	ODF001 Crack Length (mm)	ODF002 Crack Length (mm)	ODF003 Crack Length (mm)	ODF004 Crack Length (mm)
1.00%	5.15	5.24	5.5	5.27	5.42	5.51	5.2	5.55
12.50%	5.42	5.38	5.74	5.42	5.57	5.62	5.42	5.65
25.00%	5.5	5.45	5.84	5.49	5.61	5.67	5.47	5.79
37.50%	5.56	5.49	5.87	5.54	5.66	5.7	5.49	5.84
50.00%	5.57	5.5	5.89	5.55	5.69	5.72	5.49	5.9
62.50%	5.56	5.49	5.87	5.53	5.68	5.7	5.45	5.9
75.00%	5.55	5.47	5.85	5.45	5.64	5.64	5.44	5.87
87.50%	5.54	5.4	5.8	5.42	5.6	5.6	5.39	5.74
99.00%	5.44	5.25	5.69	5.25	5.52	5.55	5.21	5.65

Table 7.3: Crack length checks

		IDF001	IDF002	IDF003	IDF004	ODF001	ODF002	ODF003	ODF004
Original Crack Size (mm)		5.29	5.24	5.59	5.26	5.47	5.53	5.20	5.60
Physical Crack Size (mm)		5.49	5.42	5.80	5.45	5.61	5.64	5.41	5.78
Limits (mm)	Lower	5.20	5.13	5.51	5.16	5.32	5.35	5.12	5.49
	Higher	5.80	5.73	6.11	5.76	5.92	5.95	5.72	6.09

Bibliography

[1] World Steel Association, *The white book of steel*. World Steel Association, 2012.

[2] Q. Lu, W. Xu, and S. van der Zwaag, "Designing new corrosion resistant ferritic heat resistant steel based on optimal solid solution strengthening and minimisation of undesirable microstructural components," *Computational Materials Science*, vol. 84, pp. 198–205, 2014.

[3] N. Saeidi, F. Ashrafizadeh, and B. Niroumand, "Development of a new ultrafine grained dual phase steel and examination of the effect of grain size on tensile deformation behavior," *Materials Science and Engineering a-Structural Materials Properties Microstructure and Processing*, vol. 599, pp. 145–149, 2014.

[4] R. Rana, C. Liu, and R. K. Ray, "Evolution of microstructure and mechanical properties during thermomechanical processing of a low-density multiphase steel for automotive application," *Acta Materialia*, vol. 75, pp. 227–245, 2014.

[5] M. B. Kermani and D. Harrop, "The impact of corrosion on the oil and gas industry," *Spe Production Facilities*, vol. 11, no. 3, pp. 186–190, 1996.

[6] B. A. Burgan and M. R. Sansom, "Sustainable steel construction," *Journal of Constructional Steel Research*, vol. 62, no. 11, pp. 1178–1183, 2006.

[7] E. D. Giaouris and G.-J. E. Nychas, "The adherence of salmonella enteritidis pt4 to stainless steel: The importance of the airliquid interface and nutrient availability," *Food microbiology*, vol. 23, no. 8, pp. 747–752, 2006.

[8] World Steel Association, "World steel in figures 2017," 2017.

[9] M. Y. Demeri, *Advanced High-Strength Steels : Science, Technology, and Applications*. Materials Park, OH, USA: A S M International, 2013.

[10] J. Davis, *Alloying: Understanding the Basics*. A S M International, 2001.

[11] G. Krauss, *Steels : Processing, Structure, and Performance*. Materials Park, OH, USA: ASM International, 2005.

[12] R. Pamnani, V. Karthik, T. Jayakumar, M. Vasudevan, and T. Sakthivel, "Evaluation of mechanical properties across micro alloyed hsla steel weld joints using automated ball indentation," *Materials Science and Engineering*

a-Structural Materials Properties Microstructure and Processing, vol. 651, pp. 214–223, 2016.

[13] H. Bhadeshia and R. Honeycombe, *Steels: microstructure and properties*. Butterworth-Heinemann, 2017.

[14] G. Snieder and H. Kerr, "Effects of chromium additions and flux type on the structure and properties of hsla steel submerged arc weld metal," *Canadian Metallurgical Quarterly*, vol. 23, no. 3, pp. 315–325, 1984.

[15] L. Liu, N. H. Loh, B. Y. Tay, and S. B. Tor, "Microstructure evolution of 316l stainless steel micro components prepared by micro powder injection molding," *Powder Technology*, vol. 206, no. 3, pp. 246–251, 2011.

[16] A. S. for Metals, *ASM handbook: Vol.4*, vol. 10th. Metals Park, Ohio: American Society for Metals, 1991.

[17] B. Beidokhti, A. H. Koukabi, and A. Dolati, "Effect of titanium addition on the microstructure and inclusion formation in submerged arc welded hsla pipeline steel," *Journal of Materials Processing Technology*, vol. 209, no. 8, pp. 4027–4035, 2009.

[18] L. Aucott, S. W. Wen, and H. Dong, "The role of ti carbonitride precipitates on fusion zone strength-toughness in submerged arc welded linepipe joints," *Materials Science and Engineering a-Structural Materials Properties Microstructure and Processing*, vol. 622, pp. 194–203, 2015.

[19] B. Beidokhti, A. Dolati, and A. H. Koukabi, "Effects of alloying elements and microstructure on the susceptibility of the welded hsla steel to hydrogen-induced cracking and sulfide stress cracking," *Materials Science and Engineering a-Structural Materials Properties Microstructure and Processing*, vol. 507, no. 1-2, pp. 167–173, 2009.

[20] K. Junhua, Z. Lin, G. Bin, L. Pinghe, W. Aihua, and X. Changsheng, "Influence of mo content on microstructure and mechanical properties of high strength pipeline steel," *Materials Design*, vol. 25, no. 8, pp. 723–728, 2004.

[21] A. Yoshie and J. Sasaki, "Niobium bearing structural steels," *Warrendale, PA The Minerals, Metals and Materials Society*, p. 291, 2010.

[22] K. Nishioka and K. Ichikawa, "Progress in thermomechanical control of steel plates and their commercialization," *Sci Technol Adv Mater*, vol. 13, no. 2, p. 023001, 2012.

[23] R. Doherty, D. Hughes, F. Humphreys, J. J. Jonas, D. J. Jensen, M. Kassner, W. King, T. McNelley, H. McQueen, and A. Rollett, "Current issues in recrystallization: a review," *Materials Science and Engineering: A*, vol. 238, no. 2, pp. 219–274, 1997.

[24] R. Doherty, "Diffusive phase transformations in the solid state," in *Physical metallurgy*, pp. 1363–1505, Elsevier, 1996.

[25] F. J. Humphreys and M. Hatherly, *Recrystallization and related annealing phenomena*. Elsevier, 2012.

[26] C. M. Liao and J. L. Lee, "Effect of molybdenum on sulfide stress cracking resistance of low-alloy steels," *Corrosion*, vol. 50, no. 9, pp. 695–704, 1994.

[27] G. T. Park, S. U. Koh, H. G. Jung, and K. Y. Kim, "Effect of microstructure on the hydrogen trapping efficiency and hydrogen induced cracking of linepipe steel," *Corrosion Science*, vol. 50, no. 7, pp. 1865–1871, 2008.

[28] W. Wang, Y. Y. Shan, and K. Yang, "Study of high strength pipeline steels with different microstructures," *Materials Science and Engineering a-Structural Materials Properties Microstructure and Processing*, vol. 502, no. 1-2, pp. 38–44, 2009.

[29] H. Dong, X. Hao, and D. Deng, "Effect of welding heat input on microstructure and mechanical properties of hsla steel joint," *Metallography, microstructure, and analysis*, vol. 3, no. 2, pp. 138–146, 2014.

[30] C. Chu, Y. Qin, X. Li, Z. Yang, F. Zhang, C. Guo, X. Long, and L. You, "Effect of two-step austempering process on transformation kinetics of nanostructured bainitic steel," in *Materials*, 2019.

[31] R. J. F. Tavitas, R. S. Garcés, and V. H. L. Cortéz, "Hybrid laser–arc welding applied in longitudinal joints for hydrocarbon conduction pipes," *MRS Online Proceedings Library Archive*, vol. 1766, pp. 45–52, 2015.

[32] H. Bhadeshia, "Case study: Weld microstructures," *Materials Science & Metallurgy. Retrieved from http://www. msm. cam. ac. uk/phase-trans/2000 C*, vol. 9, 2000.

[33] R. Ghomashchi, W. Costin, and R. Kurji, "Evolution of weld metal microstructure in shielded metal arc welding of x70 hsla steel with cellulosic electrodes: A case study," *Materials Characterization*, vol. 107, pp. 317–326, 2015.

[34] F. Z. Bu, X. M. Wang, L. Chen, S. W. Yang, C. J. Shang, and R. D. K. Misra, "Influence of cooling rate on the precipitation behavior in tinbmo microalloyed steels during continuous cooling and relationship to strength," *Materials Characterization*, vol. 102, pp. 146–155, 2015.

[35] L. Y. Lan, X. W. Kong, C. L. Qiu, and D. W. Zhao, "Influence of microstructural aspects on impact toughness of multi-pass submerged arc welded hsla steel joints," *Materials Design*, vol. 90, pp. 488–498, 2016.

[36] H. Alipooramirabad, R. Ghomashchi, A. Paradowska, and M. Reid, "Residual stress- microstructure- mechanical property interrelationships in multipass hsla steel welds," *Journal of Materials Processing Technology*, vol. 231, pp. 456–467, 2016.

[37] American Petroleum Institute. Production Dept, *Specification for line pipe*. American Petroleum Institute, 1991.

[38] G. Clauss, H. Weede, and T. Riekert, "Offshore pipe laying operationsinteraction of vessel motions and pipeline dynamic stresses," *Applied ocean research*, vol. 14, no. 3, pp. 175–190, 1992.

[39] L. A. Aucott, *Mechanism of solidification cracking during welding of high strength steels for subsea linepipe.* Phd thesis, 2015.

[40] M. N. Zafar, R. Rihan, and L. Al-Hadhrami, "Evaluation of the corrosion resistance of sa-543 and x65 steels in emulsions containing h2s and co2 using a novel emulsion flow loop," *Corrosion Science*, vol. 94, pp. 275–287, 2015.

[41] E. El-Danaf, M. Baig, A. Almajid, W. Alshalfan, M. Al-Mojil, and S. Al-Shahrani, "Mechanical, microstructure and texture characterization of api x65 steel," *Materials & Design*, vol. 47, pp. 529–538, 2013.

[42] G. Pluvinage, M. B. Amara, J. Capelle, and Z. Azari, "Role of constraint on ductile brittle transition temperature of pipe steel x65," *Procedia materials science*, vol. 3, pp. 1560–1565, 2014.

[43] Y. Hua, R. Barker, G. Bermperidis, H. Zhao, L. Zhang, and A. Neville, "Comparison of corrosion behavior of x65, 1cr, 5cr and 13cr steels in water-containing supercritical co2 environments with so2/o2," in *Proceedings of Corrosion 2016*, Leeds, 2016.

[44] P. Hopkins, "Pipelines: Past, present and future," in *The 5th Asian Pacific IIW International Congress*, p. 27, 2007.

[45] M. S. J. Hashmi, "Aspects of tube and pipe manufacturing processes: Meter to nanometer diameter," *Journal of Materials Processing Technology*, vol. 179, no. 1-3, pp. 5–10, 2006.

[46] I. E. Agency, "Key oil trends," report, International Energy Agency, 2015.

[47] I. E. Agency, "Key world energy statistics," report, International Energy Agency, 2015.

[48] C. L. Jenney and A. OBrien, "Welding handbook," *Volume*, vol. 1, pp. 305–306, 2001.

[49] S. Kou, "Welding metallurgy," *New Jersey, USA*, pp. 431–446, 2003.

[50] A. Munitz, C. Cotler, A. Stern, and G. Kohn, "Mechanical properties and microstructure of gas tungsten arc welded magnesium az91d plates," *Materials Science and Engineering a-Structural Materials Properties Microstructure and Processing*, vol. 302, no. 1, pp. 68–73, 2001.

[51] S. Kou, *Welding Metallurgy.* John Wiley Sons, Inc., second ed., 2003.

[52] D. L. Olson, *ASM handbook: welding, brazing, and soldering*, vol. 6. Asm Intl, 1993.

[53] P. T. Houldcroft, *Welding process technology.* Cambridge University Press, 1977.

[54] D. Yapp and S. Blackman, "Recent developments in high productivity pipeline welding," *Journal of the Brazilian Society of Mechanical Sciences and Engineering*, vol. 26, no. 1, pp. 89–97, 2004.

[55] P. F. Mendez and T. W. Eagar, "Penetration and defect formation in high-current arc welding," *Welding Journal*, vol. 82, no. 10, p. 296, 2003.

[56] P. T. Houldcroft, *Submerged-arc welding*. Woodhead publishing, 1989.

[57] J. Nowacki and P. Rybicki, "The influence of welding heat input on submerged arc welded duplex steel joints imperfections," *Journal of Materials Processing Technology*, vol. 164, pp. 1082–1088, 2005.

[58] L. Jeffus, *Welding: principles and applications*. Nelson Education, 2011.

[59] M. D. Herynk, S. Kyriakides, A. Onoufriou, and H. D. Yun, "Effects of the uoe/uoc pipe manufacturing processes on pipe collapse pressure," *International Journal of Mechanical Sciences*, vol. 49, no. 5, pp. 533–553, 2007.

[60] L. A. S. W. H. Dong, "On the relationship of microstructure, toughness, and hardness properties in a submerged arc welded api-5l grade x65 pipeline steel section," in *International Conference on Ocean, Offshore and Arctic Engineering*, ASME, 2014.

[61] J. J. Coronado and C. Ceron, "Fracture mechanisms of ctod samples of submerged and flux cored arc welding," *Theoretical and Applied Fracture Mechanics*, vol. 53, no. 2, pp. 145–151, 2010.

[62] S. Moeinifar, A. H. Kokabi, and H. R. M. Hosseini, "Role of tandem submerged arc welding thermal cycles on properties of the heat affected zone in x80 microalloyed pipe line steel," *Journal of Materials Processing Technology*, vol. 211, no. 3, pp. 368–375, 2011.

[63] W. B. Gao, D. P. Wang, F. J. Cheng, C. Y. Deng, and W. Xu, "Underwater wet welding for hsla steels: Chemical composition, defects, microstructures, and mechanical properties," *Acta Metallurgica Sinica-English Letters*, vol. 28, no. 9, pp. 1097–1108, 2015.

[64] Y. Ito and K. Bessyo, "Weldability formula of high strength steels related to heat-affected zone cracking," *Sumitomo Search*, no. 1, pp. 59–, 1969.

[65] D. Rosenthal, "Mathematical theory of heat distribution during welding and cutting.," *Welding Journal*, vol. 20, pp. 220–234., 1941.

[66] D. G. I. K. PoorhaydariI, B. M. Patchett, "Estimation of cooling rate in the welding of plates with intermediate thickness," *Welding Journal*, 2005.

[67] A. Bochvar, N. Rykalin, N. Prokhorov, I. Novikov, and B. Movchan, "The question of hot(crystallisation) cracks," *Welding Production*, vol. 10, pp. 5–7, 1960.

[68] N. Prokhorov and N. N. Prokhorov, "Fundamentals of the theory for technological strength of metals while crystallising during welding," *Transactions of the Japan Welding Society*, vol. 2, no. 2, pp. 205–213, 1971.

[69] T. Senda, F. Matsuda, G. Takano, K. Watanabe, T. Kobayashi, and T. Matsuzaka, "Fundamental investigations on solidification crack susceptibility for weld metals with trans-varestraint test," *Transactions of the Japan welding society*, vol. 2, 1971.

[70] Y. Arata, F. Matsuda, H. Nakagawa, S. Katayama, and S. Ogata, "Solidification crack susceptibility in weld metals of fully austenitic stainless steels (report iii): Effect of strain rate on cracking threshold in weld metal during solidification," *Transactions of JWRI*, vol. 6, no. 2, pp. 197–206, 1977.

[71] Y. Arata, F. Matsuda, H. Nakagawa, and S. Katayama, "Solidification crack susceptibility in weld metals of fully austenitic stainless steels (report iv)," *Transactions of JWRI*, vol. 7, no. 2, pp. 169–172, 1978.

[72] F. Matsuda, H. Nakagawa, T. Uehara, S. Katayama, and Y. Arata, "A new explanation solidification crack for role of delta-ferrite inproving weld susceptibility in austenitic stainless steel," *Transactions of JWRI*, vol. 8, no. 1, pp. 105–112, 1979.

[73] F. Matsuda, S. Katayama, and Y. Arata, "Solidification crack susceptibility in weld metals of fully austenitic stainless steels (report ix)," *Transactions of JWRI*, vol. 12, no. 2, pp. 247–252, 1983.

[74] W. Savage and C. Lundin, "The varestraint test," *Welding Journal*, vol. 44, no. 10, p. 433, 1965.

[75] B. Alexandrov and J. Lippold, *Further development of the cast pin tear test for evaluating solidification cracking in Ni-base alloys*, pp. 317–331. Springer, 2011.

[76] M. G. Collins and J. C. Lippold, "An investigation of ductility dip cracking in nickel-based filler materials - part i," *Welding Journal*, vol. 82, no. 10, pp. 288s–295s, 2003.

[77] S. J. Norton, *Development of a Gleeble based test for post weld heat treatment cracking in nickel alloys*. Thesis, 2003.

[78] S. Mandziej, *Testing for susceptibility to hot cracking on Gleeble physical simulator*, pp. 347–376. Springer, 2005.

[79] F. Mohammadi, F. F. Eliyan, and A. Alfantazi, "Corrosion of simulated weld haz of api x-80 pipeline steel," *Corrosion Science*, vol. 63, pp. 323–333, 2012.

[80] J. C. Lippold, "Recent developments in weldability testing for advanced materials," *Joining of Advanced and Specialty Materials VII*, 2005.

[81] L. Aucott, D. Huang, H. B. Dong, S. W. Wen, J. A. Marsden, A. Rack, and A. C. Cocks, "Initiation and growth kinetics of solidification cracking during welding of steel," *Sci Rep*, vol. 7, p. 40255, 2017.

[82] H. G. Hillenbrand, K. A. Niederhoff, G. Hauck, E. Perteneder, and G. Wellnitz, "Procedures, considerations for welding x-80 line pipe established," *Oil Gas Journal*, vol. 95, no. 37, pp. 47–, 1997.

[83] U. Reisgen, S. Olschok, and S. Jakobs, "Laser submerged arc welding (lupus) with solid state lasers," *8th International Conference on Laser Assisted Net Shape Engineering (Lane 2014)*, vol. 56, pp. 653–662, 2014.

[84] S. Kyriakides and E. Corona, *Mechanics of offshore pipelines: volume 1 buckling and collapse*, vol. 1. Elsevier, 2007.

[85] A. A. Oskuie, T. Shahrabi, and A. Lajevardi, "Failure of pipeline expander segments due to undesirable edm," *Engineering Failure Analysis*, vol. 28, pp. 34–46, 2013.

[86] S. Wen, H. Dong, S. Y. Zhang, A. Bannister, and M. Connelly, "Neutron diffraction measurement of weld residual stresses in an uoe linepipe subjected to mechanical expansion," in *ASME 2013 32nd International Conference on Ocean, Offshore and Arctic Engineering*, pp. V003T03A048–V003T03A048, American Society of Mechanical Engineers, 2013.

[87] Y. H. Yang, L. Shi, Z. Xu, H. S. Lu, X. Chen, and X. Wang, "Fracture toughness of the materials in welded joint of x80 pipeline steel," *Engineering Fracture Mechanics*, vol. 148, pp. 337–349, 2015.

[88] D. R. H. Jones and M. F. Ashby, *Engineering materials 2: an introduction to microstructures and processing*. Butterworth-Heinemann, 2012.

[89] W. D. Callister and D. G. Rethwisch, *Materials science and engineering: an introduction*. Wiley New York, 1991.

[90] E. Bayraktar, D. Kaplan, L. Devillers, and J. P. Chevalier, "Grain growth mechanism during the welding of interstitial free (if) steels," *Journal of Materials Processing Technology*, vol. 189, no. 1-3, pp. 114–125, 2007.

[91] T. W. Nelson, J. C. Lippold, and M. J. Mills, "Nature and evolution of the fusion boundary in ferritic-austenitic dissimilar weld metals, part 1 - nucleation and growth," *Welding Journal*, vol. 78, no. 10, pp. 329s–337s, 1999.

[92] Y. Z. Zhou, A. Volek, and N. R. Green, "Mechanism of competitive grain growth in directional solidification of a nickel-base superalloy," *Acta Materialia*, vol. 56, no. 11, pp. 2631–2637, 2008.

[93] A. Stangeland, A. Mo, O. Nielsen, D. Eskin, and M. M'Hamdi, "Development of thermal strain in the coherent mushy zone during solidification of aluminum alloys," *Metallurgical and Materials Transactions a-Physical Metallurgy and Materials Science*, vol. 35a, no. 9, pp. 2903–2915, 2004.

[94] G. Reinhart, A. Buffet, H. Nguyen-Thi, B. Billia, H. Jung, N. Mangelinck-No[U+FFFD] N. Bergeon, T. Schenk, J. H[U+FFFD]wig, and J. Baruchel, "In-situ and real-time analysis of the formation of strains and microstructure defects during solidification of al-3.5wt pct ni alloys," *Metallurgical and Materials Transactions A*, vol. 39, no. 4, pp. 865–874, 2008.

[95] X. Kai;, Z. Shu-quan;, and Q. Zheng-lai3, "Numerical simulation research on welding temperature field of 304 stainless steel," *Advances in Engineering Research,*, vol. 113, 2016.

[96] B. Bottger, M. Apel, B. Santillana, and D. G. Eskin, "Relationship between solidification microstructure and hot cracking susceptibility for continuous casting of low-carbon and high-strength low-alloyed steels: A phase-field study," *Metallurgical and Materials Transactions a-Physical Metallurgy and Materials Science*, vol. 44a, no. 8, pp. 3765–3777, 2013.

[97] K. Nishimoto, K. Saida, K. Kiuchi, and J. Nakayama, *Influence of minor and impurity elements on hot cracking susceptibility of extra high-purity type 310 stainless steels*, pp. 183–208. Springer, 2011.

[98] M. Sistaninia, S. Terzi, A. Phillion, J.-M. Drezet, and M. Rappaz, "3-d granular modeling and in situ x-ray tomographic imaging: a comparative study of hot tearing formation and semi-solid deformation in alcu alloys," *Acta Materialia*, vol. 61, no. 10, pp. 3831–3841, 2013.

[99] D. G. Eskin and L. Katgerman, "A quest for a new hot tearing criterion," *Metallurgical and Materials Transactions a-Physical Metallurgy and Materials Science*, vol. 38a, no. 7, pp. 1511–1519, 2007.

[100] A. Phillion, S. Cockcroft, and P. Lee, "X-ray micro-tomographic observations of hot tear damage in an almg commercial alloy," *Scripta materialia*, vol. 55, no. 5, pp. 489–492, 2006.

[101] J. Aveson, G. Reinhart, B. Billia, H. Nguyen-Thi, N. Mangelinck-No[U+FFFD] T. Lafford, C. Vie, J. Baruchel, and H. Stone, "Observation of the initiation and propagation of solidification cracks by means of in situ synchrotron x-ray radiography," in *IOP Conference Series: Materials Science and Engineering*, vol. 33, p. 012040, IOP Publishing, 2012.

[102] S. Kou, "Solidification and liquation cracking issues in welding," *Jom-Journal of the Minerals Metals Materials Society*, vol. 55, no. 6, pp. 37–42, 2003.

[103] B. Santillana, R. Boom, D. Eskin, H. Mizukami, M. Hanao, and M. Kawamoto, "High-temperature mechanical behavior and fracture analysis of a low-carbon steel related to cracking," *Metallurgical and Materials Transactions a-Physical Metallurgy and Materials Science*, vol. 43a, no. 13, pp. 5048–5057, 2012.

[104] L. Aucott, D. Huang, H. B. Dong, S. W. Wen, J. Marsden, A. Rack, and A. C. F. Cocks, "A three-stage mechanistic model for solidification cracking during welding of steel," *Metallurgical and Materials Transactions a-Physical Metallurgy and Materials Science*, vol. 49a, no. 5, pp. 1674–1682, 2018.

[105] J. Andersson, *Weldability of precipitation hardening superalloysinfluence of microstructure*. Chalmers University of Technology, 2011.

[106] C. Cross, *On the origin of weld solidification cracking*, pp. 3–18. Springer, 2005.

[107] V. Shankar, T. P. S. Gill, S. L. Mannan, and S. Sundaresan, "Solidification cracking in austenitic stainless steel welds," *Sadhana-Academy Proceedings in Engineering Sciences*, vol. 28, no. 3-4, pp. 359–382, 2003.

[108] I. of British Foundrymen Welsh Engineers' Founders' Association Foundry Trades' Equipment Supplies Association, *The Foundry Trade Journal*. 1967.

[109] S. Moeinifar, A. H. Kokabi, and H. R. M. Hosseini, "Effect of tandem submerged arc welding process and parameters of gleeble simulator thermal cycles on properties of the intercritically reheated heat affected zone," *Materials Design*, vol. 32, no. 2, pp. 869–876, 2011.

[110] C. D. Lundin, C. Y. P. Qiao, T. P. S. Gill, and G. M. Goodwin, "Hot ductility and hot cracking behavior of modified 316 stainless-steels designed for high-temperature service," *Welding Journal*, vol. 72, no. 5, pp. S189–S200, 1993.

[111] W. Yeniscavich, "Correlation of hot ductility curves with cracking during welding," in *Proceedings of the Symposium on Methods of High-Alloy Weldability Evaluation.*, 1969.

[112] A. Rapetti, P. Todeschini, S. Hendili, F. Christien, and F. Tancret, "A study of ductility dip cracking of inconel 690 welding filler metal: Development of a refusion cracking test," in *ASME 2017 Pressure Vessels and Piping Conference*, pp. V06BT06A022–V06BT06A022, American Society of Mechanical Engineers, 2017.

[113] N. E. Nissley and J. C. Lippold, "Development of the strain-to-fracture test a new test has been established for evaluating ductility dip cracking susceptibility in austenitic alloys," *Welding journal*, vol. 82, no. 12, pp. 355–364, 2003.

[114] A. J. Ramirez, J. W. Sowards, and J. C. Lippold, "Improving the ductility-dip cracking resistance of ni-base alloys," *Journal of Materials Processing Technology*, vol. 179, no. 1-3, pp. 212–218, 2006.

[115] F. F. Noecker and J. N. DuPont, "Metallurgical investigation into ductility dip cracking in ni-based alloys: Part ii," *Welding Journal*, vol. 88, no. 3, pp. 62s–77s, 2009.

[116] A. Y. Jang, D. J. Lee, S. H. Lee, J. H. Shim, S. W. Kang, and H. W. Lee, "Effect of cr/ni equivalent ratio on ductility-dip cracking in aisi 316l weld metals," *Materials Design*, vol. 32, no. 1, pp. 371–376, 2011.

[117] F. Hull, "Cast-pin tear test for susceptibility to hot cracking," *Welding Journal*, vol. 38, no. 4, pp. 176s–181s, 1959.

[118] F. C. Hull, "Effect of delta ferrite on the hot cracking of stainless steel," *Welding Journal*, vol. 46, no. 9, p. 399, 1967.

[119] T. Lis, "Modification of oxygen and sulphur inclusions in steel by calcium treatment," *Metalurgija*, vol. 48, no. 2, pp. 95–98, 2009.

[120] B. Alexandrov, J. Lippold, and N. Nissley, *Evaluation of weld solidification cracking in Ni-base superalloys using the cast pin tear test*, pp. 193–213. Springer, 2008.

[121] D. P. Ryan, *Development of a Modified Cast-pin Tear Test to Evaluate the Solidification Cracking Susceptibility of Fully Austenitic Materials*. Thesis, 2003.

[122] H. Tamura, N. Kato, S. Ochiai, and Y. Katagiri, "Cracking study of aluminum alloys by the variable tensile strain hot cracking test," *transactions of the Japan Welding Sosciety*, vol. 8, 1977.

[123] T. Ogawa and E. Tsunetomi, "Hot cracking susceptibility of austenitic stainless steels.," *WELDING J.*, vol. 61, no. 3, p. 82, 1982.

[124] J. Andersson, J. Jacobsson, A. Brederholm, and H. Hänninen, *Improved Understanding of Varestraint TestingNickel-Based Superalloys*, pp. 25–36. Springer, 2016.

[125] S. Goodman, J. Lee, and E. Nichols, "Varestraint testing of cast 73-30 ni alloy," *Welding Journal*, vol. 47, no. 8, p. 371, 1968.

[126] C. Lundin and W. Savage, "Application of the varestraint technique to the study of weldability(augmented strain concept and varestraint test for hot-cracking sensitivity and weldability of filler metals)," *Welding journal, research supplement*, vol. 45, 1966.

[127] Y. Arata, F. Matsuda, K. Nakata, and I. Sasaki, "Solidification crack susceptibility of aluminum alloy weld metals (report i): characteristics of ductility curves during solidification by means of the trans-varestraint test," *Transactions of JWRI*, vol. 5, no. 2, pp. 153–167, 1976.

[128] Y. Arata, F. Matsuda, and S. Katayama, "Solidification crack susceptibility in weld metals of fully austenitic stainless steels (report ii): Effect of ferrite, p, s, c, si and mn on ductility properties of solidification brittleness," *Transactions of JWRI*, vol. 6, no. 1, pp. 105–116, 1977.

[129] F. Matsuda, H. Nakagawa, S. Katayama, and Y. Arata, "Solidification crack susceptibility in weld metals of fully austenitic stainless steels (report vi): Effect of la or rem addition on solidification crack resistance (materials metallurgy and weldability)," *Transactions of JWRI*, vol. 11, no. 1, pp. 79–94, 1982.

[130] F. Matsuda, H. Nakagawa, S. Ogata, and S. Katayama, "Fractographic investigation on solidification crack in the varestraint test of fully austenitic stainless steel: Studies on fractography of welded zone (iii)," *Transactions of JWRI*, vol. 7, no. 1, pp. 59–70, 1978.

[131] D. Hayduk, B. Damkroger, G. Edwards, and D. Olson, "Cracking susceptibility of ti-6al-2nb-1ta-0.8 mo as determined by the varestraint test," *Welding Journal*, vol. 65, no. 9, 1986.

[132] M. Dvornak, R. Frost, and D. Olson, "The weldability and grain refinement of ai-2.2 li-2.7 cu," *Welding Journal*, vol. 68, no. 8, 1988.

[133] J. Adamiec and B. Scibisz, "Investigation of hot cracking resistance of 2205 duplex steel," *Proceedings of the 11th European Workshop of the European-Microbeam-Analysis-Society (Emas) on Modern Developments and Applications in Microbeam Analysis*, vol. 7, p. 012001, 2010.

[134] J. Adamiec, "Evaluation of susceptibility of the zre1 alloy to hot cracking in conditions of forced strain," *Arch. Foundry Eng.*, vol. 10, no. 1, 2010.

[135] R. Trevisan, E. Braga, and H. Fals, "Effects of nitrogen and pulsed mean welding current in aisi 316 austenitic steel solidification cracks," *Welding international*, vol. 17, no. 4, pp. 298–302, 2003.

[136] T. Raza, J. Andersson, and L. E. Svensson, "Varestraint weldability testing of additive manufactured alloy 718," *Science and Technology of Welding and Joining*, vol. 23, no. 7, pp. 606–611, 2018.

[137] T. Senda, F. Matsuda, and G. Takano, "Solidification crack susceptibility for weld metals with the trans-varestraint test. pt. 2. commercially used aluminum and aluminum alloys," *Yosetsu Gakkai- Shi*, vol. 42, no. 1, pp. 48–56, 1973.

[138] C. L. M. d. Silva and A. Scotti, "Performance assessment of the (trans)varestraint tests for determining solidification cracking susceptibility when using welding processes with filler metal," *Measurement Science and Technology*, vol. 15, no. 11, pp. 2215–2223, 2004.

[139] J. Lippold, T. Boellinghaus, and C. Cross, *Hot Cracking Phenomena in Welds III*. Springer Berlin Heidelberg, 2011.

[140] T. Finton and J. Lippold, "Standardization of the transvarestraint test," *Edison Welding Institute Summary Report*, no. 04-05, 2004.

[141] J. Jacobsson, "Weldability and testing methodology in precipitation hardening superalloys," 2017.

[142] T. Kannengiesser and T. Boellinghaus, "Hot cracking testsan overview of present technologies and applications," *Welding in the World*, vol. 58, no. 3, pp. 397–421, 2014.

[143] A. Standard, "E3-11, 2011,standard guide for preparation of metallographic specimens, astm international, west conshohocken, pa, doi: 10.1520/e0003-11."

[144] A. S. for Testing and P. Materials (Filadelfia, "Astm e112-96 (2004) e2: Standard test methods for determining average grain size," ASTM, 2004.

[145] A. International, "Astm standards: Standards test methods and definitions for mechanical testing of steel products (a370-02).," ASTM, 2005.

[146] R. E. Chinn, "Hardness, bearings, and the rockwells," *Advanced Materials Processes*, vol. 167, no. 10, pp. 29–31, 2009.

[147] A. International, "Astm e384-99-standard test method for microindentation hardness of materials," 1999.

[148] X. K. Zhu and J. A. Joyce, "Review of fracture toughness (g, k, j, ctod, ctoa) testing and standardization," *Engineering Fracture Mechanics*, vol. 85, pp. 1–46, 2012.

[149] A. Standard, "Astm e1290-08e1, standard test method for crack-tip opening displacement (ctod) fracture toughness measurement (withdrawn 2013)," 2008.

[150] ASTM, *E399-90 Standard test method for plane-strain fracture toughness of metallic materials.* 2003.

[151] ASTM-E1820-01, "Standard Test Methods for Measurement of Fracture Toughnes," *Annual Book of ASTM Standards*, 2001.

[152] D. Hayduk, B. K. Damkrocer, G. R. Edwards, and D. L. Olson, "Cracking susceptibility of ti-6ai-2nb-1ta-0.8mo as determined by the varestraint test," *Welding Journal*, vol. 65, no. 9, p. 251, 1986.

[153] V. Shankar, T. P. S. Gill, S. L. Mannan, and S. Sundaresan, "Criteria for hot cracking evaluation in austenitic stainless steel welds using longitudinal varestraint and transvarestraint tests," *Science and Technology of Welding and Joining*, vol. 5, no. 2, pp. 91–97, 2013.

[154] J. Blitz, *Electrical and magnetic methods of non-destructive testing*, vol. 3. Springer Science Business Media, 2012.

[155] T. Aastroem, "From fifteen to two hundred ndt-methods in fifty years," in *17th world conference on nondestructive testing*, pp. 25–28, 2008.

[156] G. A. Raine and N. Smith, "Ndt of on and offshore oil and gas installations using the alternating current field measurement (acfm) technique," *Materials Evaluation*, vol. 54, no. 4, pp. 461–, 1996.

[157] A. Shukla and H. Karki, "Application of robotics in onshore oil and gas industrya review part i," *Robotics and Autonomous Systems*, vol. 75, pp. 490–507, 2016.

[158] A. International, "Standard test method for measurement of fracture toughness," 2011.

[159] D. Wildenschild and A. P. Sheppard, "X-ray imaging and analysis techniques for quantifying pore-scale structure and processes in subsurface porous medium systems," *Advances in Water Resources*, vol. 51, pp. 217–246, 2013.

[160] L. Jiang, N. Chawla, M. Pacheco, and V. Noveski, "Three-dimensional (3d) microstructural characterization and quantification of reflow porosity in sn-rich alloy/copper joints by x-ray tomography," *Materials Characterization*, vol. 62, no. 10, pp. 970–975, 2011.

[161] S. Vasic, B. Grobety, J. Kuebler, T. Graule, and L. Baumgartner, "Xrct characterisation of ti particles inside porous al2o3," *Materials Characterization*, vol. 61, no. 6, pp. 653–660, 2010.

[162] L. Pejryd and R. Eriksson, "X-ray computed tomography as a tool in joining process development," in *The 6th International Swedish Production Symposium 2014*, pp. 1–7, Citeseer.

[163] A. Standard, "E399-09," *Standard test method for linear-elastic plane-strain fracture toughness KIc of metallic materials. ASTM International*, 2009.

[164] T. Boellinghaus, J. Lippold, and C. Cross, *Cracking Phenomena in Welds IV*. Springer International Publishing, 2016.

[165] V. Quiroz, A. Gumenyuk, and M. Rethmeier, "Investigation of the hot cracking susceptibility of laser welds with the controlled tensile weldability test," *Journal of Strain Analysis for Engineering Design*, vol. 47, no. 8, pp. 587–599, 2012.

[166] J. C. Lippold, J. W. Sowards, G. M. Murray, B. T. Alexandrov, and A. J. Ramirez, "Weld solidification cracking in solid-solution strengthened ni-base filler metals," in *2007 2nd International Workshop on Hot Cracking Phenomena in Welds*, pp. 147–170, Springer Verlag, 2007.

[167] S. S. Singh, J. J. Williams, P. Hruby, X. Xiao, F. De Carlo, and N. Chawla, "In situ experimental techniques to study the mechanical behavior of materials using x-ray synchrotron tomography," *Integrating Materials and Manufacturing Innovation*, vol. 3, no. 1, p. 9, 2014.

[168] C. E. Cross and N. Coniglio, "Weld solidification cracking: Critical conditions for crack initiation and growth," in *2007 2nd International Workshop on Hot Cracking Phenomena in Welds*, pp. 39–58, Springer Verlag, 2007.

[169] G. Srinivasan, M. Divya, S. K. Albert, A. K. Bhaduri, A. Klenk, and D. R. G. Achar, "Study of hot cracking behaviour of nitrogen-enhanced austenitic stainless steels using varestraint and hot ductility tests," *Welding in the World*, vol. 54, no. 11-12, pp. R322–R332, 2010.

[170] E. J. Chun, H. Baba, K. Nishimoto, and K. Saida, "Development of laser beam welding transverse-varestraint test for assessment of solidification cracking susceptibility in laser welds," *Metals and Materials International*, vol. 21, no. 3, pp. 543–553, 2015.